(Bittel)

FINAL REPORT

FEASIBILITY STUDY FOR LONG LIFETIME HELIUM DEWAR

BY

R. T. PARMLEY

DECEMBER, 1981

PREPARED UNDER CONTRACT NO. NAS 2-10848

by

LOCKHEED MISSILES & SPACE COMPANY, INC.

Palo Alto, California 94304

FOR

AMES RESEARCH CENTER

NATIONAL AERONAUTICS AND SPACE ADMINISTRATION

MOFFET FIELD, CALIFORNIA 94035

1. Report No.	2. Government Accession No.	3. Recipient's Catalog No.
NASA-CR 166254		

4. Title and Subtitle	5. Report Date
FEASIBILITY STUDY FOR LONG LIFETIME HELIUM DEWAR	December 1981
	6. Performing Organization Code LMSC Research Lab

7. Author(s)	8. Performing Organization Report No.
R. T. Parmley	
	10. Work Unit No.

9. Performing Organization Name and Address	11. Contract or Grant No.
Lockheed Palo Alto Research Laboratory 3251 Hanover Street Palo Alto, California 94304	NAS 2-10848
	13. Type of Report and Period Covered Final Report (Jan-Dec 81)

12. Sponsoring Agency Name and Address	14. Sponsoring Agency Code
National Aeronautics & Space Administration Ames Research Center Moffett Field, California 94035	

15. Supplementary Notes Point of Contact: Dr. Peter Kittel Mail Stop 244-7
National Aeronautics & Space Administration
Ames Research Center, Moffett Field, CA 94035
Phone: 415/965-6525 FTS 448-6525

16. Abstract

The object of this study is to identify a feasible concept for a launchable 3-year lifetime helium dewar from which the required technology development tasks can be identified. Current helium dewar designs were examined to see where the largest potential reductions in parasitic heat loads can be made. For example, on the IRAS program, the single largest item, tank supports, amounted to 67%. Wire leads and multilayer insulation constituted 17 and 14%, respectively. Consequently, a large part of the study effort was devoted to examining new, promising support concepts. The support concept chosen, a Passive-Orbital-Disconnect-Strut (PODS), has an orbital support conductance that is lower by more than an order of magnitude over current tension band supports. This lower support conductance cuts the total dewar weight in half for the same 3-year lifetime requirements. Effort was also concentrated on new, efficient wire feed through designs and vapor cooling of the multilayer insulation, supports, wire feed throughs and plumbing penetrations.

The program consisted of four basic tasks. The first task examined a single-stage helium dewar vs. dual-stage dewars with a guard cryogen of nitrogen or neon. The single-stage dewar concept was selected. Next, different support concepts were analyzed from which the PODS support concept was chosen. A preliminary design of the dewar was thermally and structurally analyzed and laid out including system weights, thermal performance and performance sensitivities. Finally, a Technology Development Plan was prepared, task by task, to verify the predicted performance. A schedule and ROM costs for each task concluded the study effort.

17. Key Words (Suggested by Author(s))	18. Distribution Statement
Superfluid helium Dewar Low heat leak supports Analysis, Design 3-year lifetime STS Launch	Unlimited Star Category 18

19. Security Classif. (of this report)	20. Security Classif. (of this page)	21. No. of Pages	22. Price*
UNCLASSIFIED	UNCLASSIFIED	183	

*For sale by the National Technical Information Service, Springfield, Virginia 22161

FOREWORD

This work was conducted for the National Aeronautics and Space Administration through the AMES Research Center, Moffett Field, California, Dr. Peter Kittel, Program Manager.

The Lockheed Palo Alto Research Laboratory conducted the program within the Cryogenic Technology Group of the Materials Sciences Laboratory. Key individuals who contributed to the success of this program and their contributions are as follows:

Kevin Burns	-	Modified the PODS thermal program and developed the FTS program.
Dr. David Bushnell	-	Developed the PANDA-DEWAR program and performed the Support Selection Analysis.
Ed Cavey	-	Analyzed and laid out the dewar design.
Dr. Ike Hsu	-	Developed the thermal model for the dewar and performed the thermal analysis using the THERM program.

Ted Nast - Provided technical consultation throughout the study.

Jorgen Skogh - Performed the dewar structural analyses and the STAGS analysis.

Roger Wedel - Modified the CRYOP program for use in the Cryogen Selection Analysis. Performed parametric trade studies using the CRYOP and PRESS programs.

Some of the structural and thermal data for the Passive Orbital Disconnect Strut (PODS) system were developed under a Lockheed Independent Technology Program prior to and concurrent with this program. These data include:

- The PODS concept
- The PODS Thermal Model
- Thermal and structural test data

The results of the support and cryogen trade studies, a complete description of the selected dewar design (and its performance) and a technology development plan are provided in this report.

Richard T. Parmley
Principal Investigator

TABLE OF CONTENTS

TABLE OF CONTENTS (continued)

TABLE OF CONTENTS (continued)

FIGURES

FIGURES (continued)

TABLES

Section 1

INTRODUCTION AND SUMMARY

1.1 INTRODUCTION

The object of this study is to identify a feasible concept for a launchable three-year lifetime helium dewar from which the required technology development tasks can be identified. In order to keep the dewar size and weight within reason, it is important to reduce the parasitic heat load below those obtained on current flight dewars, designed for durations on the order of one year. In order to determine which areas provide the largest improvement potential, a breakdown of the parasitic heat loads of current helium dewar designs was examined. For example, on the IRAS program, the breakdown is as follows:

IRAS Parasitic Heat Leak [1-1]	%
Multilayer Insulation[1]	14
Tension Band Supports[2]	67
Plumbing[2]	2
Wire Leads[2]	17
	100

1. Three vapor-cooled shields
2. Vapor cooled

The tension band support represents one of the most advanced support technologies currently available yet still constitutes two-thirds of the parasitic heat load.

For this reason, Lockheed started an in-house effort in 1978 to develop a new support concept that has a thermal conductance value at least an order of magnitude below the tension band system. The passive orbital disconnect strut (PODS) that is currently being developed and is described in this report exceeds that goal and cuts the dewar weight in half (as compared to tension bands) for the same mission requirements. Consequently, qualification of the PODS supports is a key item in demonstrating the feasibility of a 3-year lifetime dewar.

Insuring the wire feeds are adequately cooled with venting helium is another key item and a design concept to accomplish this was developed on this program. Decreasing the thermal conductivity of multilayer insulations is another area of potential benefit, particularly in the low temperature range where radiation becomes less important and conduction begins to dominate.

All these technology areas are addressed in this study and development plans laid out to verify their performance.

1.2 SUMMARY

Using the dewar requirements established for this study, two trade studies were performed. The first trade study selected which cryogen(s) should be used while the second trade study examined different support concepts. A single

stage helium dewar plus PODS supports were chosen. Additional system analyses were performed so a preliminary dewar design could be laid out. The dewar performance was calculated and performance sensitivity analyses were performed. Finally a technology development plan was prepared and costed that demonstrates the recommended design approach.

Section 9 of this report provides a description of the computer programs used in the study. The thermal and structural properties of materials analyzed in the program are provided in Section 10.

Section 2

DEWAR REQUIREMENTS

The contract requirements for dewar performance were used throughout the study. The selected dewar design in Section 5 meets or exceeds all of the following requirements as shown here.

	Contract Requirements	Selected Dewar Performance (Section 5)
1. Orbit lifetime	3 Years	> 3 years for vacuum jacket temperature < 300K (< 540R)
2. Shuttle launch loads	Launch loads: 10g axial 10g lateral	Launch loads: 10g axial 10g lateral
3. Cargo bay	Must fit in 4.5M diam. (180 in) by 18M long (720 in) cargo bay.	Dewar dimensions: • Diameter 1.48m (58.3 in) • Length 4.55m (179 in)
4. Spacecraft power	Control power of 25W at 24V will be available.	Maximum control power requirements are 24 watts (momentary)
5. Support resonance requirements	> 35 Hz launch > 20 Hz orbit	35 Hz launch (min) 20 Hz orbit (min) (Assumes rigid tank and vacuum shell rings)
6. Total loaded dewar weight including helium and 200 kg (441 lb) instrument.	< 2000 kg (< 4409 lb)	989 kg (2180 lb)
7. Dewar reuse possible?	Expendable system allowed	Yes, reusable system except for aperture cover

	Contract Requirements	Selected Dewar Performance (Section 5)
8. Ground servicing	No ground servicing allowed one day before launch; intermittent servicing allowed during preceding two days.	Ground servicing required 11.1 days prior to launch; no additional servicing required.
9. Dewar orientation in space	One side assumed to always point away from Sun. Radiator considered as part of the thermal protection system.	3-year lifetime achievable as long as aperture doesn't view Sun or Earth.
10. Ground command links to dewar	Will be available.	Valves PV7 and RAV3 opening and aperture cover separation can be commanded from the ground.
11. Development program	Not last longer than 10 years.	3.5 years
12. Instrument characteristics		
• Size	1M diam x 2M long	Same
• Weight	200 KG (441 lb)	Same
• Max temperature	2K (3.6K)	Same
• Continuous heating		
• Joule	10 mW (0.03 Btu/hr)	Same
• Aperture radiation	1 mW (0.003 Btu/hr)	Same
• Wires	400 ea coax cables • 2 mil diam SS wire • 10 mil OD x 2 mil SS sheath • Teflon insulation Manganin wires • 200 ea #40 gage • 40 ea #32 gage • 10 ea #24 gage	Same (Additional wires required for valves and instrumentation)

Section 3

CRYOGEN SELECTION ANALYSIS

Analyses were performed to determine whether a single stage or dual stage dewar is optimum and which cryogens should be used. Since the instrument cooling requirement is $\leq$ 2K ($<$ 3.6R), only a superfluid helium dewar can meet this requirement. The question remains which guard cryogen should be selected for the dual stage concept and whether a single or dual stage dewar is optimum. This section provides the data to answer these questions. The major analytical tool used in these analyses is the CRYOP program described in detail in Section 9.

3.1 SELECTION OF GUARD CRYOGEN CANDIDATES

Prior to performing the single stage vs. dual stage trade studies, it is necessary to narrow the number of potential guard cryogens used on the dual stages to a reasonable number. A preliminary analysis was performed on CRYOP for He/CH_4, He/Ne, He/H_2 and He/N_2. This analysis was performed before CRYOP was modified to handle up to six vapor-cooled shields and the PODS support option.

The supports for the dual stage system consist of large-diameter folded fiberglass tubes, which provides a cantilever-type support similar to previous coolers which have been developed and flown [3.1].

The vapor cooling utilization for the helium was based on cooling the He-II/guard cryogen supports, then cooling the guard cryogen, and finally the outer shell/guard cryogen supports. A vapor-cooled shield in the multilayer insulation was not assumed.

The relative system weights were determined for several guard cryogens for the nominal parameters. Sensitivity studies were conducted for the helium/solid neon case only.

The nominal parameters at $X/X_{NOM} = 1$ are:

- Instrument heat load = 21 mW (0.07 Btu/hr)
- Multilayer insulation is double aluminized mylar with 2 silk net spacers each.
- Vacuum jacket temperature, T_H = 200K (360R)

The results shown in Fig. 3.1 indicate the He/H_2, He/N_2 and He/Ne have similar weights with the He/CH_4 somewhat heavier. The He/H_2 system represents a safety impact due to the flammable H_2 and also has a substantially larger volume than the others, so appears to be an unlikely choice, while the He/CH_4 system also has some undesirable safety features due to the flammable CH_4.

The prime candidates to be studied further are therefore He/Ne and He/N_2.

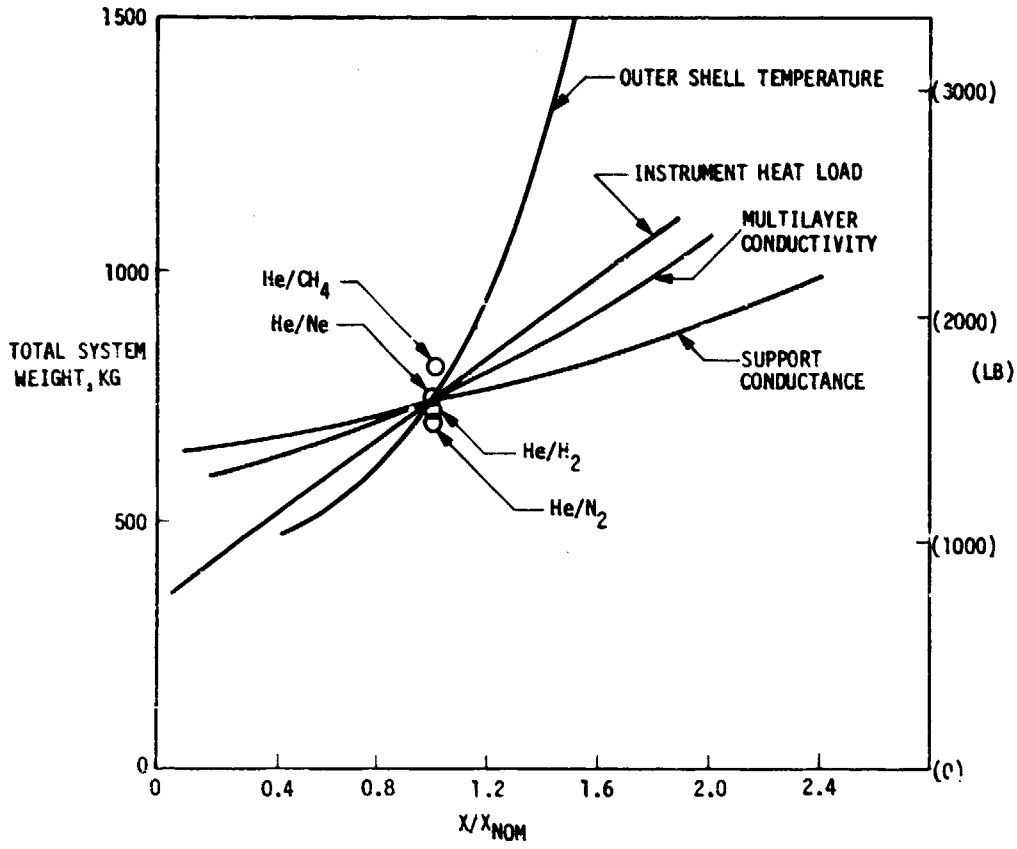

Fig. 3.1 Guard Cryogen Trade Studies

3.2 SELECTION OF TANK CONFIGURATION CANDIDATES

A trade study was performed to determine which tank configuration was most suitable for use in the single stage LHe dewar for maintaining the 1 m (39.4 in) diam. x 2 m (78.7 in) long instrument at $\leq$ 2K ($\leq$ 3.6R) for three years. General criteria normally used in selections of this type include weight, moments of inertia constraints, limitations on C.G. shift, geometric constraints, technical risk, cost and schedule.

Criteria	Contract Requirements
Weight	< 2000 kg (4409 ibs), total system including the instrument
MOI constraints	None specified
Limitations on C.G. shift	None specified
Geometric constraints	Fit into the Shuttle Cargo Bay, 4.5 m (15 ft) diam. x 18 m (60 ft) long
Technical risk, cost and schedule	Development program not to last longer than 10 years

As can be seen from the table, the contract requirements provides no sigificant constraints on any of these criteria.

The tank configurations considered in the single-stage dewar study are shown in Fig. 3.2. The tank size shown is based on a very preliminary estimate of the total heat load into the helium using three vapor cooled shields.

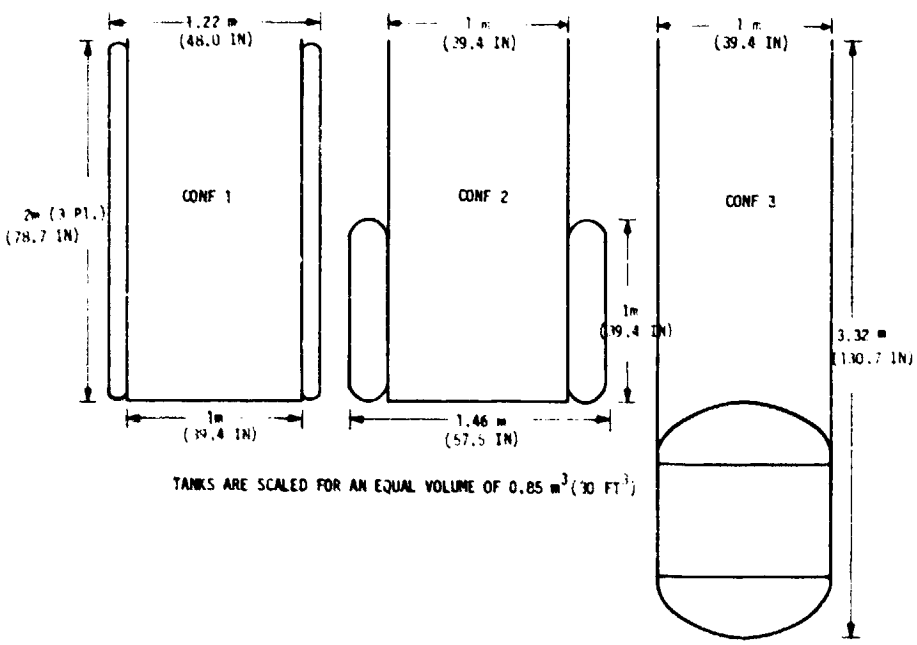

Fig. 3.2 Candidate Tank Configurations for Single Stage He Dewar

	mW	
Instrument Joule heating	10	Given
Aperture heating	1	Given
Wires (400 SS coax, 250 manganin)	4	Calculated
MLI (varied with surface area)	5*	Calculated
Supports (PODS)	1	Calculated
Fill line	1*	Calculated
25% margin (including ullage)	5	Calculated
	27 (0.092 Btu/hr)	

*Ratioed from data in Ref. 3.2

The candidate configurations consist of 1) a toroidal tank that extends the full 2 m (78.7 in) length of the instrument; a conduction shield closes off one end of the instrument cavity; the other end is opened to space after achieving orbit; 2) a toroidal tank that extends halfway, 1 m (39.4 in), along the cylinder with a conduction shield extending the other half of the cylinder; one end is also closed off with a conduction shield as in configuration 1; 3) a cylindrical tank with $\sqrt{2}$ /1 ellipsoidal ends and a 2 m (78.7 in) long by 1 m (39.4 in) diameter conduction shield extending around the instrument cavity.

Table 3.1 provides the criteria used to rank the three tank configurations. All of the factors affecting system weight are summarized in Table 3.2. Configuration 3 is the lightest weight system followed by configurations 1 and 2. Although the instrument/C.G. load path will decrease this weight advantage for configuration 3, it is doubtful it would be large enough to change these

Table 3.1 CRITERIA FOR RANKING TANK CONFIGURATIONS (SINGLE STAGE DEWAR)

Criteria	Configuration 1	2	3
Objective Criteria			
Delta weight, kg (lb) (see Table 3.2)	36(79)	42(93)	0
External (T_H) surface area, normalized	1.0	1.09	1.12
Tank surface area, normalized	3.3	1.9	1.0
Spacecraft dimension, normalized			
• Length	1.0	1.0	1.66
• Diameter	1.22	1.46	1.0
Subjective Criteria(1)			
Tank manufacturing complexity	3	2	1
Vacuum shell manufacturing complexity	1	2	1
Fill time based on mass to be cooled	3	2	1

(1) 1 is most desirable ranking

Table 3.2 PRELIMINARY WEIGHT COMPARISON FOR TANK CONFIGURATIONS

Item	Configuration 1	2	3
Tank(1)	142	111	69
Vacuum Jacket	221	240(2)	223
Conduction shield around instrument	1.1	5.4	17.8
Vapor-cooled shields (3) (t = 0.05 cm or .02 in)	49	53(2)	54.5
MLI	9.8	10.7(2)	11.0
Helium	103	112	115
Instrument CG/load path			(3)
Total Wt., kg (lb)	526(1160)	532(1173)	490(1080)
ΔWt., kg (lb)	36(79)	42(93)	0

(1) Includes 1.7% aluminum foam
(2) Weights ratioed from data in Ref. 3.2
(3) These weights will be higher for configuration 3 than either 1 or 2, but were not calculated due to lack of design detail.

preliminary weight rankings. Configurations 1 and 2 have a significant length advantage over configuration 3.

When considering these criteria plus the others listed, there was no clear cut choice between the three configurations. Configuration 3 is the lightest; on the other hand, configurations 1 and 2 are considerably shorter and the dewar CG will change less as the tank is drained; configuration 3 is judged to be the least complex design to manufacture and assemble. Due mainly to the lighter weight and lower manufacturing complexity, configuration 3 was selected over configurations 2 and 3. This selection of tank configuration 3 was made for representing the tank weight and envelope during the cryogen selection analysis. This choice should be re-examined when more detailed system requirements are defined.

The analyses performed in Section 3.1 narrowed the selection of the secondary cryogen to solid nitrogen or solid neon to go along with the primary superfluid helium tank. These same preliminary studies showed the secondary tank volume to be considerably smaller than the primary tank volume. For this reason a small toroidal, secondary cryogen tank (to minimize dewar length) plus an ellipsoidal LHe tank was selected for the dual stage cryogen selection analyses. Fig. 3.3 shows both single and dual stage tank layouts. Note the primary tank and conduction shield are supported off the secondary tank. The secondary tank is supported off the vacuum shell.

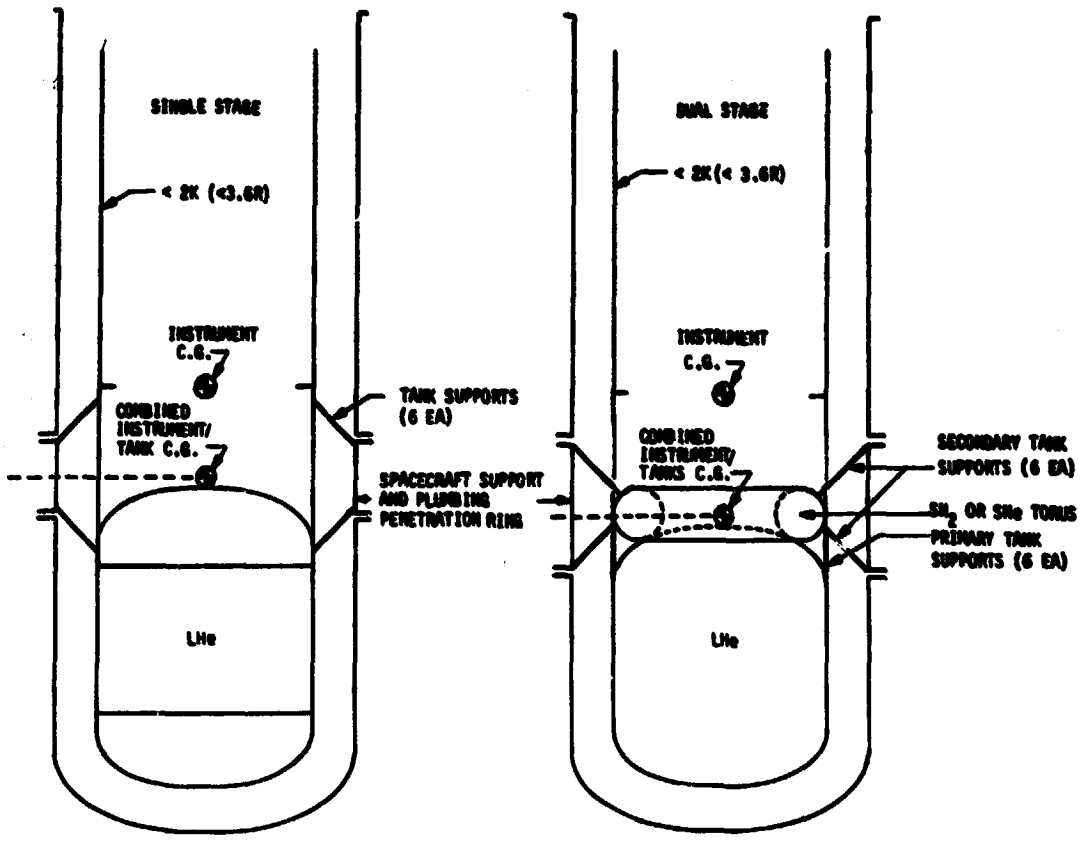

Fig. 3.3 Selected Tank Configurations for Use in the Cryogen Selection Analysis

3.3 SINGLE VS. DUAL STAGE TRADE STUDIES

These studies were performed using the CRYOP program described in Section 9. When these analyses were performed initially, an error in the modified vapor shield optimization subroutine caused the calculated heat rates to be too low. This error was discovered after the design of the selected single stage dewar was well advanced and the detailed thermal nodal model of the design showed higher heat rates than were calculated previously by CRYOP. Consequently, all these trade studies were rerun to see if the conclusions reached previously were still valid. They were, in most cases examined, but the selection of a

single stage dewar over a dual stage dewar was not as clear cut as shown previously by the incorrect analyses.

Using the corrected CRYOP program, the trade study was repeated for both single and dual stages using the tank configurations shown in Section 3.2 and the assumptions shown in Table 3.3. Parameters that were varied include the instrument heat load, warm boundary temperature, and number of vapor cooled shields.

Nominal case tabular outputs from the CRYOP program are shown in Table 3.4 (He), Table 3.5 (He/N_2) and Table 3.6 (He/Ne). The output includes the dewar length (minus the aperture cover), dewar diameter, design lifetime (including a 20% margin), optimum insulation thickness, location and temperature of the vapor cooled shields, parasitic heat load with and without vapor cooling, tank volume and a weight breakdown of the dewar (minus the aperture cover). The aperture cover length and weight were added in manually after the runs were completed.

Note that under "EXPERIMENT WT", 17.6 kg (39 lb) was added to 200 kg (441 lb) of experiment weight 218 kg (480 lb) total to account for the inner conduction shield extending up from the helium tank surrounding the 2 m (78.4 in) long instrument and providing a $\leq$ 2K ($\leq$ 3.6 R) boundary. The nominal values used for the cryogen selection studies are shown in Table 3.7.

Table 3.3 ASSUMPTIONS USED IN CRYOGEN SELECTION ANALYSIS

	SINGLE STAGE	DUAL STAGE	
		PRIMARY	SECONDARY
Cryogen	Helium	Helium	Nitrogen or Neon
Tank Configuration (Filled with 1.7% Aluminum Foam)	6061 Aluminum Cylinder, Ring Stiffened Plus $\sqrt{2}$/1 Ellipsoidal Ends	6061 Aluminum Cylinder, Ring Stiffened Plus $\sqrt{2}$/1 Ellipsoidal Ends	6061 Aluminum Torus
Vacuum Shell	6061 Aluminum Cylinder, Ring Stiffened Plus $\sqrt{2}$/1 Ellipsoidal Ends	6061 Aluminum Cylinder, Ring Stiffened Plus $\sqrt{2}$/1 Ellipsoidal Ends	
Supports(Vapor Cooled)	PODS, 6 EA.	PODS, 6 EA.	PODS, 6 EA.
Primary Conduction Shield Around Instrument	6063 Aluminum, 17.8 Kg (39 lb)	6063 Aluminum, 17.8 Kg (39 lb)	-
Vapor Cooled Shields, 0.05 cm (0.02 in) Thick	6063 Aluminum	6063 Aluminum	6063 Aluminum
Multilayer Insulation	Double Aluminized Mylar/Silk Net Spacers		
Aperture Cover	39 kg (86 lb) Weight 0.5 m (19.7 in) Length	39 kg (86 lb) Weight 0.5m (19.7 in) Length	
Plumbing (Vapor Cooled)	1 Fill, 1 Vent	1 Fill, 1 Vent	1 Fill, 1 Vent, 2 Coolant Lines
Wire Leads(Vapor Cooled)	400 Coax, 250 Manganin	400 Coax, 250 Manganin	
Supplemental Cooling (Radiators, Shadow Shields, Refrigerators)	No	No	

Table 3.4 CRYOP OUTPUT, 4½ DEWAR

OPTIMIZATION OF MLI THICKNESS

APES BASELINE COOLER, 0 INST=11, RU, 200 K SHELL, 5 AL VENT SHIELDS CASE 3

SYSTEM OUTER DIA= 94.28 IN, TOTAL LENGTH= 168.61 IN, TANK WALL= .19 IN
PRIMARY TANK LENGTH= 78.37 IN
DESIGN LIFETIME=1095. DAYS, SHELL TEMP= 200. K

CRYOGEN	TEMP. DES K	HOT BOUND-ARY TEMP,K	HT SUBL BTU/ LB	DENSITY LB/CU FT	SPEC HT BTU/LB-F	R OUT IN.	R IN IN.	VENT SHDS	PLB LINES
HELIUM	2.	200.	8.8	9.0	1.24	19.70	.88	5	2

MLI TYPE	COND.,BTU/ HR-FT-F	LAYERS PER INCH	DENSITY LB/CU FT	THICKNESS IN.	ACCELER. AXIAL	FACTOR TRANS	RAD MLI IN.
MLI/SILK NET	.788-04	37.	1.92	6.28	-.0	-.00	1.00

PODS SUPPORT SYSTEM

PRIM. VC SHIELD LOCATIONS (X/TOTAL)	.12	.25	.48	.57	.78
PRIM. VC SHIELD TEMPERATURES (K)	21.7	39.7	65.4	101.1	146.6

	HEAT LOAD (WATTS) PRIMARY	SECONDARY	RADIATOR
EXPERIMENT	.011	.000	
NO VENT COOLING, TOTAL	.486	.000	
WITH VENT COOLING, TOTAL	.025	.000	.000
INSULATION	.014	-.000	.000
SUPPORTS	.004	-.000	.000
LEAD WIRES	.005	-.000	.000
PLUMBING	.002	-.000	.000
HEAT REMOVAL, TOTAL		-.000	-.000
INSULATION		.000	-.000
SUPPORTS		.000	-.000
LEAD WIRES		.000	-.000
PLUMBING		.000	-.000
HT REMOVAL BY VENT GAS		-.000	-.000
TOTAL	.036	.000	.000

CALCULATED LIFETIME (DAYS)	1095.05	.00	
TANK VOLUME (CU FT)	48.6431	.0000	
CRYOGEN WT (LB)	448.22	.00	
DRY TANK WT (LB)	229.89	.00	
INSULATION WT (LB)	163.55	.00	.00
VENT SHIELD WT (LB)	229.85	.00	
SHIELD WT (LB)		.00	.00
VACUUM TANK WT (LB)			394.15
MOUNTING PLATE WT (LB)			.00
MISC. WT (LB)			102.06
SUPPORT WT (LB)			3.19

EXPERIMENT WT (LB)	400.00
TOTAL DRY WT (LB)	1682.71
TOTAL WEIGHT WITH CRYOGENS (LB)	2842.93
CYLINDRICAL VOLUME (CU FT)	221.736

Table 3.5 CRYOP OUTPUT, He/N2 DEWAR

OPTIMIZATION OF MLI THICKNESS

APES-1 HE/N2 COOLER, 0 INST=11. NO. 200 K SHELL, 1 HE SHD,3 N2 SHDS CASE 1

SYSTEM OUTER DIA= 94.00 IN, TOTAL LENGTH= 133.46 IN, TANK WALL= .19 IN
PRIMARY TANK LENGTH= 40.31 IN
SECONDARY TANK LENGTH= 4.33 IN

DESIGN LIFETIME=1095. DAYS, SHELL TEMP= 200. K

CRYOGEN	TEMP, DEG K	HOT BOUNDARY TEMP,K	HT SUBL BTU/ LB	DENSITY LB/CU FT	SPEC HT BTU/LB-F	R OUT IN.	R IN IN.	VENT SHDS	PLG LINES
HELIUM	2.	43.	8.4	9.8	1.24	19.73	.03	1	2
N2	43.	200.	108.0	55.8	.25	21.59	.01	3	2

MLI TYPE	COND.,BTU/ HR-FT-F	LAYERS PER INCH	DENSITY LB/CU FT	THICKNESS IN.	ACCELER. FACTOR AXIAL	TRANS	RAD PLT IN.
MLI/SILK NET	.102-05	37.	1.92	1.75	-.0	-.00	1.00
MLI/SILK NET	.027-05	37.	1.92	4.25			

FCOS SUPPORT SYSTEM

PRIM. VC SHIELD LOCATIONS (X/TOTAL) .26
PRIM. VC SHIELD TEMPERATURES (K) 13.6
SEC. VC SHIELD LOCATIONS (X/TOTAL) .25 .50 .75
SEC. VC SHIELD TEMPERATURES (K) 78.8 118.9 160.3

	HEAT LOAD (WATTS) PRIMARY	SECONDARY	RADIATOR
EXPERIMENT	.011	.000	
NO VENT COOLING, TOTAL	.029	.945	
WITH VENT COOLING, TOTAL	.007	.253	.000
INSULATION	.005	.084	.000
SUPPORTS	.001	.145	.000
LEAD WIRES	.001	.019	.000
PLUMBING	.001	.005	.000
HEAT REMOVAL, TOTAL		-.196	-.000
INSULATION		-.025	-.000
SUPPORTS		-.029	-.000
LEAD WIRES		-.003	-.000
PLUMBING		-.003	-.000
HT REMOVAL BY VENT GAS		-.135	-.000
TOTAL	.018	.057	.000
CALCULATED LIFETIME (DAYS)	1093.19	1093.56	
TANK VOLUME (CU FT)	24.4676	1.0373	
CRYOGEN WT (LB)	221.43	57.94	
DPT TANK WT (LB)	121.10	9.13	
INSULATION WT (LB)	32.63	91.69	.00
VENT SHIELD WT (LB)	32.75	113.70	
SHIELD WT (LB)		37.90	.00
VACUUM TANK WT (LB)			299.72
MOUNTING PLATE WT (LB)			.00
MISC. WT (LB)			74.08
SUPPORT WT (LB)			2.15
EXPERIMENT WT (LB)	400.00		
TOTAL DRY WT (LB)	1294.05		
TOTAL WEIGHT WITH CRYOGENS (LB)	1573.32		
CYLINDRICAL VOLUME (CU FT)	188.315		

Table 3.6 CRYOP OUTPUT, He/Ne DEWAR

OPTIMIZATION OF MLI THICKNESS

AMES-6 HE/NE COOLER, Q INST=11. MW, 200 K SHELL, 0 HE SHD.1 NF SHDS CASE 6

SYSTEM OUTER DIA= 54.98 IN, TOTAL LENGTH= 132.87 IN, TANK WALL= .18 IN
PRIMARY TANK LENGTH= 41.75 IN
SECONDARY TANK LENGTH= 7.16 IN

DESIGN LIFETIME=1095. DAYS, SHELL TEMP= 200. K

CRYOGEN	TEMP, DEG K	MCT BOUNDARY TEMP,K	HT SUBL BTU/ LB	DENSITY LB/CU FT	SPEC HT BTU/LB-F	R OUT IN.	R IN IN.	VENT SHDS	PLG LINES
HELIUM	2.	14.	8.8	9.0	1.24	19.70	.00	0	2
NEON	14.	200.	43.0	81.0	.25	20.55	.60	3	2

MLI TYPE	COND.,BTU/ HR-FT-F	LAYERS PER INCH	DENSITY LB/CU FT	THICKNESS IN.	ACCELER. AXIAL	FACTOR TRANS	RAD MLI IN.
MLI/SILK NET	.354-06	37.	1.92	.75	-.0	-.00	1.00
MLI/SILK NET	.747-06	37.	1.92	5.50			

PODS SUPPORT SYSTEM

SEC. VC SHIELD LOCATIONS (X/TOTAL)	.16	.37	.65
SEC. VC SHIELD TEMPERATURES (K)	39.6	78.2	133.1

	HEAT LOAD (WATTS) PRIMARY	SECONDARY	RADIATOR
EXPERIMENT	.012	.000	
NO VENT COOLING, TOTAL	.006	.493	
WITH VENT COOLING, TOTAL	.006	.138	.000
INSULATION	.004	.039	.000
SUPPORTS	.001	.093	.000
LEAD WIRES	.000	.011	.000
PLUMBING	.001	.003	.000
HEAT REMOVAL, TOTAL		-.057	-.000
INSULATION		-.004	-.000
SUPPORTS		-.001	-.000
LEAD WIRES		-.000	-.000
PLUMBING		-.001	-.000
HT REMOVAL BY VENT GAS		-.052	-.000
TOTAL	.017	.080	.000

CALCULATED LIFETIME (DAYS)	1095.00	1097.72	
TANK VOLUME (CU FT)	22.8715	2.4854	
CRYOGEN WT (LB)	296.99	201.32	
DRY TANK WT (LB)	113.92	21.87	
INSULATION WT (LB)	13.42	115.75	.00
VENT SHIELD WT (LB)	.00	110.91	
SHIELD WT (LB)		36.97	.00
VACUUM TANK WT (LB)			299.77
MOUNTING PLATE WT (LB)			.00
MISC. WT (LB)			71.51
SUPPORT WT (LB)			2.46

EXPERIMENT WT (LB)	480.00
TOTAL DRY WT (LB)	1266.58
TOTAL WEIGHT WITH CRYOGENS (LB)	1674.89
CYLINDRICAL VOLUME (CU FT)	182.529

Table 3.7 NOMINAL VALUES USED IN THE CRYOGEN SELECTION ANALYSIS

	Single Stage	Dual Stage	
		Primary	Secondary
Vacuum Shell Temperature, K (R)	200(360)	200(360)	
No. of Vapor Cooled Shields	5	0 He/Ne 1 He/N_2 (Between Primary and Secondary Tank)	3 (Between Secondary Tank and Vacuum Shell)
Support Conductance (Vapor Cooled)	6 ea. PODS	6 ea. PODS	6 ea. PODS
Instrument Heat Load, mW (continuous)	11	11	

3.3.1 Single Stage Results

The study results for the single stage helium dewar are shown in Figs. 3.4 and 3.5. The nominal case value shown by a square was varied, one parameter at a time, to examine the sensitivity of the system to a change in different parameters. Note in Fig. 3.5 the launch weight is relatively insensitive to changes in instrument heat load (7% increase for a doubled heat load). As instrument heat loads are increased, parasitic heat loads are reduced due to greater vapor cooling. Launch weight is optimum at 5 vapor cooled shields. Changes in warm boundary temperature had the largest effect on launch system weight, i.e., -17% at 150K and -31% at 100K vacuum shell temperature. The

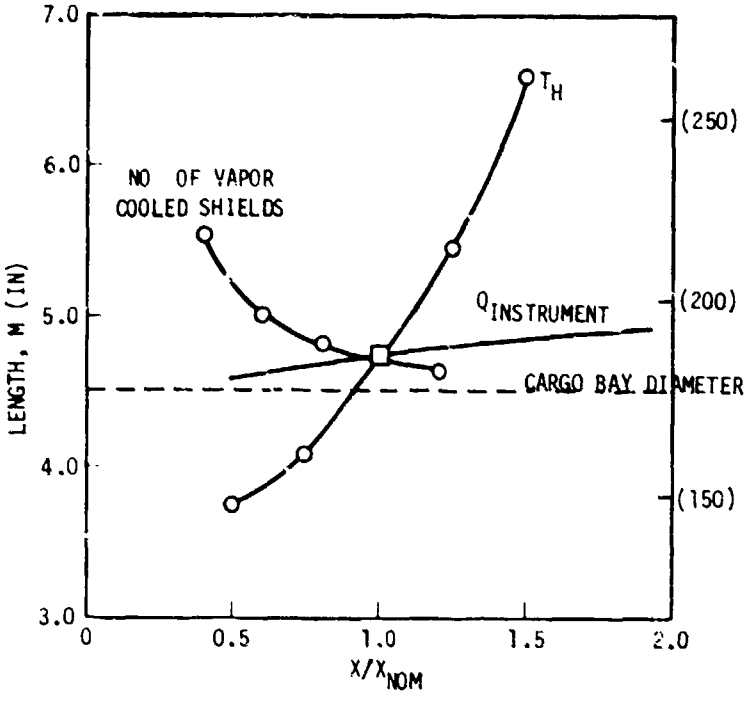

Fig. 3.4 Single-Stage Helium Dewar Length Sensitivities

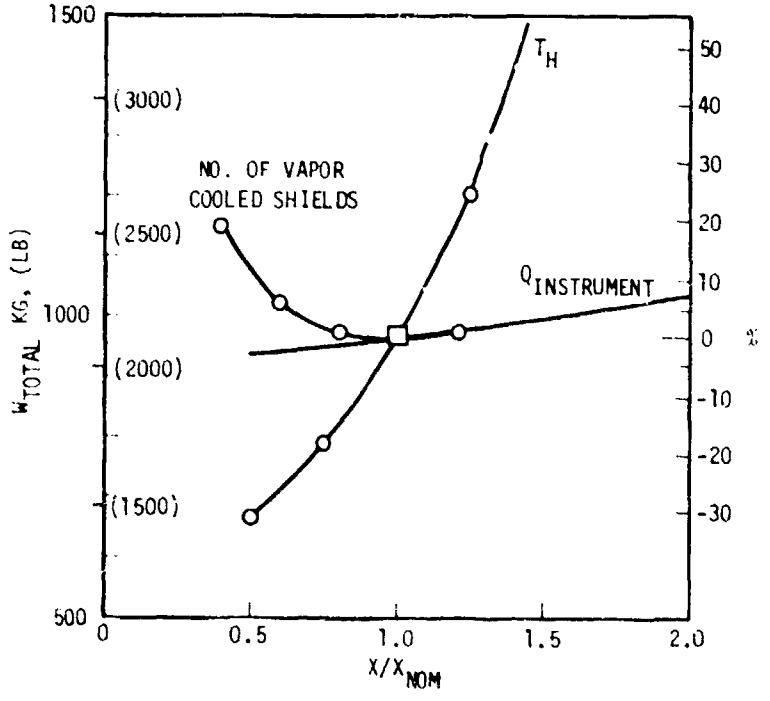

Fig. 3.5 Single Stage Helium Dewar Weight Sensitivities

added weight of shadow shields, radiators, etc., required to obtain these lower temperatures was not included in Fig. 3.5.

Fig. 3.4 shows the effect of parameter changes on the total dewar length including the aperture cover. Note the nominal length will not fit into the cargo bay, crosswise. Lengthwise, of course, there is no problem.

3.3.2 Dual Stage Results

The study results for the dual stage helium/nitrogen dewar are shown in Figs. 3.6 and 3.7; Figs. 3.8 and 3.9 summarize the helium/neon dewar results. The data for both dual-stage dewars follows the same trends. The launch weight is near optimum when three vapor-cooled shields are used for either dual stage candidate. The helium/nitrogen dewar's launch weight is less than the helium/neon dewar above T_H = 178K (320R). Between T_H = 178K (320R) and 110K (198R), the helium/neon dewar is the lightest. Below T_H = 152K (274R) for nitrogen and T_H = 110K (198R) for neon, the weight of the secondary cryogen went to zero showing the single stage helium dewar is optimum in this temperature regime.

Note in Fig. 3.9 the He/Ne launch weight is slightly more sensitive to doubling the instrument heat load (11%) than the single stage system (7%). When the instrument heat load was doubled for the He/N_2 case, the nitrogen weight went to zero, indicating a single stage helium system was optimum for this case. Both dual stage dewar weights were sensitive to warm boundary temperature changes, but not as sensitive as the single stage dewar.

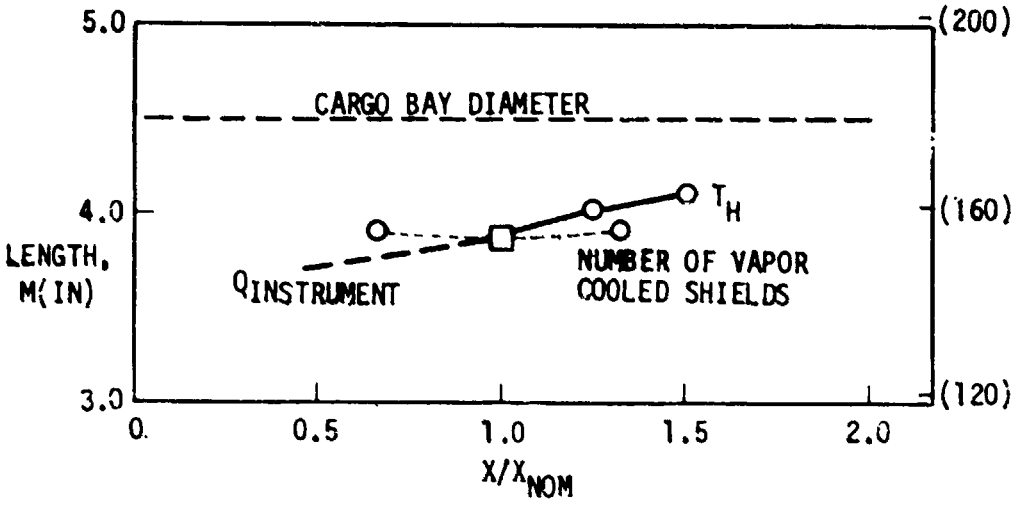

Fig. 3.6 Dual-Stage Helium/Nitrogen Dewar Length Sensitivities

NOTE: 1) FOR Q_{INST} = 22 MW (0.08 Btu/Hr) SINGLE STATE He DEWAR IS OPTIMUM

2) BELOW T_H = 150K (270R) SINGLE STAGE HELIUM DEWAR IS OPTIMUM

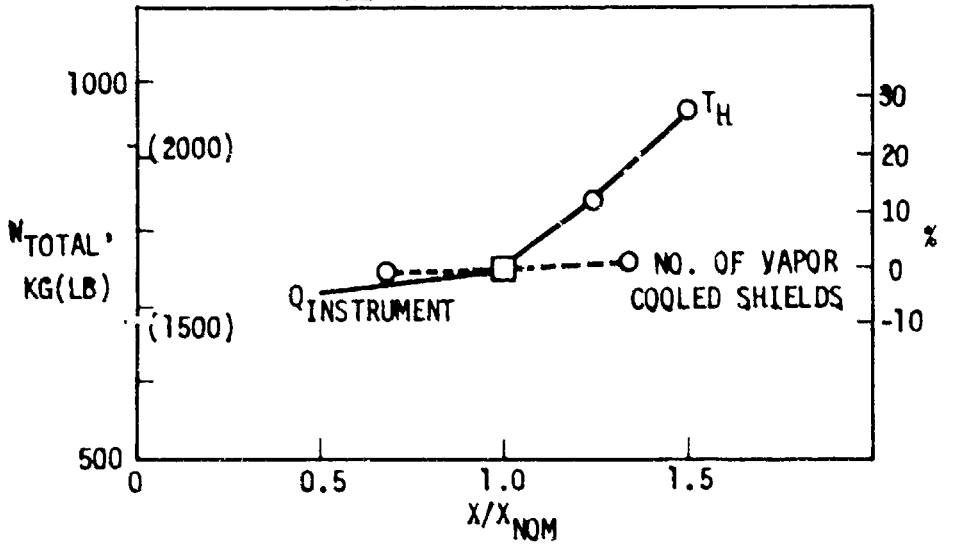

Fig. 3.7 Dual-Stage Helium/Nitrogen Dewar Weight Sensitivities

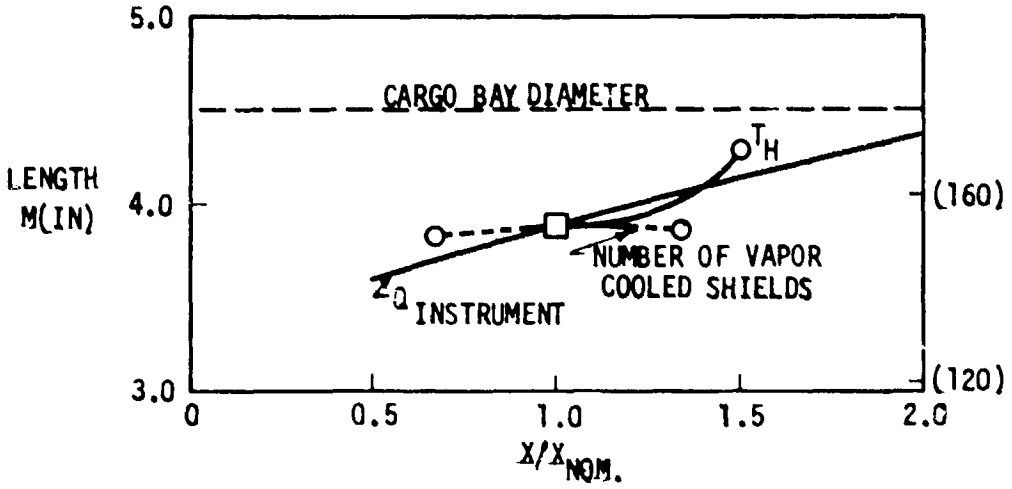

Fig. 3.8 Dual-Stage Helium/Neon Dewar Length Sensitivities

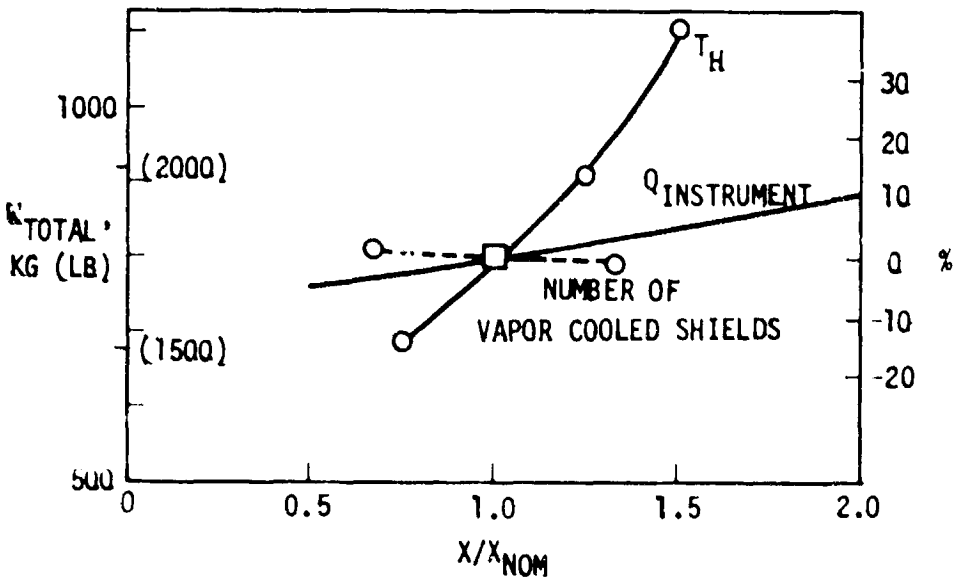

Fig. 3.9 Dual-Stage Helium/Neon Dewar Weight Sensitivities

Figs. 3.6 and 3.8 show the effect of parameter changes on the total dewar length including the aperture cover. Note the nominal length will fit into the cargo bay, crosswise, if it is desired to mount it in that orientation.

3.4 SELECTED CRYOGEN

Using the data developed in Section 3.3, selection criteria were prepared for the single and dual stage dewars. Fig. 3.10 provides a comparison of dewar lengths including the aperture cover; Fig. 3.11 provides a weight comparison of the dewars. Additional selection criteria are provided in Table 3.8.

Based on these data, the single-stage helium dewar was selected for the following reasons.

The average orbit warm boundary temperature will probably be less than 200K (360R) judging by the predicted temperatures for programs of a similar nature, i.e., the superfluid helium dewar on IRAS [3.2] and the neon/methane dewar on Teal Ruby [3.3]. These orbit temperatures are achieved using thermal control coatings, insulation, radiators and active orientation systems. At these temperatures of 170K (306R) and 150K (270R) respectively, weight penalties incurred using a single-stage helium dewar are on the order of 17% to 15% when compared to the lightest helium/neon dewar. [At 200K (360R), the weight penalty is 28% when compared to the lightest helium/nitrogen dewar.] This weight penalty is not considered excessive when balanced against the lower cost and lower complexity of the single stage design as discussed in Section 6.3. (The dual-stage dewar requires an additional tank for the neon or nitrogen, low heat leak tank supports, fill line, vent line, coolant inlet

and exit lines and associated plumbing components. The GSE also requires a neon or nitrogen loading module.)

Secondly, the single-stage helium dewar weight is less sensitive to changes in the instrument heat rate as shown in Table 3.8.

Third, although the dual-stage dewars by themselves are shorter than the single-stage dewar and will fit into the Shuttle Cargo Bay crosswise as well as lengthwise, when a spacecraft is added to the dewars it is highly likely both the single- and dual-stage dewars can only fit into the Shuttle Bay lengthwise.

Finally, the single-stage dewar weight of 966 kg (2130 lb) is considerably lower than the 2000 kg (4409 lb) contract requirement, providing more than adequate margin for the weight growth that normally occurs as a design matures.

Table 3.8 CRITERIA FOR CRYOGEN SELECTION

Selection Criteria	Dewar Type		
	He	He/Ne	He/N_2
Lightest-weight dewar when T_H is:	< 110K (198R)	110 to 178K (198 to 320R)	> 178K (320R)
Nominal dewar launch weight*, kg (lb)	966 (2130)	799 (1761)	753 (1660)
Shortest length dewar when T_H is:	< 110K (198R)	110 to 280K (198 to 504R)	> 280K (504R)
Fits into Shuttle Bay			
• Crosswise	NO	YES	YES
• Lengthwise	YES	YES	YES
% change in dewar weight for doubled instrument heat rate, 22 mW (0.08 Btu/hr)	+7	+11	Single-stage He dewar is optimum for this case
Cost and complexity of analysis, design, manufacturing, cryogen loading, test			
• Dewar	1**	2	2
• GSE	1	2	2

* T_H = 200K (360R)
** 1 is the most desirable

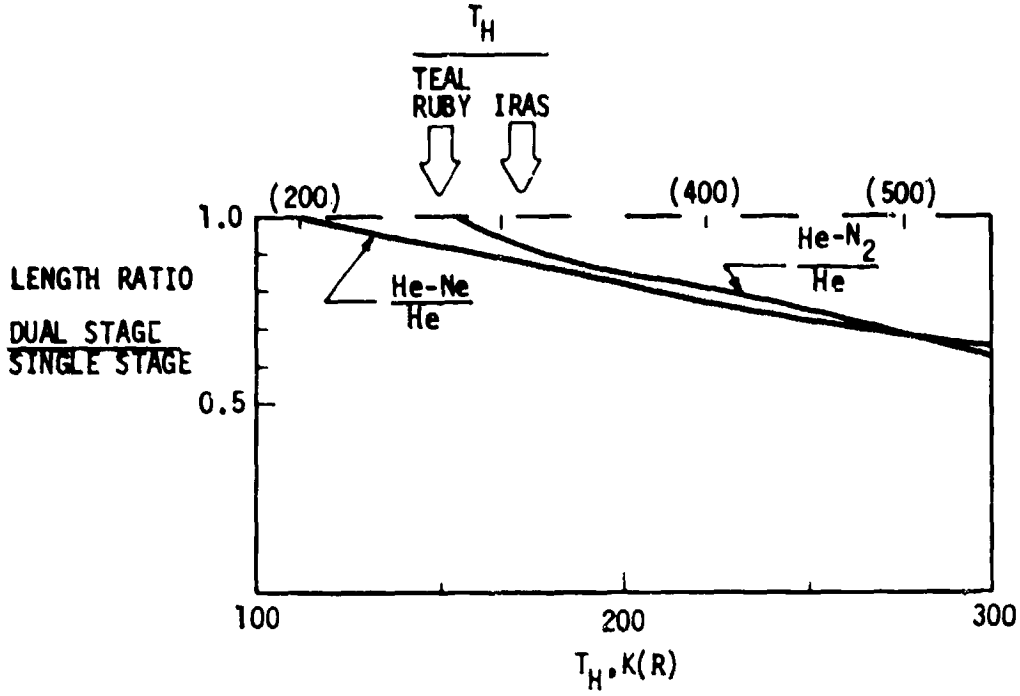

Fig. 3.10 Dewar Length Comparison

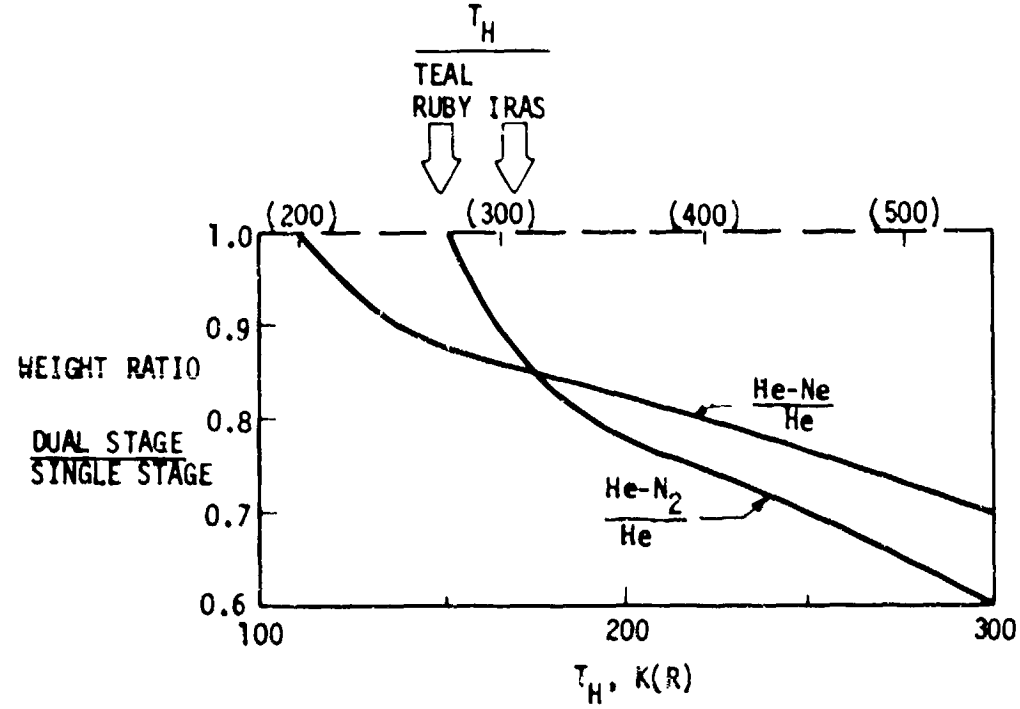

Fig. 3.11 Dewar Weight Comparison

Section 4

SUPPORT SELECTION ANALYSIS

4.1 SUPPORT SYSTEM SCREENING

For state-of-the-art helium dewar flight systems, the support heat leak can be the major parasitic heat load to the cryogen. For example, the heat leak breakdown for the IRAS program [4.1] shows the tension bands constitute two thirds of the parasitic heat load. (Note the shift in heat load for the PODS support system selected in this study as shown later in Fig. 5.30.)

Parasitic Heat Leak, Percent	IRAS	PODS Dewar
Multilayer insulation	14[1]	30[3]
Supports[2]	67 (Tension Band)	22 (PODS)
Plumbing[2]	2	4
Wire leads[2]	17	44
	100	100

1. Three vapor-cooled shields
2. Vapor-cooled
3. Five vapor-cooled shields

If this support heat leak can be lowered an order of magnitude or more, dewar weight can be decreased substantially or dewar lifetime extended significantly.

An extensive literature search was performed to define the state of the art in helium support systems and uncover any advanced support concepts that are under development. The unclassified literature surveyed included:

- Advances in Cryogenic Engineering (Vols. 1-25)
- National Technical Information Service (1964 to date)
- Science Abstracts: Physics, Electrical and Electronic, Engineering and Computers and Control (1970 to date)
- Defense Technical Information Center Data Base (1970 to date)
- NASA Research Facilities Data Base (1970 to date)

and was performed using the DIALOG literature search program.

The most extensive research work on alternate support concepts was performed by Lockheed [4.2] on 12 different concepts. The concepts include monocoques (both passive and pyrotechnically detached), honeycomb cone, vapor-cooled cone, fiberglass struts, and three active disconnect struts (torque tube, ball and clamp, and retracting wedge). Six concepts were fabricated and tested thermally. The selected concept, a fiberglass support tube, also had extensive structural tests performed at cryogenic temperature [4.3].

Most of the helium dewar flight systems use some version of the fiberglass tension band support as shown in Table 4.1. The Stanford Relativity Experiment [4.4] has a combination of fiberglass bands and titanium support tubes. The titanium tubes are actively retracted in orbit. GIRL uses compound fiberglass bands to take advantage of the higher strengths of fiberglass at low temperature and the contact resistance of multiple band parts. No new advanced support concepts were uncovered in the literature survey that had not already been considered by Lockheed previously.

In 1978, Lockheed started a research program to develop a support system with a thermal conductance value at least an order of magnitude lower than present

Table 4.1 COMPARISON OF STATE-OF-THE-ART HELIUM SUPPORT SYSTEMS

System Description*	Tank Volume, Liters (ft3)	Helium Mass, Kg (lb)	Instrument Heat Load, watt (Btu/hr)	Total Heat Load, watt (Btu/hr)	Support General Class	System Description	Mass Supported, kg (lb)	Minimum Resonance (Hz)	A/L, cm (in)	KA/L, W/K (Btu/hr R)
IRAS (1 yr)	466 (16.5)	70 (154)	9 (0.03)	37 (0.13)	Point Support Tension	9 F.G. Bands/Supports both tank & vc shield	309 (681)	21	0.388 (0.15)	1.58 E-3 (0.01)
LST IR Expmt ADL (Study) (1 yr)	517 (18.3)	71 (157)	42 (0.14)	53 (0.18)	Point Support Tension/Compr.	6 F.G. tube pairs to form 3 truss at one end. 3 F.G. bands in tension at other end.	217 (478)			
Stanford Relativity Expmt (Study) (1 yr)		135 (300)	31 (0.11)	Orbit: 81 (0.28) Launch: 6400 (22.00)	Point Support Disconnect	F.G. bands (orbital). Retractable titanium tubes for launch.	340 (750)			
Helium Test Program for IRAS (11 mo)	590 (20.8)	86 (190)	50 (0.17)	100 (0.34)	Point Support Disconnect	6 filament wound F.G. bands. Retractable supports for launch.				
CLIR (Phase I) Study (30 day)	701 (24.8)	80 (176)	8600 (29.00)	415 (1.4)	Continuous Tension/ Compression	Continuous F.G. tube	140 (309)	25.4	0.32 (0.13)	1.39 E-3 (0.009)
GIRL	300 (10.6)	35 (77)	442 (151.0)	522 (1.8)	Point Support Tension	16 F.G. chains (glass fiber composite)	150 (331)			
CHRESUS (30 day)		75 (165)		89 (0.3)	Point Support Tension	24 R-glass fiber reinforced plastic containing 75% glass			1.52 (0.6)	8.36 E-3 (0.05)
Apollo LEM (5 day)	175 (6.2)	22 (48)		2340 (8.0)	Point Support Compression	Foamed fiberglass pads				
Apollo LEM Ground Service Tank	670 (23.7)	84 (185)		322 (1.1)	Point Support Compression					
FOOS Dewar**	1000 (35.3)	137 (302)	11 (0.04)	24.5 (0.08)	Point Support Disconnect	12 ea FOOS, cold end only	431 (950)	35 Launch 20 Orbit		1.1 E-3 (0.007) Launch 7 E-5 (5 E-4) Orbit

*Hardware Program Unless Annotated (Study)

**The selected system from this study is shown for comparison purposes.

state-of-the-art support systems. Hundreds of different concepts were examined of the generic types summarized in Table 4.2. Screening criteria used (updated for this program) are shown in Table 4.3. From this screening, one support concept was selected for development. This system, the passive orbital disconnect strut (PODS), was analyzed, designed, fabricated, structurally tested, and is currently under thermal test. The PODS system is the first candidate to be selected for this program.

The contract specifies a minimum of two advanced support system concepts shall be analyzed. Consequently, since no promising new support system concepts were uncovered in the literature survey, the second best of the support systems developed from the screening analysis was selected. This concept, the folded tube strut, is a combination of three support system concepts listed in Table 4.2: the point support, the large folded tube support and the alternate load path support. Details of the two candidate support system concepts plus a reference state-of-the-art system follows.

4.1.1 Concept No. 1 - Passive Orbital Disconnect Strut (PODS)

The concept is a modified version of a developed and qualified fiberglass strut system. The design combines the desirable features of a thermal disconnect in orbit with the high reliability of a completely passive design.

The portion of the point support strut design that makes it unique is shown in Fig. 4.1. The gold-coated Invar stem is suspended inside the gold-coated Invar body by prestressed S-glass filaments. In low-g or under specified load conditions in 1-g, heat transfer occurs in vacuum between the gold-coated stem and body by radiation and by conduction along the S-glass strands.

Table 4.2 DEMONSTRATED* AND ADVANCED SUPPORT CONCEPTS EXAMINED

Tension	Compression/Tension	Disconnect
High-strength steel wires	Fiberglass/epoxy monocoque*	Differential temperature expansion
S-glass/epoxy*	Fiberglass/epoxy honeycomb cylinders	Mechanical (electrical, pyrotechnic, pneumatic)
Kevlar 49	Dusted plates	Piezoelectric expansion
Bands*	Fiberglass pads*	Sublimation
Chains or compound bands*	Point supports*	Magnetic (active feedback loop)
	Folded tube*	Cut filaments
		Alternate load path (PODS)
		NiTi memory alloy

Table 4.3 CRITERIA FOR SUPPORT SYSTEM SELECTION

- Minimum parasitic heat leak on ground and in orbit for 3-year lifetime
- Minimum weight
- Minimum cost
- Resonance > 35 Hz during launch and > 20 Hz in orbit
- Passive design
- Can be demonstrated thermally in one-G qualification tests
- Applicable to different tank sizes, weights and shapes
- Suitable for use in Shuttle launch and abort modes
- Orbit heat rates independent of launch loads
- Support configuration to simplify MLI installation and minimize thermal degradation of MLI
- Support vapor-cooled shields

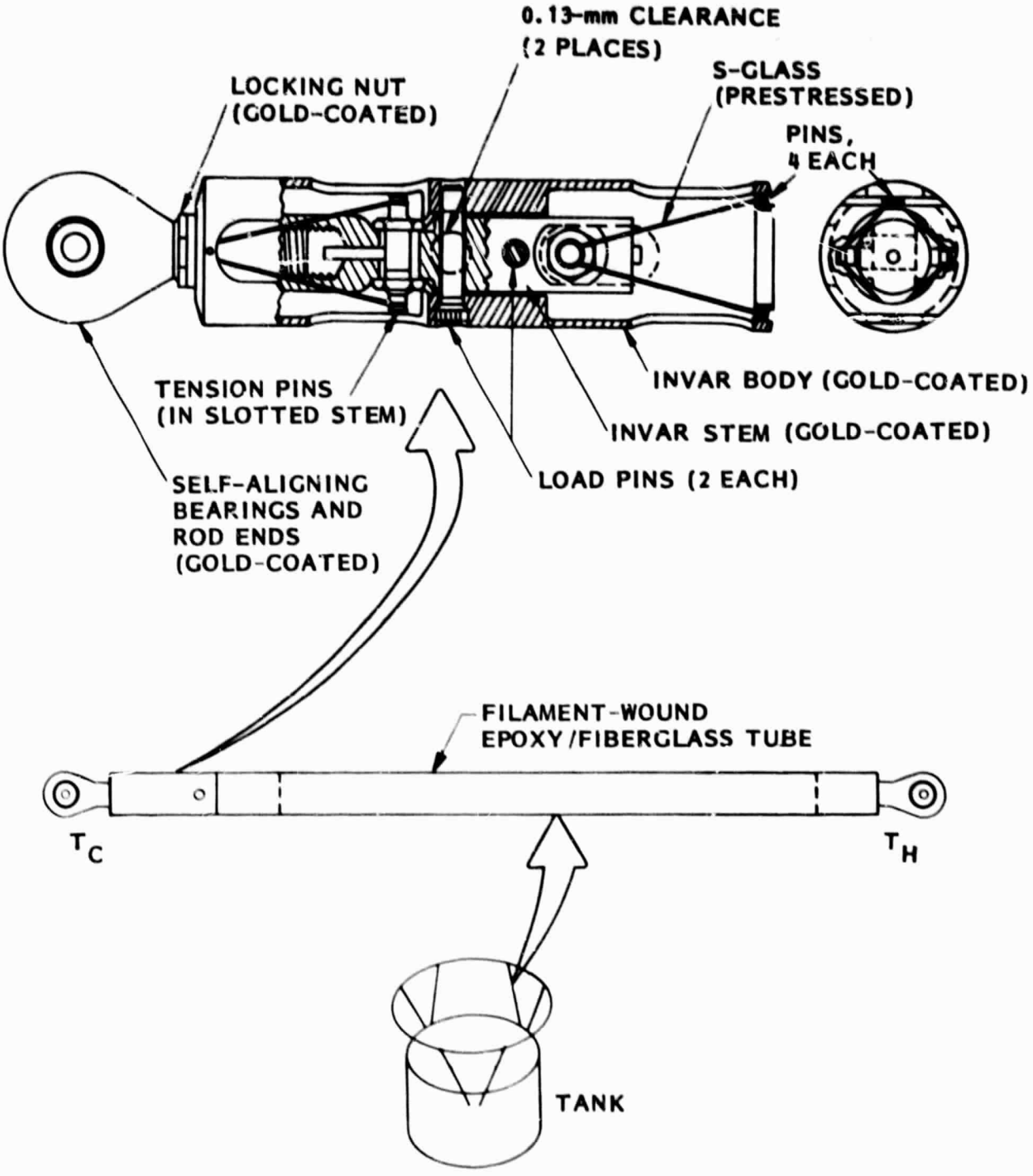

Fig. 4.1 Passive Orbital Disconnect Strut (PODS) System, PODS at Cold End Only

Under the high-g load conditions of launch, the S-glass filaments stretch elastically to the point where the stem holes bottom out against the two metal load pins. The high loads are transmitted through the pins until orbit is achieved. Once the load is removed, the Invar stem recenters itself inside the body and the load pins no longer touch the stem. This passive orbital disconnect support (PODS) concept greatly reduces the strut heat leak in orbit, yet is designed to handle the high structural loads of launch. The strut performance can be tailored separately for the launch loads (sizing of fiberglass tube and load pins) and desired orbit resonance (length and area of S-glass filaments). The parts required for a PODS strut at both the warm and cold ends are shown in Fig. 4.2. The design that was selected for this program (based on analyses described later) uses the PODS mechanism only at the cold end of the strut.

4.1.2 Concept No. 2 -Folded Tube Strut (FTS)

The FTS concept consists of 3 concentric, folded fiberglass tubes connected together to form a single strut as shown in Fig. 4.3. During launch, tube No. 1 is designed to take the launch loads at a resonance of 35 Hz. The loads are transmitted through the wedge-shaped Invar ring shown (due to elastic strains in fiberglass tubes 2 and 3). In orbit, the wedge disconnects passively when the load is removed; the fiberglass conduction path length is approximately tripled while the strut resonance drops to 20 Hz.

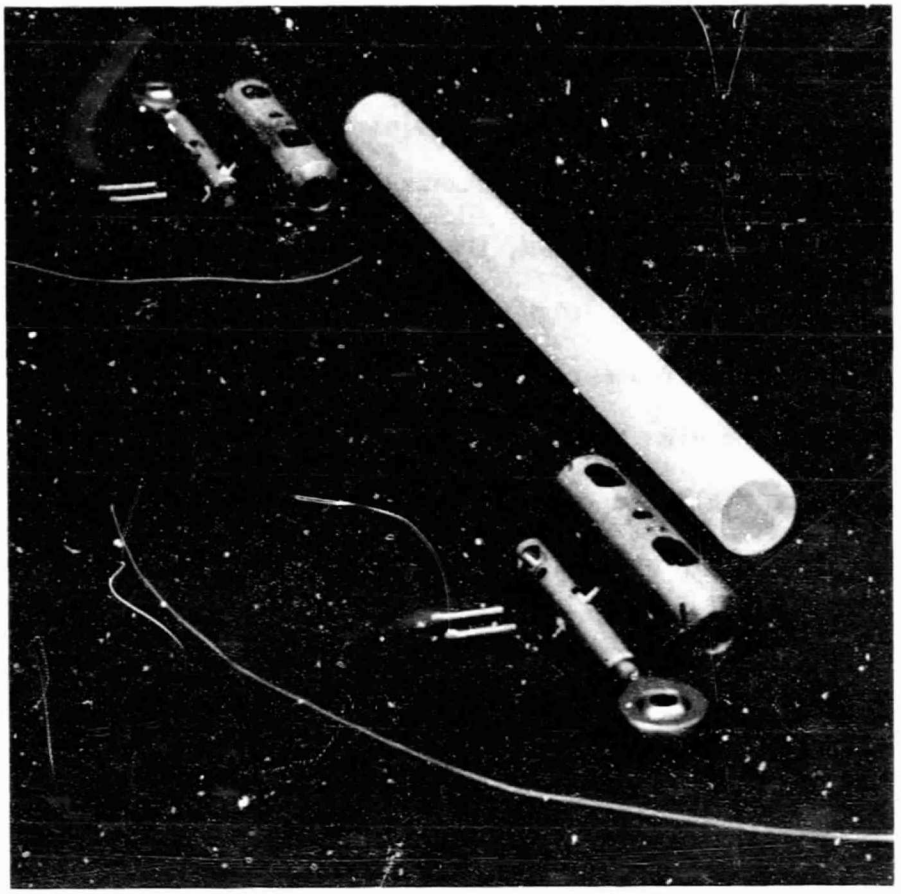

ORIGINAL PAGE
BLACK AND WHITE PHOTOGRAPH

Fig. 4.2 Exploded View of PODS Support (PODS Both Ends)

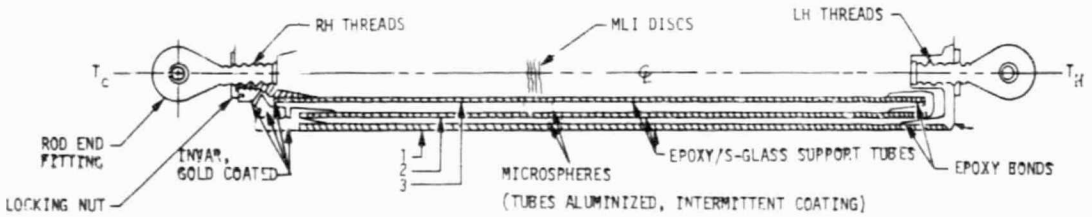

TUBE 1. DESIGNED FOR LAUNCH, ABORT LOADS AND RESONANCE
TUBES 1, 2, 3 DESIGNED FOR ORBIT RESONANCE AND MIN Q

Fig. 4.3 Folded Tube Strut (FTS) Concept

4.1.3 Reference-State-of-the-Art Tension Band Support System

In order to determine the potential performance improvement possible with advanced support concepts 1 and 2, a reference state-of-the-art support system was selected so comparative analyses can be made. As shown previously in Table 4.1, the tension band support is used on several helium flight dewars and represents one of the most advanced systems currently in use. A typical support system is shown in Fig. 4.4 for a superfluid helium dewar and LO_2/LH_2 Orbiter Power Reactant Storage Assemblies. The support consists of opposing sets of uniaxial S-glass/epoxy bands wrapped over metal end-spools. The bands are pretensioned so the supports never go slack under changing pressures, temperatures, or launch loads.

4.2 THERMAL/STRUCTURAL OPTIMIZATION TRADE STUDIES

The support system is used to support the helium tank, cold plumbing components, the instrument, the vapor-cooled shields and the insulation off the vacuum shell. Twelve supports are used, three pairs in opposition to three other pairs. They are located so the center-of-gravity of the supported mass is midway between the supports as represented in Fig. 4.5. The actual dewar configuration is shown later in Section 5.

The objective of this task is to optimize each support system candidate in such a way as to minimize the flow of heat from the vacuum shell to which they are attached, while maintaining enough structural rigidity to keep the lowest frequencies at launch and during orbital conditions above certain specified

ORBITER POWER REACTANT
STORAGE ASSEMBLY

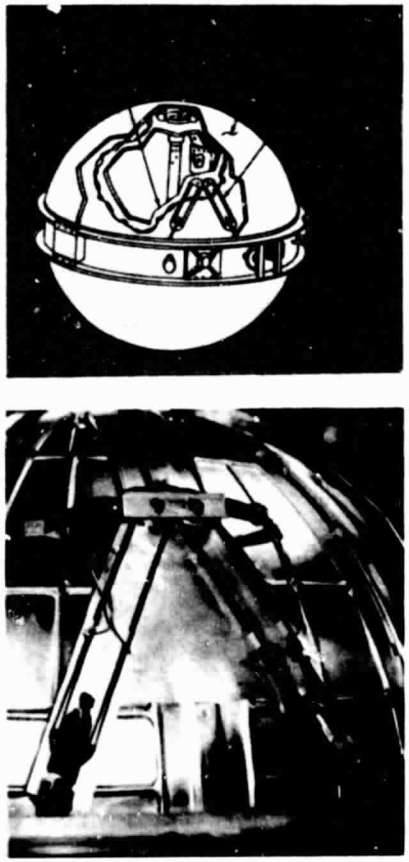

BEECH AIRCRAFT

ORIGINAL PAGE
BLACK AND WHITE PHOTOGRAPH

IRAS

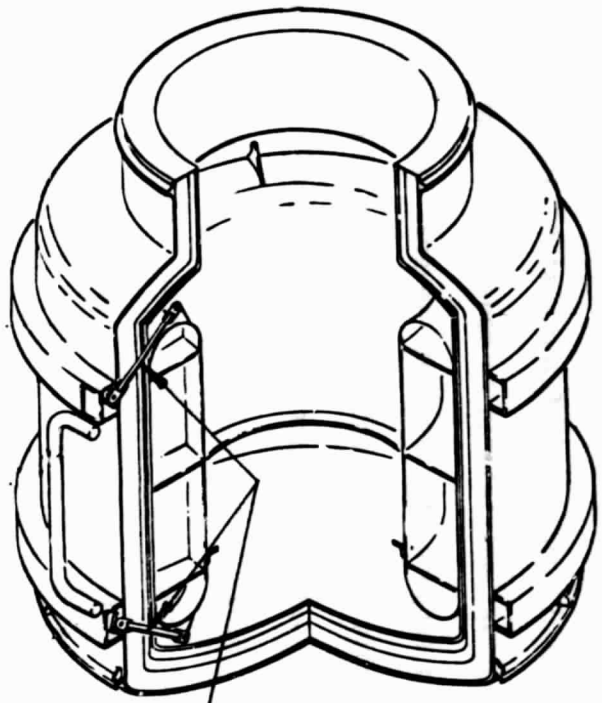

BALL BROTHERS RESEARCH CORP.

Fig. 4.4 State-of-the-Art Tension Supports

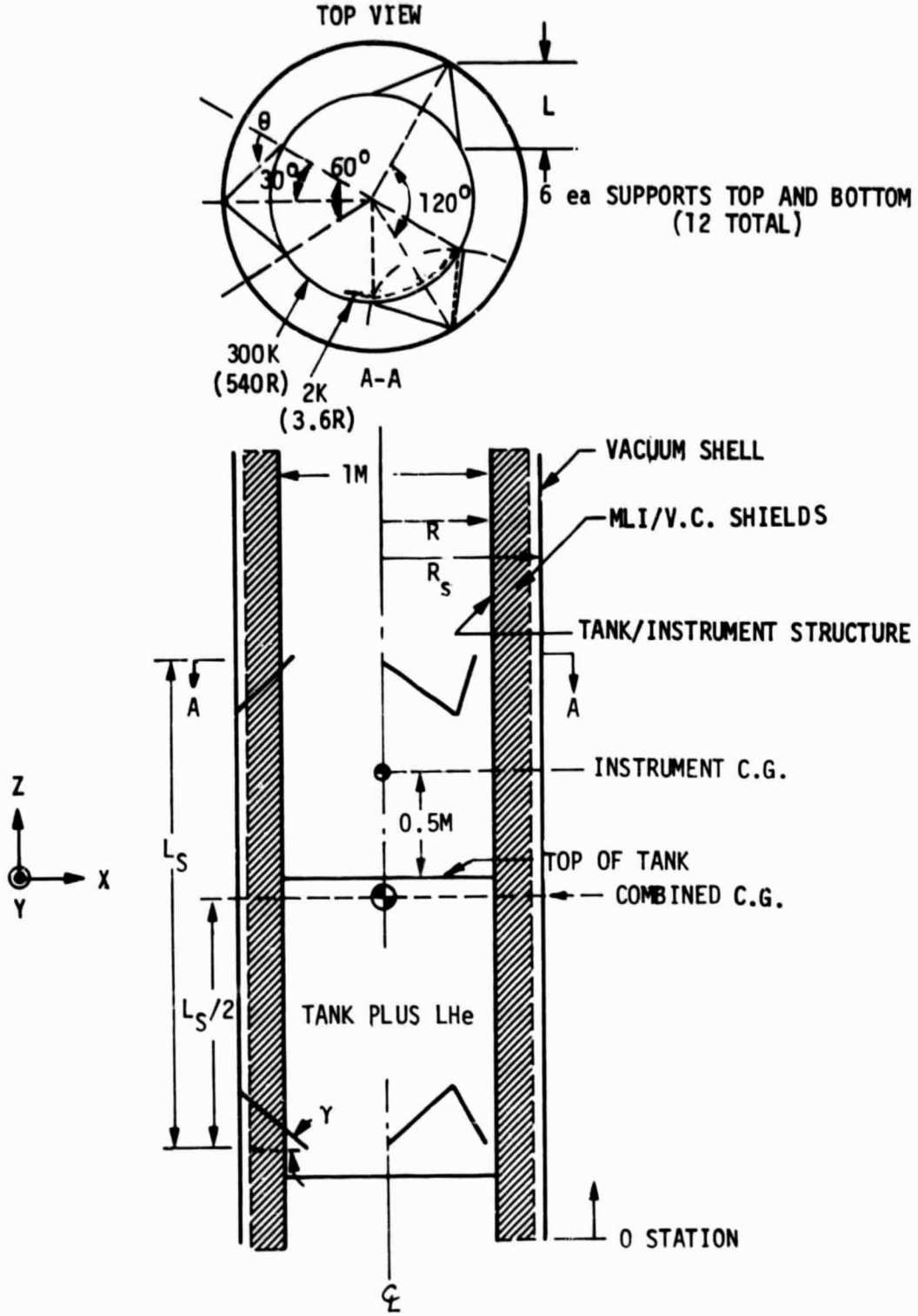

Fig. 4.5 Geometry Used in PANDA-DEWAR Analysis

values, and stresses due to assembly and launch loads below those that would cause buckling or material failure.

In this analysis, the vacuum shell and the tank/instrument structure to which it is attached are assumed to be rigid and the supports to be massless. It is also assumed that the tank, vapor-cooled shields, insulation and payload are rigid, supported by elastic struts or tension bands which carry loads only along their axes (pinned ends). The three concepts that were analyzed are:

- The passive orbital disconnect strut (PODS)
- The folded tube support (FTS)
- The reference tension band system

In the PODS and FTS concepts, the effective axial stiffness $(EA)_{eff}$ and heat flow conductance $(KA/L)_{eff}$ change abruptly from the launch condition to the orbital conduction due to "disconnect" features within each strut, so that design of each of these support systems involves the solution of two optimization problems, one corresponding to the launch phase and the other corresponding to the orbital phase. The tension band concept involves solution of one optimization problem, corresponding to the launch condition only, since the nature of this support system does not change for the orbital phase and the launch phase represents the more severe environment.

Trade studies are conducted with the use of a computer program called PANDA, originally designed for weight minimization of composite cylindrical panels subjected to destabilizing loads [4.5]. For application to the problem of dewar support design, this program has been modified by replacement of the expression for weight by an expression for heat flow and replacement of expressions for

local and general buckling loads with expressions for vibration frequencies. This modified program is called PANDA-DEWAR and is described in detail in Section 9.

The program inputs include:

1) Weights and dimensions of supported equipment;

2) Launch and orbital frequency constraints;

3) Young's modulus and the maximum allowable stress of the fiberglass tube or band; and

4) Thermal conductivities of the tube, band and S-glass filaments.

Program outputs include:

1) Center-of-gravity locations and polar and tilting moments of inertia of supported equipment;

2) Launch design margins of maximum stress , tube column (Euler) buckling, tube shell (local) buckling, and tube or band thermal stress;

3) Strut length and diameter, strut spacing and angles, cross sectional area and wall thickness, and pretension load (tension band only);

4) Launch and orbital frequency margins in lateral, tilt, axial and torsional modes; and

5) The axial length and cross-sectional area of the S-glass filaments for the PODS support.

Optimization is carried out by a nonlinear programming algorithm called CONMIN [4.6, 4.7]. This program, written by Vanderplaats in the early 1970's, is based on a nonlinear constrained search algorithm due to Zoutendijk [4.8]. The basic analytic technique used in CONMIN is to minimize an objective function (heat flow, for example) until one or more constraints, in this case vibration

frequencies, buckling loads, maximum stress or strain, and upper and lower bounds on design variables, become active. The minimization process then continues by following the constraint boundaries in design variable space in a direction such that the value of the objective function continues to decrease. When a point is reached such that no further decrease in the objective function is obtained, the process is terminated.

An example of this optimization process is shown in Fig. 4.6 for the PODS support system. Note approximately 13 design iterations were required before the launch conditions were optimized; the orbit case required seven design iterations. Once the optimum values are achieved, the results are printed out in the tabular format shown in Tables 4.4 through 4.7 for the PODS support (both ends), PODS support (cold end only), FTS and the tension band system.

A separate optimization run was conducted for each support system as a function of the supported weight. The parametric results are plotted in Fig. 4.7 for the launch case. Note in Fig. 4.7 that putting the PODS at the cold end only is superior to putting the PODS mechanism at both the cold and warm ends of the strut. This result is due to the longer fiberglass tube length possible for the same rod-end-to-rod-end length of the strut.

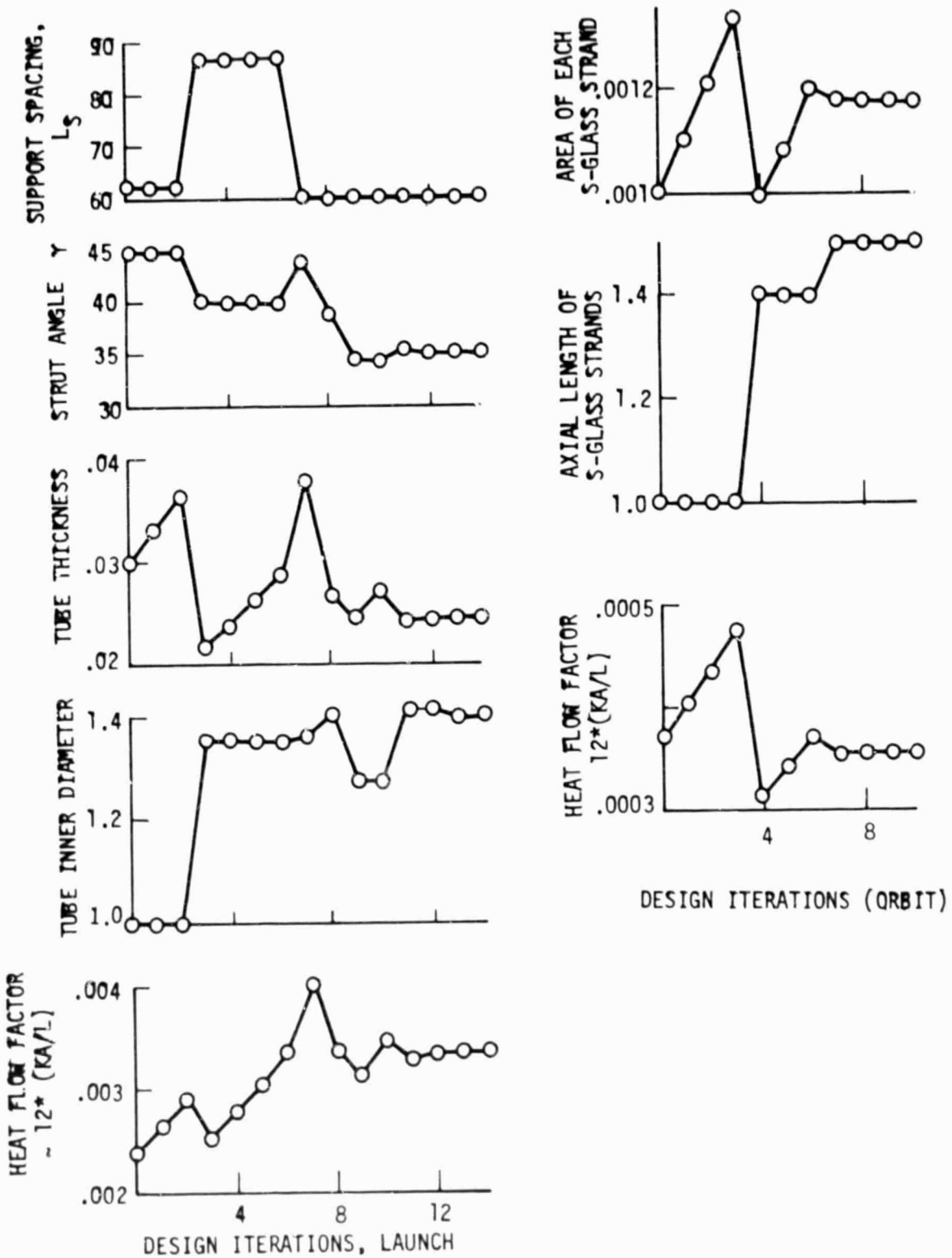

Fig. 4.6 PANDA-DEWAR Design Iterations for the PODS Support

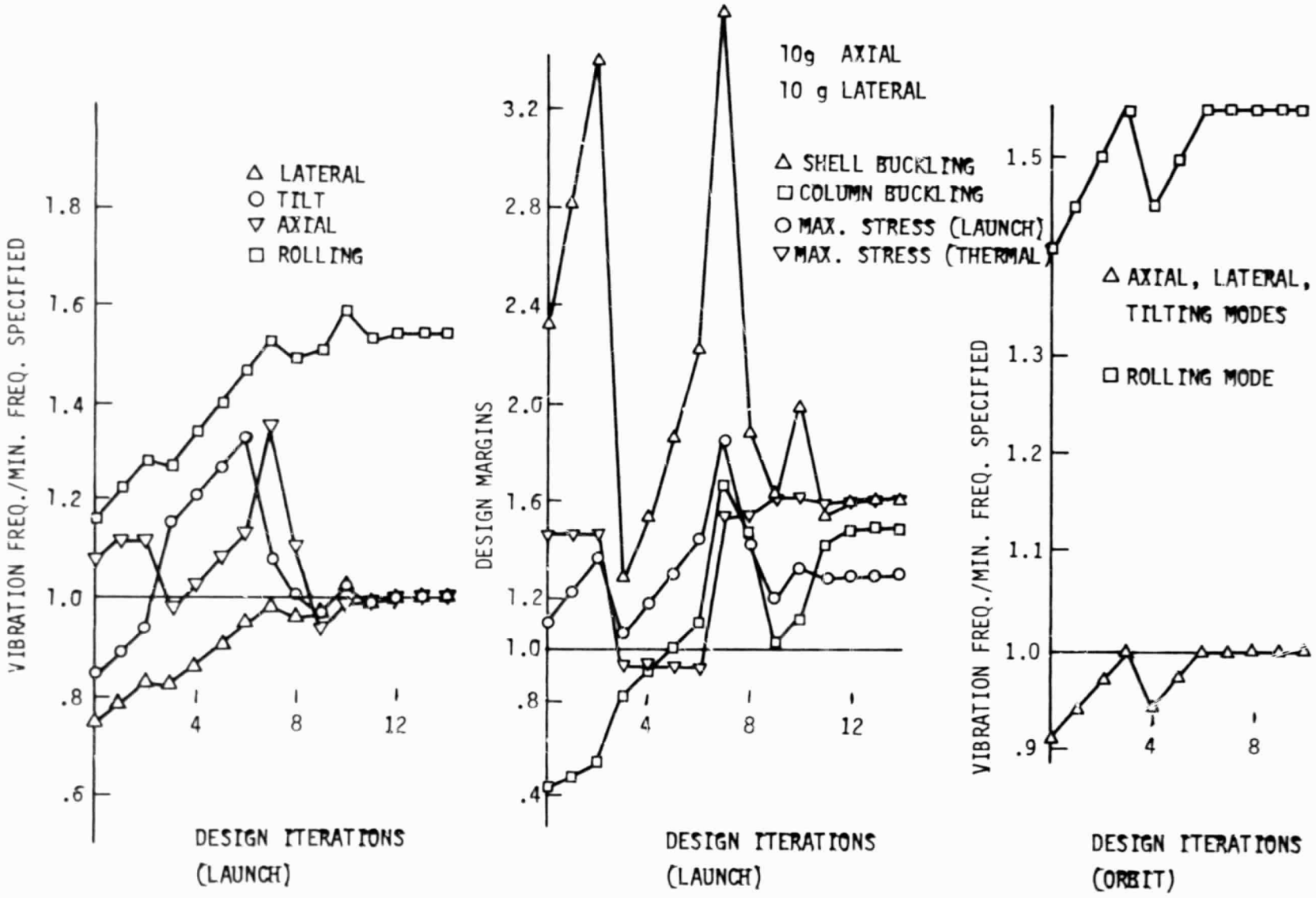

Figure 4.6 (continued)

Table 4.4 PODS, BOTH ENDS OF STRUT

DEWAR POD CONCEPT, 1200 LBS.

EFFECTIVE HEAT LOSS FACTORS FOR LAUNCH AND ORBIT...

(KA/L) FOR LAUNCH, ORBIT =	3.5102E-03	2.8354E-04

WEIGHT AND LENGTH OF SUPPORTED EQUIPMENT...

TOTAL WEIGHT . . . . . =	1.2000E+03	
PAYLOAD WEIGHT (INSTRUMENT PACK) =	4.8000E+02	
TANK WEIGHT (CRYOGEN + CONTAINER) =	3.9656E+02	
VAPOR SHIELD + INSULATION WEIGHT =	3.2344E+02	
LENGTHS OF TANK, SHIELD	5.2700E+01	1.3150E+02

CG LOCATION AND MOMENTS OF INERTIA OF SUPPORTED EQUIP

CG LOCATION (FROM AFT END OF TANK) . .=	5.5390E+01	
POLAR MOMENT OF INERTIA. . . . . .=	9.1321E+02	
MOMENT OF INERTIA FOR TILTING. . . . .=	3.2180E+03	
TANK + CRYOGEN TILTING . . . . . .=	1.2038E+03	
VAPOR SHIELD + INSULATION TILTING=	1.5337E+03	
PAYLOAD (INSTRUMENT PACKAGE) TILT =	4.8047E+02	
LAUNCH & ORBITAL FREQUENCY CONSTRAINTS=	3.5000E+01	2.0000E+01
AXIAL AND LATERAL LAUNCH ACCEL. IN G S=	1.0000E+01	1.0000E+01
YOUNGS MODULUS OF TUBE MATERIAL .... =	6.0000E+06	
MAX. ALLOWABLE STRESS OF TUBE MATERIAL=	5.0000E+04	

CONDUCTIVITIES [BTU/(HR-IN.-DEG.F)] FOR SUPPORT..

CONDUCTIVITY, K1, OF TUBE OR STRAP. . =	2.7900E-02	
CONDUCTIVITIES (SGLAS) OF HOT,COLD END=	5.2000E-02	7.2200E-03
INNER RADIUS OF CRYOGENIC TANK. . . . =	1.2000E-06	
OUTER RADIUS OF TANK AND PAYLOAD. . . =	1.9700E+01	
INNER RADIUS OF VACUUM SHELL. . . . . =	2.7200E+01	
LENGTH OF RIGID PART OF SUPPORT, EXCLUDING LENGTHS OF SGLAS MEMBERS=	2.4000E+00	
MARGIN ON MAXIMUM STRESS DURING LAUNCH=	1.2959E+00	
MARGIN ON COLUMN BUCKLING AT LAUNCH . =	1.2588E+00	
MARGIN ON SHELL BUCKLING AT LAUNCH . =	1.4115E+00	
MARGIN ON TUBE THERMAL STRESS . . . . =	1.8292E+00	
STRUT LENGTH, TUBE LENGTH (PL, TUBEL) =	1.7304E+01	8.9040E+00
AXIAL SPACING OF DEWAR SUPPORT RINGS =	5.5390E+01	
STRUT ANGLES (THETA, GAMMA) =	7.4171E+01	3.5222E+01
TUBE CROSS SECTION (AREA, INNER DIAM) =	9.3354E-02	1.3803E+00
TUBE WALL THICKNESS, R/T RATIO . . . .=	2.1203E-02	3.3051E+01
PRETENSION (ONLY FOR TENSION STRAP) =	0.0000E+00	
LAUNCH FREQ. MARGINS, (LATERAL, TILT) =	1.0005E+00	1.0639E+00
LAUNCH FREQ. MARGINS, (AXIAL, TORSION)=	9.9890E-01	1.5646E+00
AXIAL LENGTH OF SGLASS TENSION MEMBER =	1.5000E+00	
CROSS SECTION AREA OF SGLASS MEMBER =	9.0697E-04	
ORBITAL FREQ. MARGINS, (LATERAL, TILT)=	9.9532E-01	1.0584E+00
ORBITAL FREQ. MARGINS, (AXIAL,TORSION)=	9.9375E-01	1.5566E+00

Table 4.5 PODS, COLD END OF STRUT

DEWAR POD CONCEPT, 1200 LBS. (POD AT ONE END ONLY OF STRUT)

EFFECTIVE HEAT LOSS FACTORS FOR LAUNCH AND ORBIT...
K A/L) FOR LAUNCH, ORBIT = 2.6217E-03 1.7197E-04

WEIGHT AND LENGTH OF SUPPORTED EQUIPMENT...

TOTAL WEIGHT	=	1.2000E+03
PAYLOAD WEIGHT (INSTRUMENT PACK)	=	4.8000E+02
TANK WEIGHT (CRYOGEN + CONTAINER)	=	3.9656E+02
VAPOR SHIELD + INSULATION WEIGHT	=	3.2344E+02
LENGTHS OF TANK, SHIELD	5.2700E+01	1.3150E+02

CG LOCATION AND MOMENTS OF INERTIA OF SUPPORTED EQUIP

CG LOCATION (FROM AFT END OF TANK) . .	=	5.5390E+01
POLAR MOMENT OF INERTIA.	=	9.1321E+02
MOMENT OF INERTIA FOR TILTING.	=	3.2180E+03
TANK + CRYOGEN TILTING	=	1.2038E+03
VAPOR SHIELD + INSULATION TILTING	=	1.5337E+03
PAYLOAD (INSTRUMENT PACKAGE) TILT	=	4.8047E+02

LAUNCH & ORBITAL FREQUENCY CONSTRAINTS	= 3.5000E+01	2.0000E+01
AXIAL AND LATERAL LAUNCH ACCEL. IN G S	= 1.0000E+01	1.0000E+01
YOUNGS MODULUS OF TUBE MATERIAL	= 6.0000E+06	
MAX. ALLOWABLE STRESS OF TUBE MATERIAL	= 5.0000E+04	

CONDUCTIVITIES [BTU/(HR-IN.-DEG.F)] FOR SUPPORT..

CONDUCTIVITY, K1, OF TUBE OR STRAP. .	= 2.7900E-02	
CONDUCTIVITIES (SGLAS) OF HOT,COLD END	= 1.0000E+06	7.2200E-03

INNER RADIUS OF CRYOGENIC TANK. . . .	= 1.0000E+00	
OUTER RADIUS OF TANK AND PAYLOAD. . .	= 1.9700E+01	
INNER RADIUS OF VACUUM SHELL.	= 2.7200E+01	
LENGTH OF RIGID PART OF SUPPORT, EXCLUDING LENGTHS OF SGLAS MEMBERS	= 2.4000E+00	

MARGIN ON MAXIMUM STRESS DURING LAUNCH	= 1.2945E+00	
MARGIN ON COLUMN BUCKLING AT LAUNCH .	= 1.3914E+00	
MARGIN ON SHELL BUCKLING AT LAUNCH .	= 1.3616E+00	
MARGIN ON TUBE THERMAL STRESS	= 2.2820E+00	

STRUT LENGTH, TUBE LENGTH (PL, TUBEL)	= 1.7309E+01	1.1909E+01
AXIAL SPACING OF DEWAR SUPPORT RINGS	= 5.5390E+01	
STRUT ANGLES (THETA, GAMMA)	= 7.4171E+01	3.5246E+01
TUBE CROSS SECTION (AREA, INNER DIAM)	= 9.3255E-02	1.4046E+00
TUBE WALL THICKNESS, R/T RATIO	= 2.0824E-02	3.4225E+01
PRETENSION (ONLY FOR TENSION STRAP)	= 0.0000E+00	
LAUNCH FREQ. MARGINS, (LATERAL, TILT)	= 9.9947E-01	1.0631E+00
LAUNCH FREQ. MARGINS, (AXIAL, TORSION)	= 9.9879E-01	1.5631E+00

AXIAL LENGTH OF SGLASS TENSION MEMBER	= 1.5000E+00	
CROSS SECTION AREA OF SGLASS MEMBER	= 4.8292E-04	
ORBITAL FREQ. MARGINS, (LATERAL, TILT)	= 9.9964E-01	1.0633E+00
ORBITAL FREQ. MARGINS, (AXIAL, TORSION)	= 9.9895E-01	1.5633E+00

Table 4.6 FOLDED TUBE SUPPORT

```
DEWAR FOLDED TUBE CONCEPT, 1200 LBS.

EFFECTIVE HEAT LOSS FACTORS FOR LAUNCH AND ORBIT...
 (A/L) FOR LAUNCH, ORBIT  =  2.0935E-03  2.0075E-04

WEIGHT AND LENGTH OF SUPPORTED EQUIPMENT...
    TOTAL WEIGHT . . . . . .=  1.2000E+03
    PAYLOAD WEIGHT (INSTRUMENT PACK)  =  4.8000E+02
    TANK WEIGHT (CRYOGEN + CONTAINER) =  3.9656E+02
    VAPOR  SHIELD + INSULATION WEIGHT =  3.2344E+02
    LENGTHS OF TANK, SHIELD  5.2700E+01  1.3150E+02

CG LOCATION AND MOMENTS OF INERTIA OF SUPPORTED EQUIP
CG LOCATION (FROM AFT END OF TANK) . .=  5.5390E+01
POLAR MOMENT OF INERTIA. . . . . .=  9.1321E+02
MOMENT OF INERTIA FOR TILTING. . . . .=  3.2180E+03
    TANK + CRYOGEN TILTING . . . . . .=  1.2038E+03
    VAPOR  SHIELD + INSULATION TILTING=  1.5337E+03
    PAYLOAD (INSTRUMENT PACKAGE) TILT =  4.8047E+02

LAUNCH & ORBITAL FREQUENCY CONSTRAINTS=  3.5000E+01  2.0000E+01
 XIAL AND LATERAL LAUNCH ACCEL. IN G S=  1.0000E+01  1.0000E+01
YOUNGS MODULUS OF TUBE MATERIAL ....  =  6.0000E+06
MAX. ALLOWABLE STRESS OF TUBE MATERIAL=  5.0000E+04

CONDUCTIVITIES [BTU/(HR-IN.-DEG.F)] FOR SUPPORT..
CONDUCTIVITY, K1, OF TUBE 1 AT LAUNCH =  2.7900E-02
CONDUCTIVITY OF TUBE 1 IN ORBIT . . . =  3.5600E-02
 ONDUCTIVITY OF TUBE 2 IN ORBIT . . . =  2.5500E-02
CONDUCTIVITY OF TUBE 3 IN ORBIT . . . =  1.4900E-02

INNER RADIUS OF CRYOGENIC TANK  . . . =  1.4900E-02
OUTER RADIUS OF TANK AND PAYLOAD. . . =  1.9700E+01
INNER RADIUS OF VACUUM SHELL. . . . . =  2.7200E+01
LENGTH OF RIGID PART OF SUPPORT . . . =  5.0000E+00

MARGIN ON MAXIMUM STRESS DURING LAUNCH=  1.2940E+00
MARGIN ON COLUMN BUCKLING AT LAUNCH . =  1.3652E+00
MARGIN ON SHELL  BUCKLING AT LAUNCH . =  1.0692E+00
MARGIN ON TUBE THERMAL STRESS . . . . =  2.2121E+00

STRUT LENGTH, TUBE LENGTH (PL, TUBEL) =  1.7308E+01  1.2308E+01
AXIAL SPACING OF DEWAR SUPPORT RINGS  =  5.5390E+01
STRUT ANGLES            (THETA, GAMMA) =  7.4171E+01  3.5242E+01
TUBE CROSS SECTION (AREA, INNER DIAM) =  7.6962E-02  1.4443E+00
TUBE WALL THICKNESS, R/T RATIO . . . .=  1.6767E-02  4.3569E+01
PRETENSION  (ONLY FOR TENSION STRAP ) =  0.0000E+00
LAUNCH FREQ. MARGINS, (LATERAL, TILT) =  9.9936E-01  1.0629E+00
LAUNCH FREQ. MARGINS, (AXIAL, TORSION)=  9.9852E-01  1.5629E+00


LENGTHS OF FOLDED TUBES NOS. 2 AND 3  =  1.1692E+01
OUTER RADIUS OF TUBE NO. 2 . . . . . .=  6.7214E-01
THICKNESS OF TUBE NO. 2  . . . . . .=  3.7617E-02
OUTER RADIUS OF TUBE NO. 3 . . . . . .=  2.4373E-01
THICKNESS OF TUBE NO. 3  . . . . . .=  1.0000E-02
ORBITAL FREQ. MARGINS, (LATERAL, TILT)=  9.9683E-01  1.0602E+00
ORBITAL FREQ. MARGINS, (AXIAL,TORSION)=  9.9600E-01  1.5589E+00
```

Table 4.7 TENSION BAND SUPPORT

DEWAR TENSION STRAP CONCEPT, 2000 LBS.

EFFECTIVE HEAT LOSS FACTORS FOR LAUNCH AND ORBIT...
(KA/L) FOR LAUNCH, ORBIT = 5.0889E-03 4.6174E-03

WEIGHT AND LENGTH OF SUPPORTED EQUIPMENT...

TOTAL WEIGHT	=	2.0000E+03
PAYLOAD WEIGHT (INSTRUMENT PACK)	=	4.8000E+02
TANK WEIGHT (CRYOGEN + CONTAINER)	=	8.8360E+02
VAPOR SHIELD + INSULATION WEIGHT	=	6.3640E+02
LENGTHS OF TANK, SHIELD	1.0630E+02	1.8510E+02

CG LOCATION AND MOMENTS OF INERTIA OF SUPPORTED EQUIP

CG LOCATION (FROM AFT END OF TANK) . .	=	8.3171E+01
POLAR MOMENT OF INERTIA.	=	1.6153E+03
MOMENT OF INERTIA FOR TILTING. . . .	=	1.2160E+04
TANK + CRYOGEN TILTING	=	4.4407E+03
VAPOR SHIELD + INSULATION TILTING	=	5.3173E+03
PAYLOAD (INSTRUMENT PACKAGE) TILT	=	2.4017E+03

LAUNCH & ORBITAL FREQUENCY CONSTRAINTS	=	3.5000E+01 2.0000E+01
AXIAL AND LATERAL LAUNCH ACCEL. IN G S	=	1.0000E+01 1.0000E+01
YOUNGS MODULUS OF TUBE MATERIAL	=	7.5000E+06
MAX. ALLOWABLE STRESS OF TUBE MATERIAL	=	5.6000E+04
CONDUCTIVITY OF STRAP AT LAUNCH . . .	=	3.1300E-02
CONDUCTIVITY OF STRAP IN ORBIT . . .	=	2.8400E-02
INNER RADIUS OF CRYOGENIC TANK. . . .	=	1.0000E-08
OUTER RADIUS OF TANK AND PAYLOAD. . .	=	1.9700E+01
INNER RADIUS OF VACUUM SHELL.	=	2.7200E+01
LENGTH OF RIGID PART OF SUPPORT . . .	=	2.0000E-02
MARGIN ON MAXIMUM STRESS DURING LAUNCH	=	1.1488E+00
MARGIN ON SLACK STRAP DURING LAUNCH .	=	9.9994E-01
MARGIN ON STRAP THERMAL STRESS . . .	=	9.8381E-01
STRUT LENGTH, TUBE LENGTH (PL, TUBEL)	=	2.2162E+01 2.2142E+01
AXIAL SPACING OF DEWAR SUPPORT RINGS	=	7.1287E+01
STRUT ANGLES (THETA, GAMMA)	=	7.4171E+01 5.0369E+01
TUBE CROSS SECTION (AREA, INNER DIAM)	=	3.0000E-01 0.0000E+00
TUBE WALL THICKNESS, R/T RATIO	=	0.0000E+00 0.0000E+00
PRETENSION (ONLY FOR TENSION STRAP)	=	7.3117E+03
LAUNCH FREQ. MARGINS, (LATERAL, TILT)	=	9.9979E-01 9.8951E-01
LAUNCH FREQ. MARGINS, (AXIAL, TORSION)	=	1.7072E+00 1.5177E+00

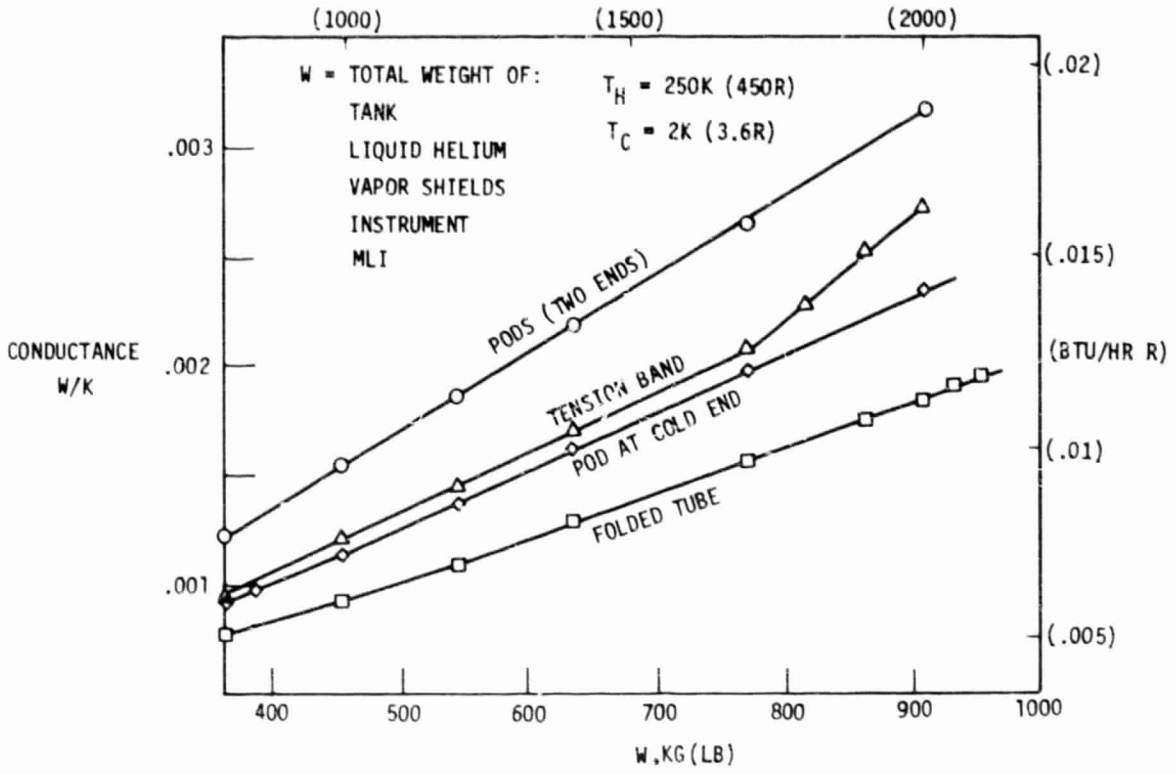

Fig. 4.7 Launch Support Conductance

The inflection in the tension band support curve at 770 kg (1698 lb) is due to a change in which margin requirement designs the supports. Below ~ 770 kg (1698 lb) the lateral frequency margin is the designing criteria. Above 770 kg (1698 lb), the tilt frequency margin designs the supports (due to the increasingly longer helium tank). The folded tube data shows it is the optimum support for launch conditions. This analysis, however, is too optimistic for the FTS since it does not account for radiation heat flow from the outer tube to the inner tubes.

Fig. 4.8 plots the orbit support conductance as a function of supported weight. Here, the PODS (cold end only) is the optimum support system. Since the calculated conductance values in Fig. 4.8 are based on solid conduction heat transfer only (no radiation), a check was made on the PODS system (cold end) to see if this assumption was valid. The PODS thermal model was used to calculate the conduction and radiation heat transfer as a function of the first vapor cooled shield temperature, T_1. Note in Fig. 4.9 that radiation is negligible below 30K (54R) so the conduction only assumption used is valid for the PODS support system. The inflection in the conduction curve in Fig. 4.9 at ~ 15K (27R) is due to the change in slope of S-glass conductivity at this temperature as shown in Fig. 4.10.

Using the FTS thermal model, analyses show radiation cannot be neglected for the FTS as indicated by the temperature distributions shown in Fig. 4.11. Note the temperature goes up from tube 1, 180K (324R), to tube 2, 209K (376R), and then back down to 125K (225R) at tube 3 showing radiation heat transfer between tubes is significant. Consequently, the FTS conductance data shown previously in Fig. 4.8 that ignores radiation heat transfer is too optimistic (low). Note the tension band support system conductance in Fig. 4.8 is over an order of magnitude higher than the optimum system, PODS (cold end only).

The effect of support conductance on single-stage dewar weight was calculated using the CRYOP program as shown in Fig. 4.12. Note the PODS system (cold end only) was the lowest weight; FTS is 4% higher and the tension band dewar weight is double the PODS dewar weight. Also note the PODS system will support a full helium tank minus the instrument, without shorting thermally. Consequently, simulated space parasitic heat rates for the supports can be measured in one-g

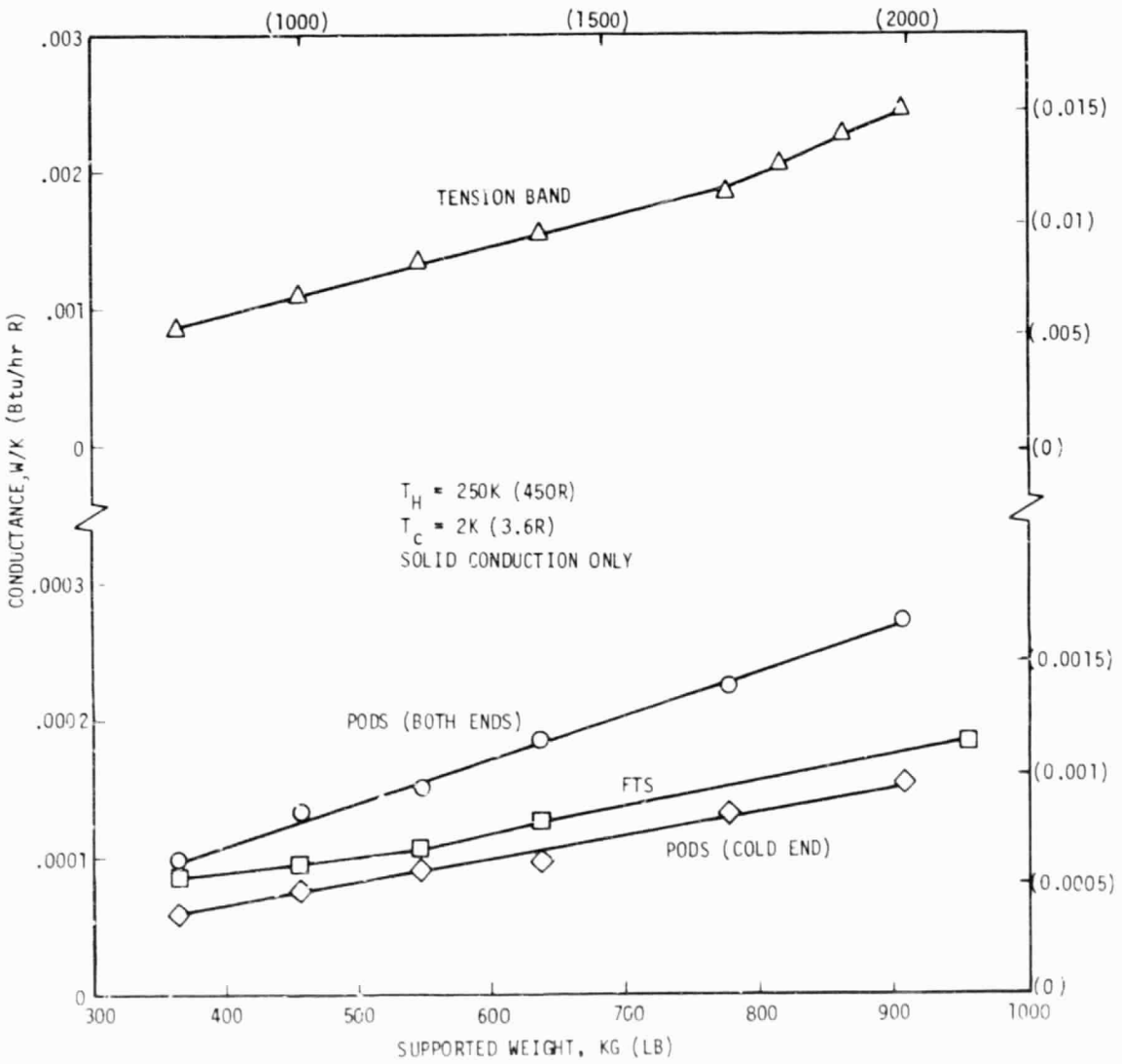

Fig. 4.8 Orbit Support Conductance

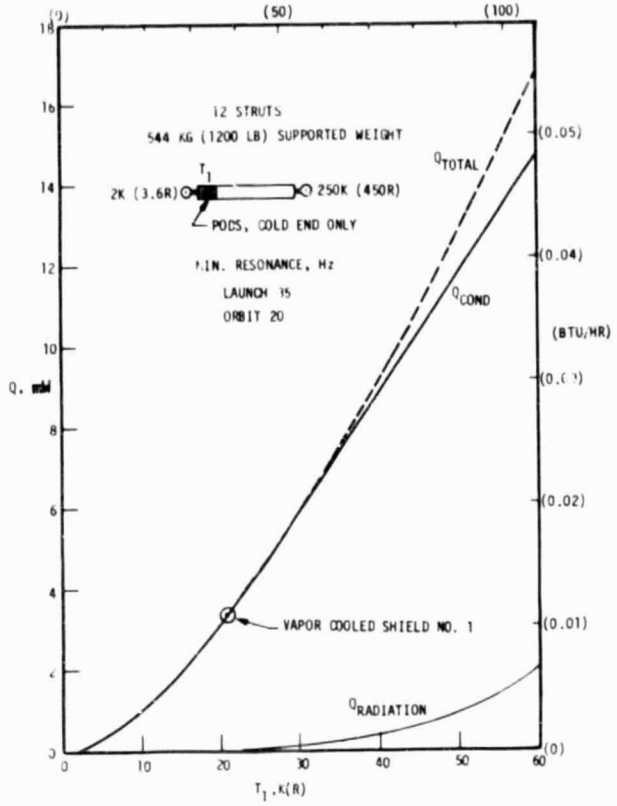

Fig. 4.9 PODS Heat Rate

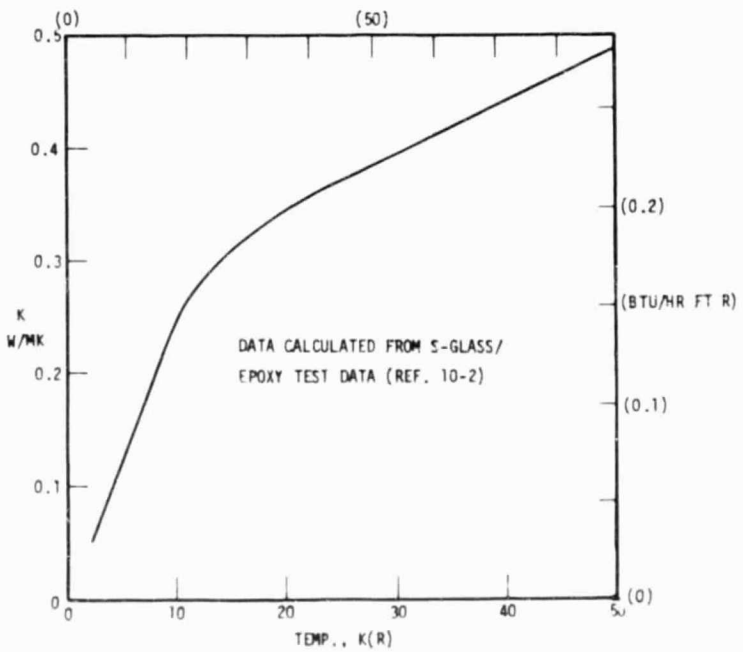

Fig. 4.10 Thermal Conductivity of S-Glass

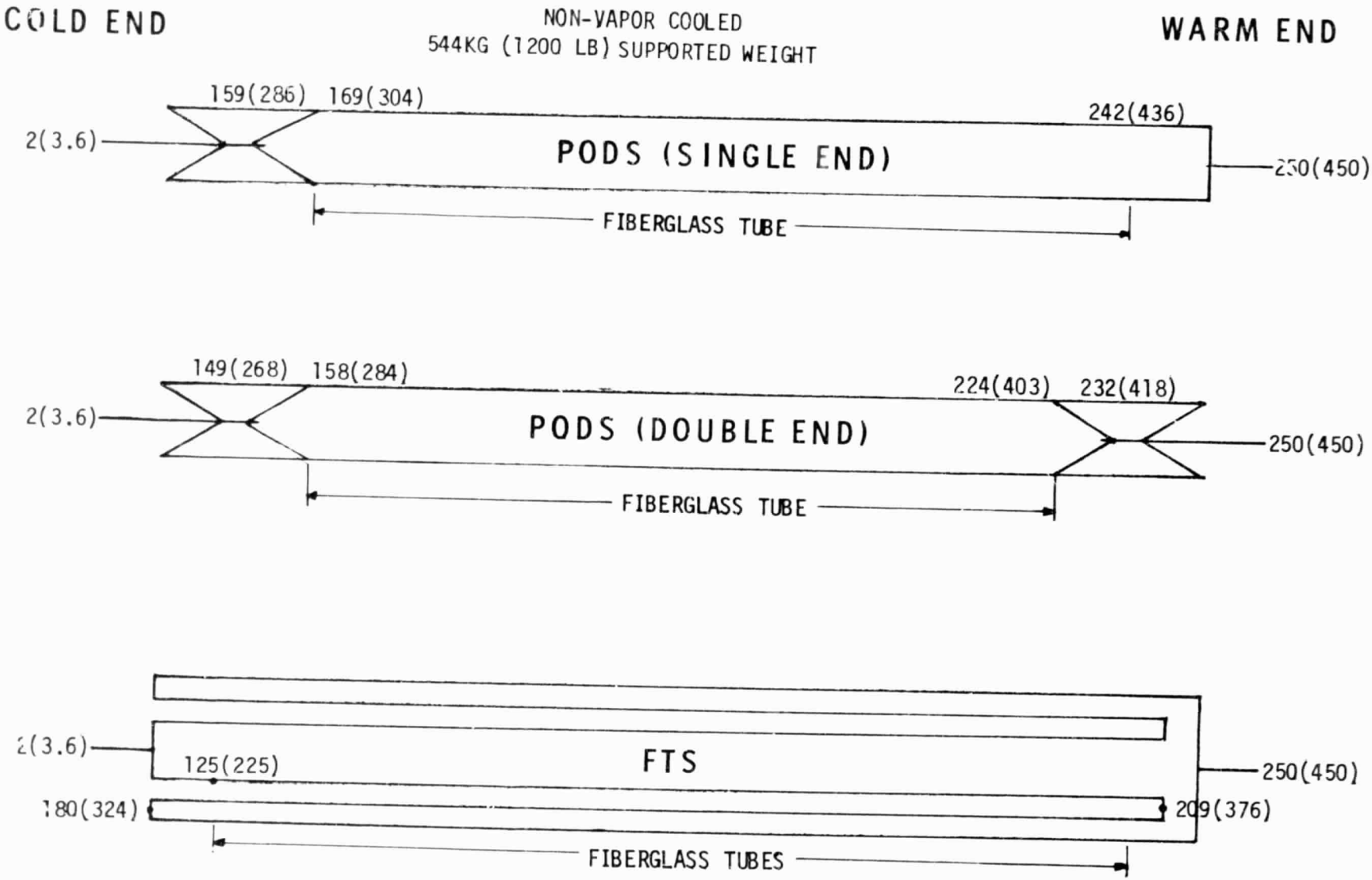

Fig. 4.11 Support Temperature Distributions, K (R)

* The final support design shown later in Fig. 5.24 will support 600 kg (1322 lb)

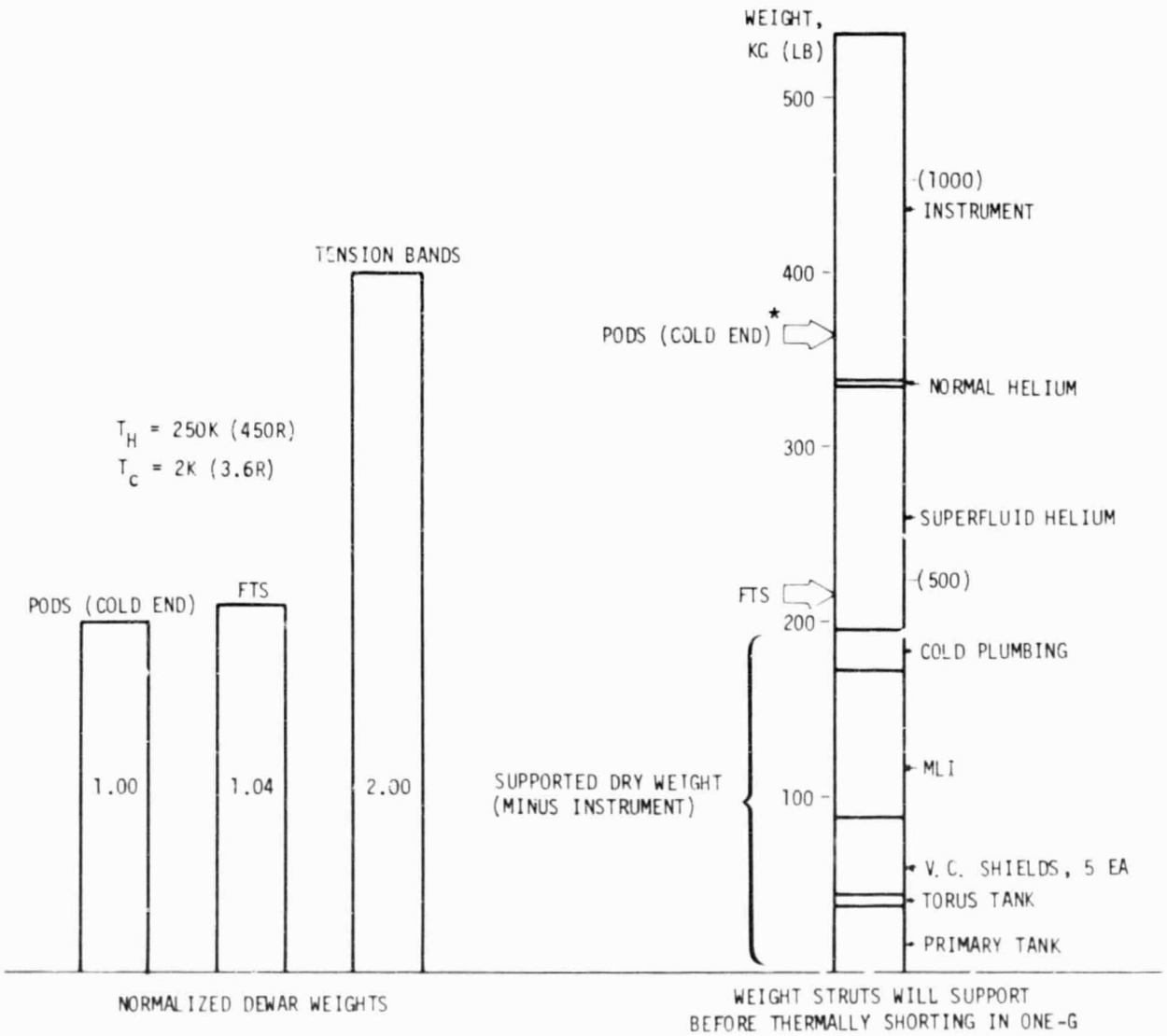

Fig. 4.12 Comparison of Weight Factors for Support System Candidates

thermal tests. For the FTS, it is marginal whether this type of test could be performed even with a partially filled tank.

4.3 SUBJECTIVE TRADE STUDIES

Fabrication and assembly costs were estimated per strut for both strut candidates. These estimates assume all the manufacturing processes have been demonstrated and all required tooling or assembly fixtures are available. The estimate per strut is based on a total build of 18 struts. No product assurance hours are included in the estimates. The material costs and hour estimates for the PODS struts are based on records kept while the engineering model strut was being fabricated and assembled on the Lockheed Independent Research Program. The folded tube strut estimate was kept consistent with the PODS numbers where comparable materials or assembly tasks are used. As can be seen from Table 4.8, the total cost per strut and the delta are:

FTS	$2882
PODS (cold end)	$2459
	Δ $ 423

The cost differential is insignificant compared to total program costs.

The steps required to install a tank within the Invar vacuum shell ring using the strut supports is given as follows.

Table 4.8 COMPARISON OF STRUT FABRICATION AND ASSEMBLY COSTS (PER STRUT)

FOLDED TUBE		PODS (COLD END ONLY)	
Estimated Purchased Material Costs ($1980)		Based on Actual Purchased Material Costs ($1980)	
Machined Invar Parts, S.S. Parts	490	Machined Invar, S.S. Parts	307
Rod Ends	700	Rod Ends	700
F.G. Tubes	150	F.G. Tube	50
Misc	50	Misc	50
	$1390		$1107
ESTIMATED HOURS		BASED ON ACTUAL HOURS	
Dimensional Check	2	Dimensional Check	3
Gold Coat Parts	16	Gold Coat Parts	8
Bond Operation	1.5	Bond S-Glass, 4 Times	8
Insulation Discs	0.8	Epoxy On-9 Pins, 2 Times	2
MLI Wrap	4	Prestress Bond, 2 Times	4
Bond Operation	1.5	Al Washer Bond, 2 Times	0.5
MLI Wrap	4	Install Insulation Discs	0.8
Bond Operation	1.5	F.G. Tube Bond	1.5
Clearance Adj Locknut	2	Outer Insulation Wrap	2
Load Test	2	Load Test	2
Vacuum Bakeout	2	Vacuum Bakeout	2
TOTAL HRS/STRUT	37.3	TOTAL HRS/STRUT	33.8
AT $40/HR	$1492	AT $40/HR.	$1352
TOTAL COST/STRUT	$ 2882	TOTAL COSTS/STRUT	$2459

Δ COST PER DEWAR

12(2882-2459) = $5076

FTS	PODS
• Prefit struts to tank and vacuum shell (with load gap locked). • Tighten locking nuts. • Remove struts and reset load gap. • Reinstall struts. Check nonshorting of strut across the load gap with an ohmeter.	• Prefit struts to tank and vacuum shell with "zero" clearance load pins installed. • Tighten locking nuts. • Remove "zero" clearance load pins and install flight load pins. (If access is a problem, the struts can be removed and installed one at a time for this operation.) Check non-shorting between the stem and the body with an ohmeter.

The analysis, design and fabrication complexity for accepting point loads into the vacuum shell or tank are comparable for either support system.

Installation complexity of multilayer insulation around the struts is the same for either support candidate. However, vapor cooling the PODS supports is easier than the FTS because of the restricted access to tubes 2 and 3 of the FTS.

The operational reliability of both support systems is comparable since they both operate in a passive mode with design stress levels set low enough (25% of ultimate) to preclude fatigue failures.

Therefore, from a cost, fabrication/assembly complexity or reliability viewpoint, the PODS has a slight but not significant edge.

4.4 SELECTED SUPPORT SYSTEM

The PODS (cold end only) support system has been selected over the FTS system based on the analyses performed in Sections 4.2 and 4.3. A summary of the reasons for this selection are:

- Lower orbital support conductance
- Dewar weight lower by 4%
- Orbit performance can be demonstrated in one-g
- For lower orbit resonances, PODS heat rate can be decreased; FTS tube #13 is at minimum gage.
- PODS geometry is ideal for vapor cooling. Tubes 2 and 3 of FTS require separate cooling circuit.
- Other factors are about equal:
    - Cost
    - Reliability
    - Effect of point loads on weight
    - Ease of MLI and vapor-cooled shield installation

Section 5

DEWAR DESIGN AND PERFORMANCE

Based on the analyses performed in Sections 3 and 4, a single-stage helium dewar (with 5 vapor-cooled shields and 12 PODS struts) was selected for further analysis and design. Initially, some additional system analyses were performed to further define the dewar design. Using the results of these analyses, the design was drawn using CADAM, the thermal performance was analyzed and weights were calculated.

5.1 SYSTEM ANALYSES

Prior to finalizing the dewar design, a number of system analyses were required to make design choices or to optimize system performance. These analyses included modeling the system thermal performance; selecting the optimum vapor-cooled shield thickness and attachment design to the struts; analyzing the struts' unique attachment requirements based on system operating temperature ranges; sizing the porous plug, vent lines and burst discs; selecting the optimum ground hold concept and selecting the optimum tank and vacuum shell material and design.

5.1.1 System Thermal Modeling

A thermal nodal network of the dewar was setup for both the ground hold and orbital cases as shown in Figs. 5.1 and 5.2. The thermal analysis was

Fig. 5.1 Ground Hold Thermal Model

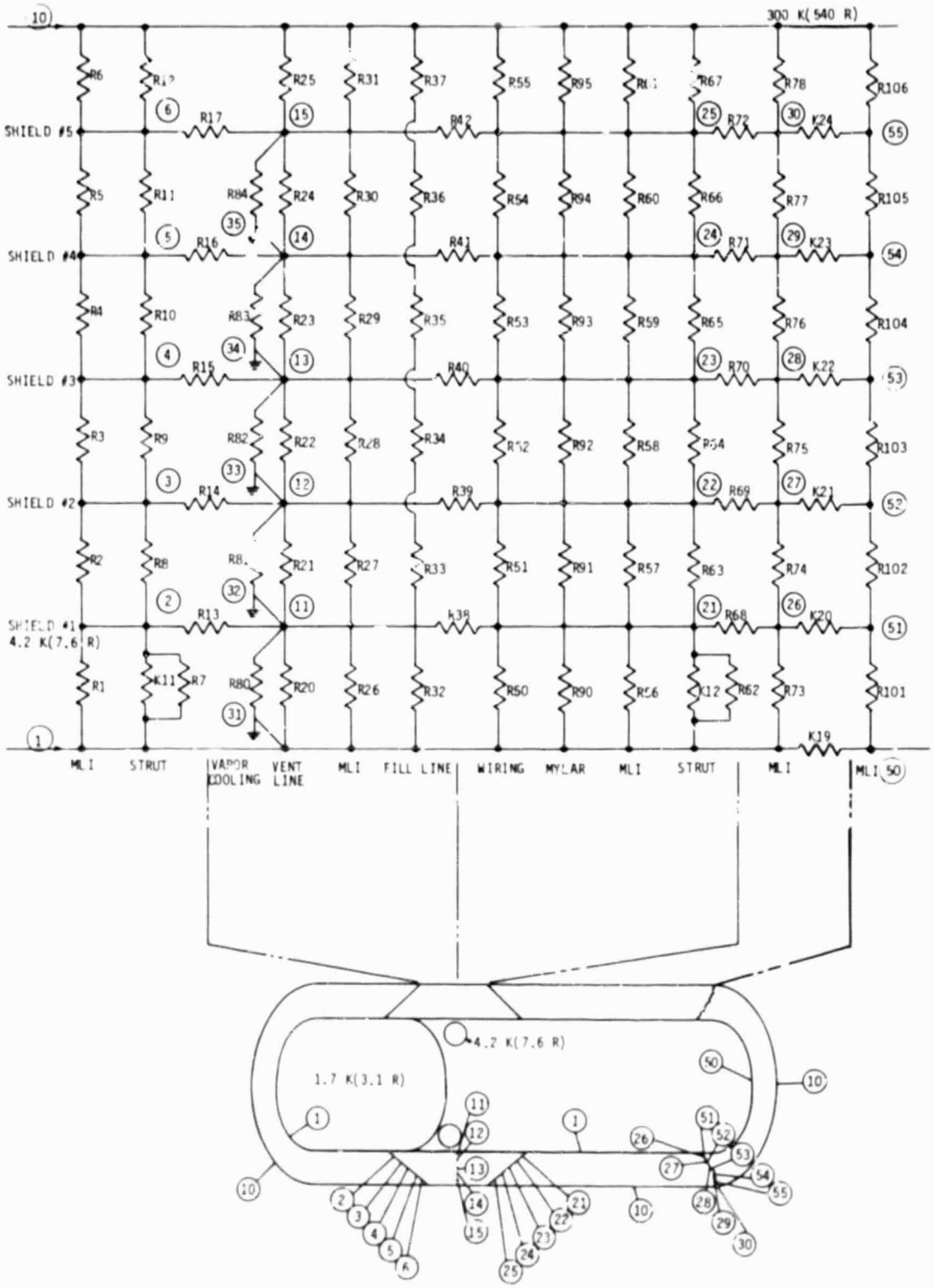

Fig. .2 Orbit Thermal Model

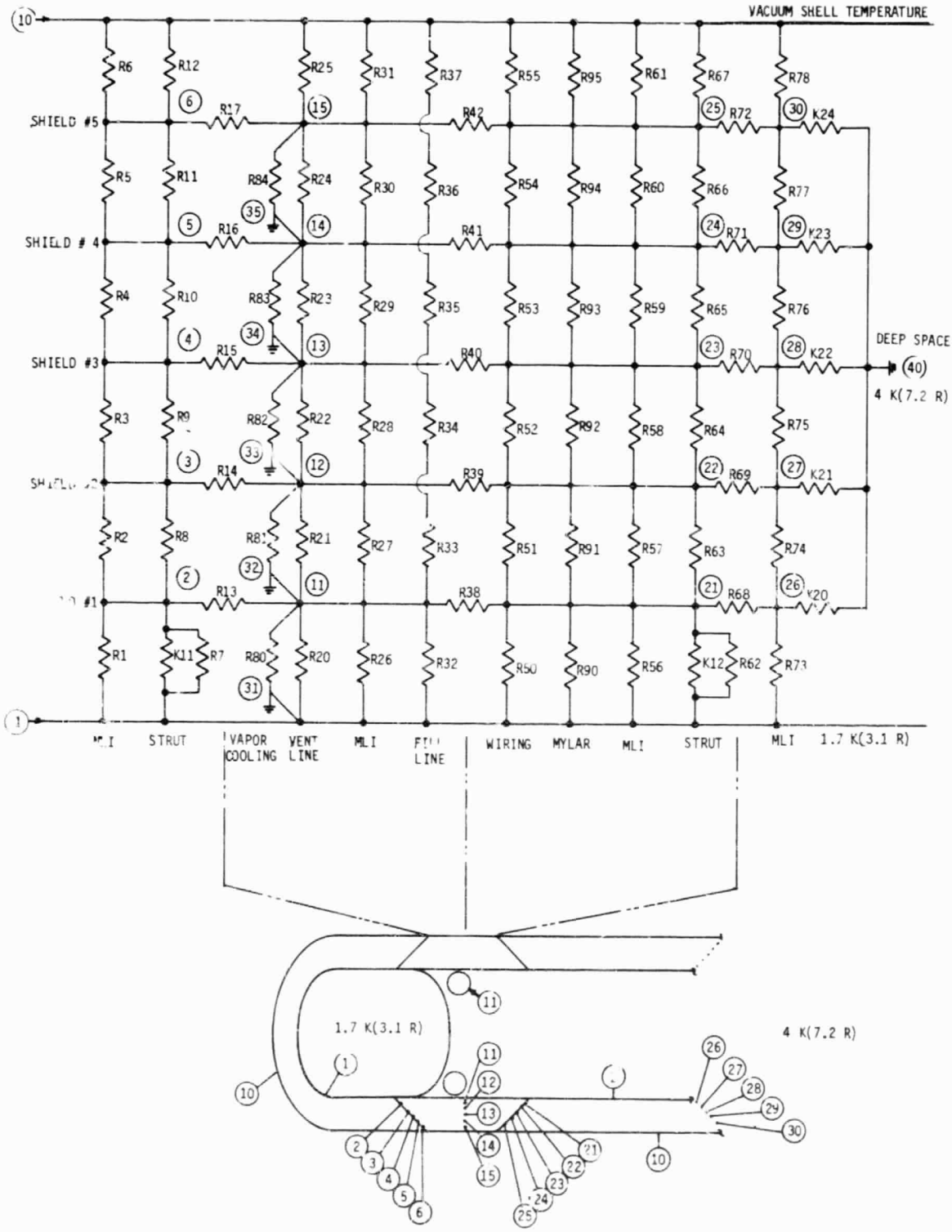

performed using the THERM program. In the figures, R represents conduction resistors and K radiation resistors.

For the ground hold model, note the PODS supports have both conduction (R7, R62) and radiation (K11, K12) resistors at the cold end since the design described later in this section does not short out against the load pins in one-g. The first vapor-cooled shield is shorted (mounted) to the torus tank, node 11 (described later in Section 5.1.5), and consequently runs at 4.2K (7.6R). Heat sink nodes 31 through 35 represent the heat removed by the normal helium vent gas. Note the fill line is only shorted to the first vapor-cooled shield; otherwise, fill with superfluid helium would not be possible. The wire feed throughs are divided into the parallel wire resistors (R50-R55) and Mylar cone resistors (R90-R95) shown later in Fig. 5.23. The aperture cover is radiatively coupled to the dewar through resistors K19 (inner surface) and K20 through K24 (the ends of the shields viewing each other).

The orbit case shown in Fig. 5.2 is similar to the ground hold case with the following changes. The aperture cover is ejected in orbit so nodes 26-30 (the flanged ends of the vapor-cooled shields) radiate to deep space. Also, the first vapor-cooled shield temperature and torus tank are not set at 4.2K (7.6R) but float.

5.1.2 Vapor-Cooled Shield Analyses

Three analyses were conducted on the vapor-cooled shields. The first analysis determined the minimum thickness required, from a thermal standpoint, to minimize system weight. The second analysis determined if the minimum

thickness required thermally was adequate structurally while the third analysis calculated the flexure capability required at the shield/strut attachment point due to differential contractions of the tank, vacuum shell, struts and vapor-cooled shields.

5.1.2.1 Shield Thickness Analysis. Using the orbit thermal model described in Section 5.1.1, the vapor-cooled shield thickness was varied parametrically. The overall dewar heat range did not increase more than 1.7% going from 0.5 mm (0.020 in) thickness down to 0.127 mm (0.005 in). Consequently, from a thermal standpoint, a 0.127 mm (0.005 in) thick vapor-cooled shield is adequate.

5.1.2.2 Shield Structural Analysis. The vapor shield must carry its own weight plus the weight of the insulation blanket wrapped on top of it. The 0.127 mm (0.005 in) shield must be stiffened to carry this load. The most efficient means is to bond an aluminum honeycomb core on one side only (no gas can be trapped in the cells with this arrangement).

The face plate is made of 0.127 mm (0.005 in) thick 6063 aluminum and the core is aluminum honeycomb designated as 5052/F40-.0013 with a density of 33.7 kg/m^3 (2.1 lb/ft^3). There are 1.3 cells per cm and the gage is 0.033 mm (0.0013 in).

The loading on the vapor shield is the weight of the shield and the insulation between two concentric vapor shields. The weight of the thickest layer of insulation weighs 1.22 kg/m^2 (0.25 lb/ft^2). A load factor of 10 is to be carried by the shield.

For the analysis, the shield is assumed to be loaded by a hydrostatic pressure rather than the gravity loading of the shield and insulation blanket. This is a slightly conservative approach which allows a simplified analysis. The dimensions are that of the outermost shell: 1.32 m (52 in) diameter and 2.32 m (91.5 in) length. The PANDA code was used to investigate the effect of the height of the honeycomb core on the buckling pressure.

In the first analysis, the faceplate/honeycomb combination was treated as a shell wall consisting of two homogeneous layers. In this case, the honeycomb modulus was taken as 4.5×10^8 N/m^2 (65000 psi), in accordance with the 1981 revision of the publication "Mechanical Properties of Hexcel Honeycomb Materials, TSB120". The following table gives results from this series of analyses:

Skin Thickness mm (in)	Core Height cm (in)	Loading N/m^2 (psi)	Buckling Pressure N/m^2 (psi)
0.13 (0.005)	0.64 (0.25)	175 (0.0254)	3,700 (0.537) [1,5]
0.13 (0.005)	0.89 (0.35)	183 (0.0266)	7,500 (1.087) [1,5]
0.13 (0.005)	1.3 (0.5)	196 (0.0284)	16,200 (2.351) [1,4]
0.25 (0.010)	0.64 (0.25)	210 (0.0304)	4,600 (0.665) [1,5]

In the above table, the "Loading" is the combined weight of the shield and insulation blanket. The buckling pressure is the general instability pressure and the numbers within the brackets give the axial and circumferential numbers of buckling waves. The table seems to indicate a substantial margin between the buckling pressure and the applied loading (3700/175=21) in the first case, for example), but we have to remember that the honeycomb is treated as a homogeneous layer and not as a structure built up of very thin plates,

unsupported on one edge. To make an assessment of the local buckling modes, a second series of PANDA analyses were made as follows.

The honeycomb was modeled as "rings" and "stringers" spaced 0.76 cm (0.3 in) apart (1.3 spaces per cm, as in the honeycomb). Thus, a square pattern results, not a hexagonal as in the honeycomb. The ring/stringer model is conservative; there is a smaller amount of stiffening material than in the honeycomb, and the "ring" and "stringer" stiffeners are not attached to each other at their intersections. The results obtained in this analysis are listed in the following table:

Skin Thickness mm (in)	Core Height cm (in)	Loading N/m^2 (psi)	Buckling Pressure N/m^2 (psi)
0.13 (0.005)	0.64 (0.25)	175 (0.0254)	515 (0.0747), ring buckling, n=272

Here the "ring" part of the honeycomb buckles (or rolls) at a much lower load than the general instability load found for the two-layer shell model discussed above. (General instability loads for the ring/stringer model was 2455 N/m^2 (0.355 psi). These loads are lower than the corresponding loads for the two-layer skin model; this is so because of the smaller amount of stiffening in the square stiffener pattern.) The 272 waves correspond to a wave length of 0.76 cm (0.3 in), which is the same as the spacing of the rings. The actual honeycomb material, with its shorter unsupported plate lengths, must have a higher buckling load than the one given in the table above.

To summarize: the above-described analyses indicate that the vapor shield with a 0.13 mm (0.005 in) face and a 0.64 cm (0.25 in) high honeycomb core will survive a 10-g loading with an extra margin of 515/175=2.9.

5.1.2.3 Shield Attachment Analysis. Since the vapor-cooled shields are supported off the 12 PODS struts, it is important they do no exert enough force on the struts to thermally short out the load pins in orbit. This load can develop due to the different contraction values for the vacuum shell, struts, tank and the vapor-cooled shields as the temperatures change from ground hold values to orbit values. Worst case mismatch values between the strut and the vapor-cooled shield were calculated to be, for a T_H = 200K (360R) case:

	Δ Movement mm (in)	
Radial	0.89 (0.035)	Based on the selected design shown later in Fig. 5.22
Axial	0.48 (0.019)	
Circumferential	0.13 (0.005)	

These values require an attachment design that permits this amount of movement by either shield deflection or attachment deflection.

5.1.3 Support System Analyses

In order to prevent the PODS support system from thermally shorting out in orbit, the six supports attached to the tank and the six supports attached to the instrument flange support must either:

1. Be allowed to move independently of each other in the axial direction as the tank and instrument cooldown to < 2K (< 3.6R) and the vacuum shell temperature fluctuates in orbit; or

2. The strut spacing between the six pairs of struts must be set so the forced change in length of a strut is < 0.13 mm (< 0.005 in) with the primary tank and instrument structurally joined.

Six supports can be used to independently support the primary tank and another six struts support the instrument as long as the six attach points are in a common plane. Six supports provide a statically determinate support system but the tilt loads can be higher than when the tank and experiment are tied together structurally, i.e., the first alternative requires the use of a mechanical link between the tank and instrument such that axial movement can occur but lateral movement is restricted. A linear ball bushing or scissors links satisfies this requirement although there are questions whether the links would be stiff enough in the lateral direction and whether cryodeposits might freeze the linkage and prevent movement. The magnitude of the required movement is set by the axial spacing of the six pairs of struts, i.e., 0.086 cm (0.034 in) for a typical spacing of 1.3 m (52.8 in).

The second alternative requires setting the strut spacing, L_S, such that the forced change in length of the strut is < 0.13 mm (< 0.005 in). Figs. 5.3, 5.4 and 5.5 illustrate in three different views how the pinned end struts move when both the tank and the vacuum shell temperatures are reduced. The movements are artificially divided along separate axes for each effect, i.e., tank shrinkage, strut shrinkage, and vacuum jacket shrinkage, to better illustrate how the movements were calculated. In actuality, this movement occurs simultaneously.

For tank cooldown, the "thermal null" point occurs when:

$$L_S/2\ (\Delta L/L) = BC + CD$$

where

- $L_S/2$ is defined in Fig. 5.3
- $\Delta L/L$ is the unit change in length of aluminum going from 300 to 2K (540 to 3.6R)
- Lengths BC and CD are defined in Fig. 5.3

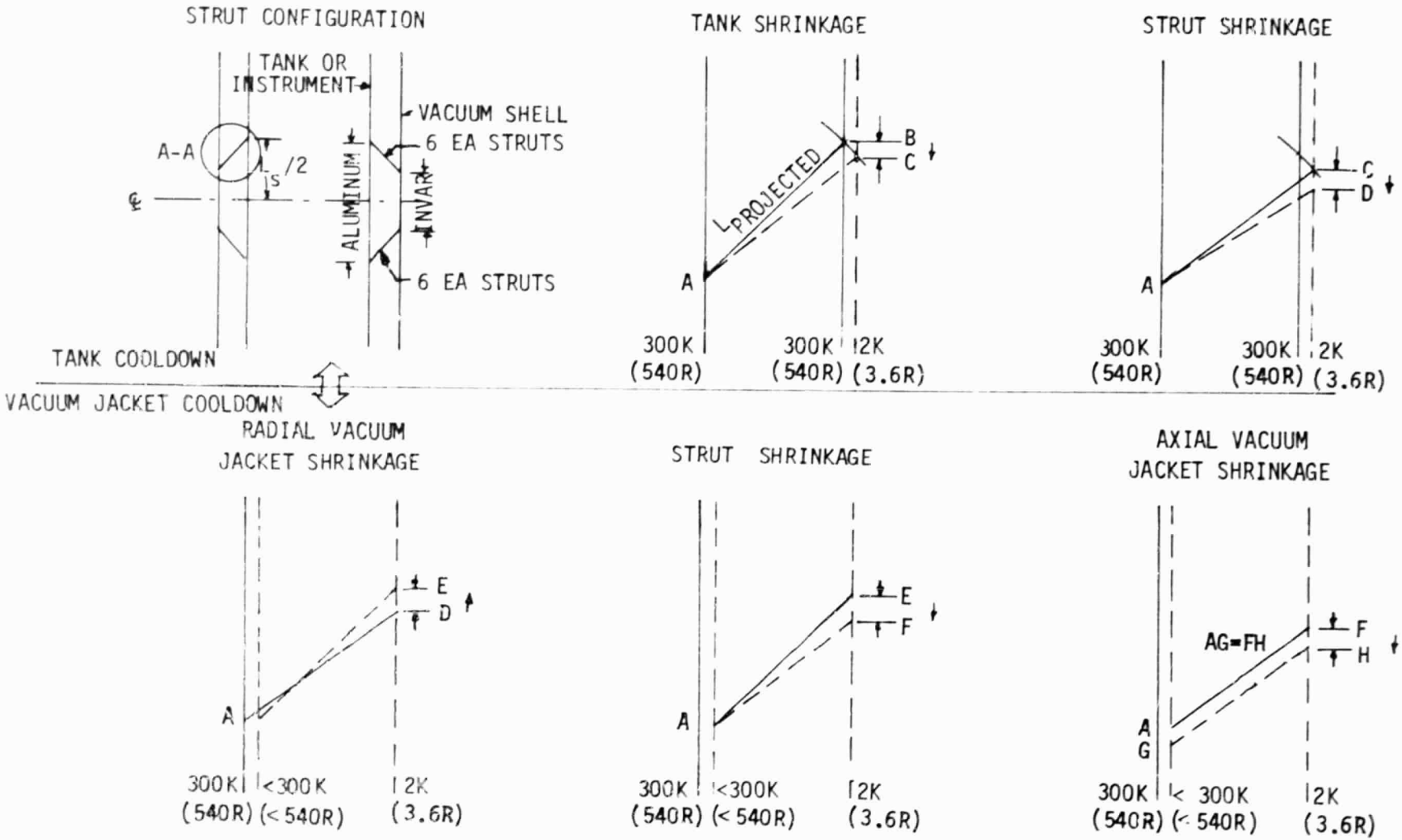

Fig. 5.3 Thermally Induced Strut Movement, Cross Section Side View No. 1

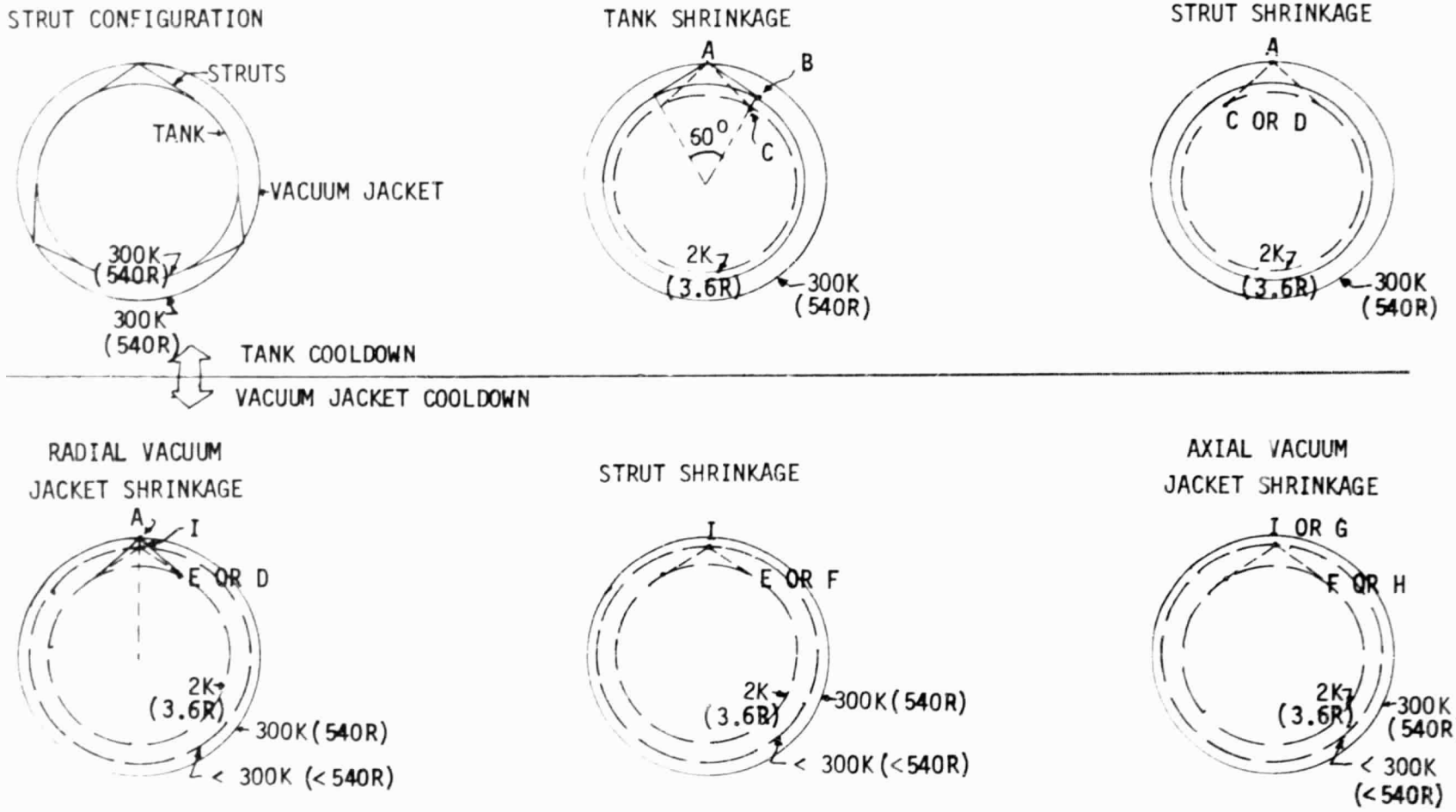

Fig. 5.4 Thermally Induced Strut Movement, Top View

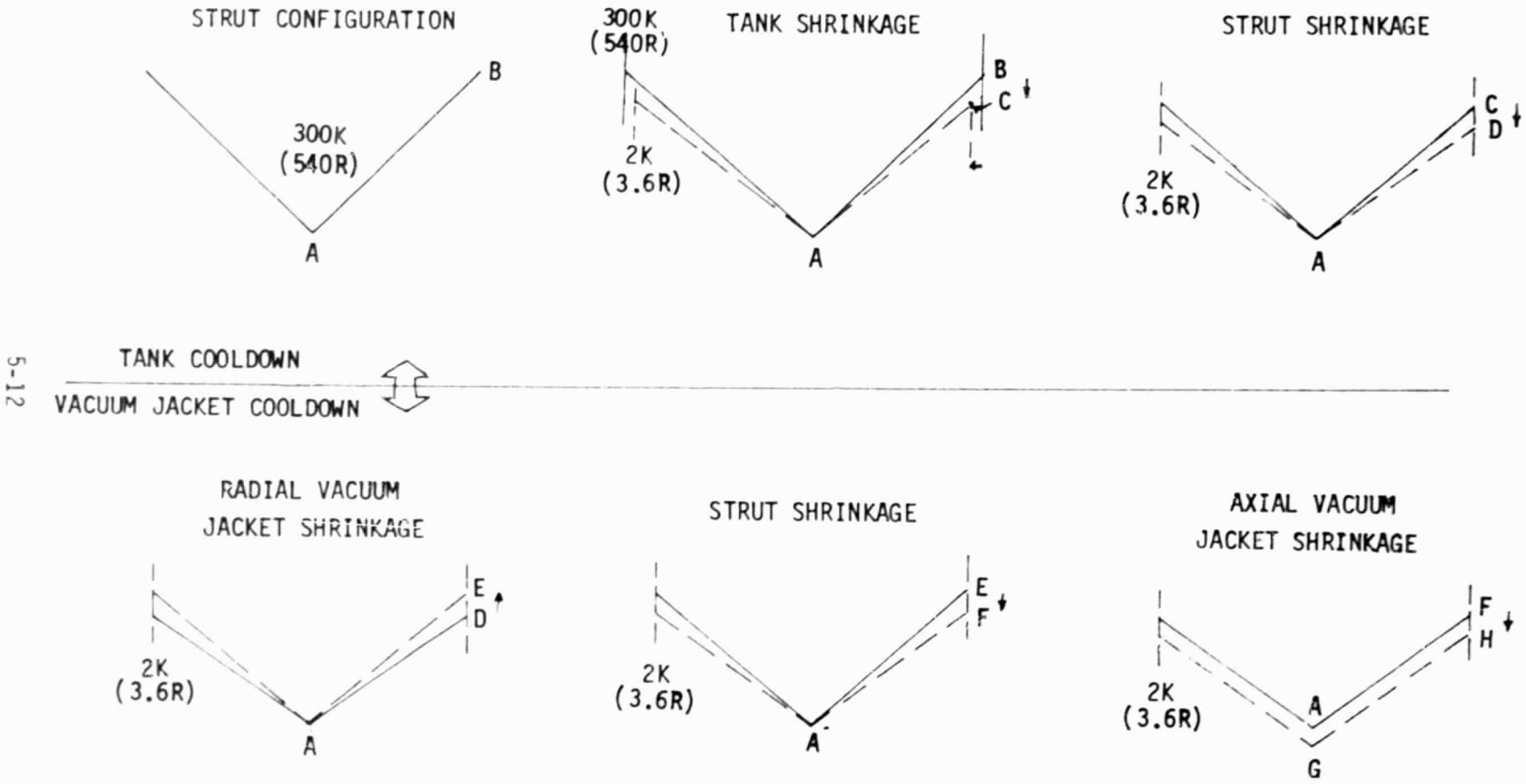

Fig. 5.5 Thermally Induced Strut Movement, Side view No. 2

For vacuum shell cooldown (after the tank and instrument are at 2K (3.6R)), the "thermal null" point occurs when:

$$L_S/2\ (\Delta L/L) = BC + CD + EF + FH - ED$$

where lengths EF, FH and ED are defined in Fig. 5.3.

The thermal null value for L_S was calculated and plotted vs. the vacuum shell temperature in Fig. 5-6.

An average value of L_S was then chosen, 93.6 cm (36.85 in) that minimized the forced change in strut length as the Invar vacuum shell temperature changed over a typical range in orbit. Note in Fig. 5.7 the forced change in strut length over the vacuum jacket temperature range of 100 to 250K (180 to 450R) never exceeded 0.044 mm (0.0017 in), well within the allowable limits of 0.127 mm (0.005 in). Also note the L_S value can be varied slightly without affecting the forced strut length change significantly.

A PANDA/DEWAR run was performed using the selected L_S value of 93.6 cm (36.85 in) as shown in Table 5.1. The orbit conductance value was increased 63% over a system where L_S was allowed to optimize based on structural and resonance considerations only. (If the helium tank configuration was changed to a toroid surrounding the instrument, this orbit increase would be much less because the tilt frequency margins are sizing the supports (Table 5.1) due to the long, narrow design. A dewar with a toroidal tank is 40% shorter than the current design.)

The prelaunch conductance drops to near the orbital value (depending on T_H) because the larger S-glass strands can now support the fully loaded tank and

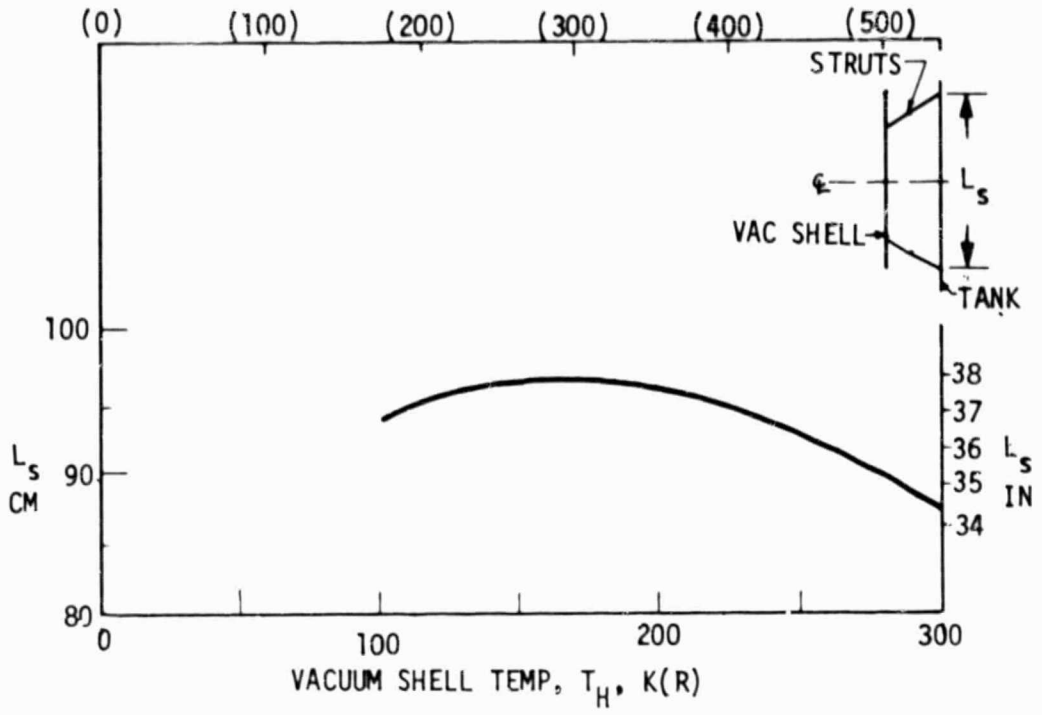

Fig. 5.6 Thermal Null Value of L_S

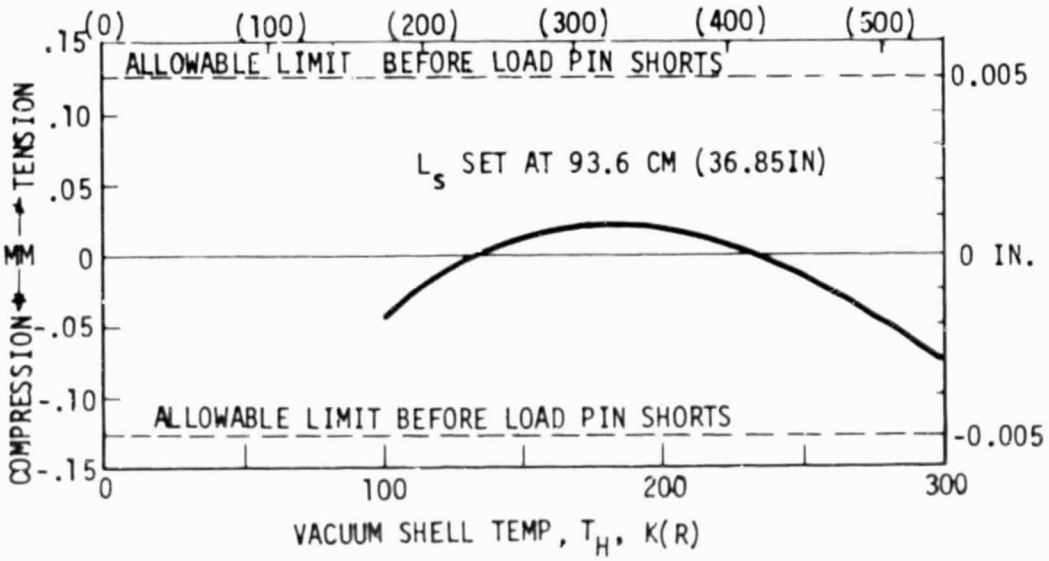

Fig. 5.7 Forced Changes in Strut Length Due to Changes in the Vacuum Shell Temperature

Table 5.1 SUPPORT ANALYSIS

```
   DEWAR PODS CONCEPT (ONE POD).  1215 LBS.  Ls = 36.85

EFFECTIVE HEAT LOSS FACTORS FOR LAUNCH AND ORBIT
(KA/L) FOR LAUNCH, ORBIT  =  4.1732E-03  2.8009E-04

WEIGHT AND LENGTH OF SUPPORTED EQUIPMENT.
    TOTAL WEIGHT                              =  1.2200E+03
    PAYLOAD WEIGHT (INSTRUMENT PACK)          =  4.8000E+02
    TANK WEIGHT (CRYOGEN + CONTAINER)         =  4.0874E+02
    VAPOR  SHIELD + INSULATION WEIGHT         =  3.3126E+02
    LENGTHS OF TANK  SHIELD  5.4040E+01  1.3284E+02

CG LOCATION AND MOMENTS OF INERTIA OF SUPPORTED EQUIP
CG LOCATION (FROM AFT END OF TANK)            =  5.6100E+01
POLAR MOMENT OF INERTIA                       =  9.3077E+02
MOMENT OF INERTIA FOR TILTING                 =  3.3589E+03
    TANK + CRYOGEN TILTING                    =  1.2559E+03
    VAPOR  SHIELD + INSULATION TILTING=  1.5954E+03
    PAYLOAD (INSTRUMENT PACKAGE) TILT =  5.0760E+02

LAUNCH & ORBITAL FREQUENCY CONSTRAINTS=  3.5000E+01  2.0000E+01
AXIAL AND LATERAL LAUNCH ACCEL  IN G S=  1.0000E+01  1.0000E+01
YOUNGS MODULUS OF TUBE MATERIAL               =  6.0000E+06
MAX  ALLOWABLE STRESS OF TUBE MATERIAL=  5.0000E+04

CONDUCTIVITIES (BTU/(HR-IN -DEG F)) FOR SUPPORT
CONDUCTIVITY, K1, OF TUBE OR STRAP            =  2.7900E-02
CONDUCTIVITIES (SGLAS) OF HOT,COLD END=  1.0000E+06  7.2200E-03

INNER RADIUS OF CRYOGENIC TANK                =  0.0000E+00
OUTER RADIUS OF TANK AND PAYLOAD              =  1.9700E+01
INNER RADIUS OF VACUUM SHELL                  =  2.7200E+01
LENGTH OF RIGID PART OF SUPPORT,
    EXCLUDING LENGTHS OF SGLAS MEMBERS=  2.4000E+00

MARGIN ON MAXIMUM STRESS DURING LAUNCH=  2.0803E+00
MARGIN ON COLUMN BUCKLING AT LAUNCH           =  2.3287E+00
MARGIN ON SHELL  BUCKLING AT LAUNCH           =  5.5495E+00
MARGIN ON TUBE THERMAL STRESS                 =  4.2965E+00

STRUT LENGTH, TUBE LENGTH (PL. TUBEL)         =  1.7618E+01  1.2218E+01
AXIAL SPACING OF DEWAR SUPPORT RINGS          =  3.6801E+01
STRUT ANGLES                (THETA, GAMMA)    =  7.4171E+01  3.6542E+01
TUBE CROSS SECTION (AREA, INNER DIAM)         =  1.5229E-01  1.1015E+00
TUBE WALL THICKNESS, R/T RATIO                =  4.2380E-02  1.3495E+01
PRETENSION  (ONLY FOR TENSION STRAP )         =  0.0000E+00
LAUNCH FREQ. MARGINS, (LATERAL, TILT)         =  1.2319E+00  1.0000E+00
LAUNCH FREQ. MARGINS, (AXIAL, TORSION)        =  1.2958E+00  1.9240E+00


AXIAL LENGTH OF SGLASS TENSION MEMBER         =  1.5000E+00
CROSS SECTION AREA OF SGLASS MEMBER           =  7.9578E-04
ORBITAL FREQ. MARGINS, (LATERAL, TILT)=  1.2318E+00  1.0000E+00
ORBITAL FREQ. MARGINS, (AXIAL,TORSION)=  1.2957E+00  1.9240E+00
```

instrument without thermally shorting out the load pins. (For purposes of optimizing the fiberglass tube dimensions for launch, the PANDA-DEWAR program assumes the load pins are shorted; consequently, the launch conductance value shown in Table 5.1 is correct for launch but not for prelaunch ground hold.) Since the orbit heat leak for the vapor cooled struts with the selected L_S value is currently 3.1 mW, this amounts to a 1.2 mW increase over supports where L_S is allowed to optimize (a 5% increase in the total heat rate, not a significant change). Consequently, this method of support (Invar vacuum ring plus a thermal null value of L_S) was selected over the use of linear ball bushings or scissor linkages, because it is completely passive requiring no moving parts and has a minimal thermal impact.

During the dewar development program, accurate thermal contraction data will be obtained on assembled struts, invar and aluminum to set an accurate value of L_S.

5.1.4 Plumbing Analyses

Sizing analyses were performed on the porous plug, vent line and burst discs.

5.1.4.1 Porous Plug Sizing. The porous plug was sized based on the test data obtained by Lockheed [5.1] and shown in Fig. 5.8.
The helium vent rate for this dewar is ~ 9 cc/sec (0.06 in^3/sec). It is desired to keep the pressure drop across the plug down to < 1.0 torr (0.02 psi) so the flow area has to be increased (using a safety factor of 10) to

$$10\left(\frac{9\ \text{cc/sec}}{2.5\ \text{cc/sec}}\right) 1.27\ \text{cm}^2 = 45.7\ \text{cm}^2\ (7.1\ \text{in}^2)$$

or a diameter of 7.6 cm (3.0 in).

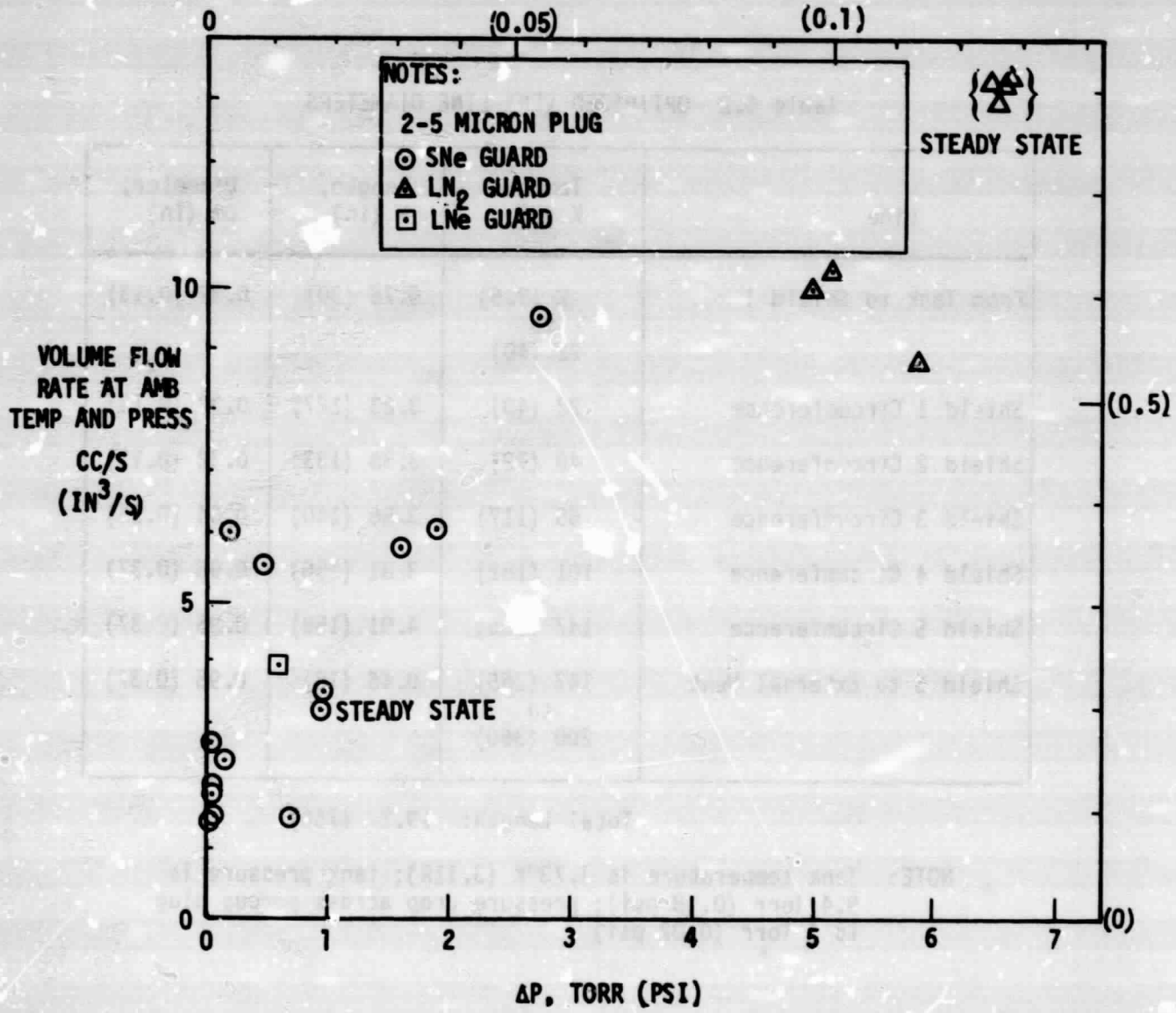

Fig. 5.8 Porous Plug Test Data

5.1.4.2 Vent Line Sizing. The vent line size was optimized for a helium dewar temperature of 1.73K (3.11R) using the PRESS program as shown in Table 5.2. Note the line diameters for shields 4 and 5 are larger than the honeycomb thickness of the shield, 0.64 cm (0.25 in). Consequently, elliptical or rectangular tubing of an equivalent area is required for these shields to prevent the tubing from protruding beyond the shield.

Table 5.2 OPTIMIZED VENT LINE DIAMETERS

Line	Temp, K (R)	Length, M (in)	Diameter, cm (in)
From Tank to Shield 1	2 (3.6) to 22 (40)	0.76 (30)	0.32 (0.13)
Shield 1 Circumference	22 (40)	3.23 (127)	0.32 (0.13)
Shield 2 Circumference	40 (72)	3.38 (133)	0.32 (0.13)
Shield 3 Circumference	65 (117)	3.56 (140)	0.64 (0.25)
Shield 4 Circumference	101 (182)	3.81 (150)	0.95 (0.37)
Shield 5 Circumference	147 (265)	4.01 (158)	0.95 (0.37)
Shield 5 to External Vent	147 (265) to 200 (360)	0.46 (18)	0.95 (0.37)

Total Length: 19.2 (756)

NOTE: Tank temperature is 1.73°K (3.11R); tank pressure is 9.4 Torr (0.18 psi); pressure drop across porous plug is 1 Torr (0.02 psi)

5.1.4.3 Burst Disc Sizing. An extreme emergency condition was postulated where the vacuum shell is punctured and air is rapidly solidifying on the

superfluid helium tank and instrument shroud and on the normal helium torus tank and first vapor cooled shield. The heat rate to each tank was taken from Fig. 5.9 [5.2] based on their respective surface areas. The "Cryostat with MLI" curve was used.

	Area m^2 (ft^2)	Max. Heat Rate W (Btu/hr)
Superfluid tank plus instrument shroud	19.5 (210)	0,000 (375,000)
Torus tank plus first vapor cooled shield	23.9 (257)	140,000 (475,000)

Since the heat rates were about equal, calculations of the required burst disc diameter were made using the PRESS program for only the higher value . The diameter is plotted as a function of the tank pressure in Fig. 5.10.

This calculation assumes the helium is dumped directly into the instrument cavity. A burst disc on the vacuum shell Invar ring then dumps the helium outside the dewar. The gas couldn't be routed directly out of the dewar because the line sizes were getting so large the orbit heat rates down the lines became excessive.

For the torus tank, a burst disc diameter of 5.1 cm (2.0 in) was selected. For the primary tank, the burst disc should be larger because air will also be solidifying on an instrument of unknown area that is conductively coupled to the tank. The primary tank burst disc diameter was arbitrarily doubled to 10.2 cm (4.0 in) to account for the instrument.

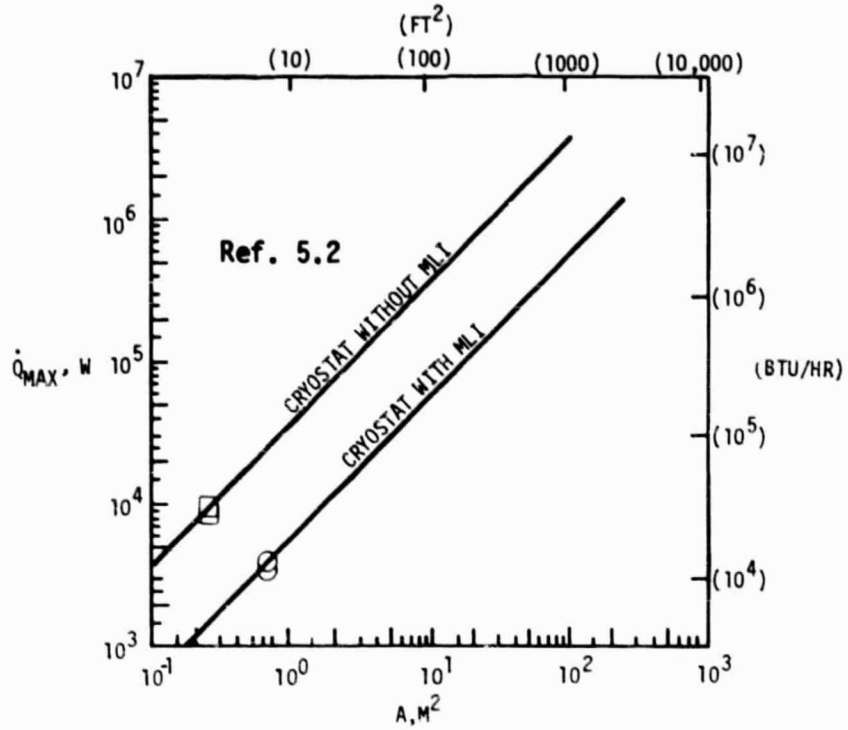

Fig. 5.9 Measured Peak Heat Rates of Helium Dewars Exposed to Air

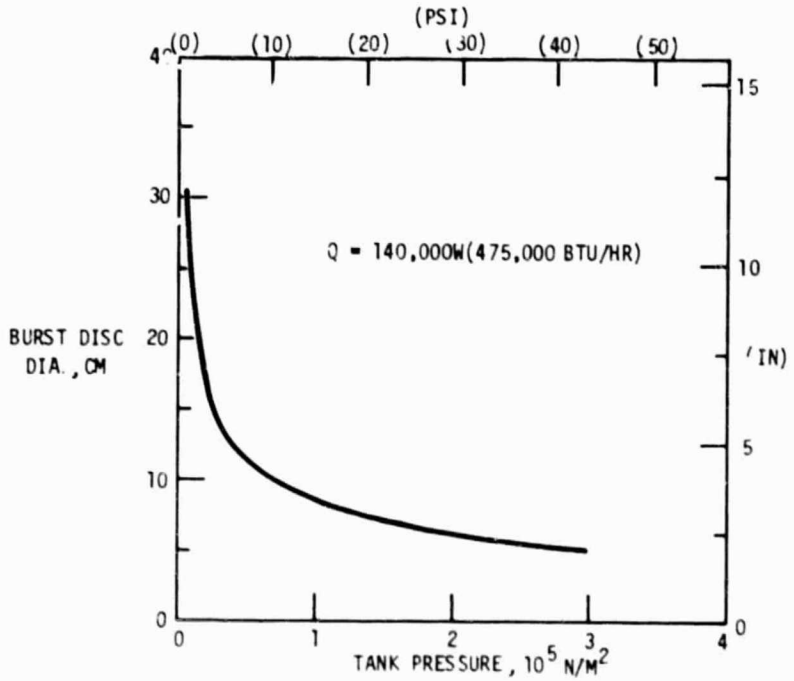

Fig. 5.10 Burst Disc Diameter as a Function of Tank Pressure

5.1.5 Ground Hold Analyses

Once the single stage helium dewar is installed in the Orbiter and loaded with superfluid helium, it is desirable, from an Orbiter servicing point of view, not to require further dewar servicing. From the Orbiter timelines, it appears desirable to have greater than a 10-day prelaunch hold capability for the dewar (although servicing up to a day prior to launch is feasible).

To see what ground hold capability the reference subatmospheric pressure superfluid helium dewar has, a calculation was made on the time it takes for the nonvented tank temperature to rise from 1.73 to 2.0K (3.1 to 3.6R). From Table 5.3, the maximum allowable ground hold time is 0.6 days.

Table 5.3 COMPARISON OF GROUND HOLD METHODS

No.	Concept	Ground Hold Time Without Servicing (Days)	$\frac{Q_{GROUND\ HOLD}}{Q_{ORBIT}}$ Superfluid Helium Tank	Added Weight (Dewar or Flight Equipment)	Comments
Ref	Hold Superfluid Helium Tank Non-vented	0.6(1)	65	---	This method is unacceptable unless ground hold times are kept very short.
1	Add Normal Helium, Helium Tank for Ground Hold Cooling (see Fig. 5.11)	12	0.13(3)	3.5 LHe 4.3 Torus 1.0 Plumbing 8.8 Kg (19 lb)	The helium tank can be sized for any ground hold period. Minimal shuttle interfaces.
2	Shuttle Onboard Pumping System (See Fig. 5.11)	As long as required (2)	1.3(4)	24.5 Pump(5) 2.0 Controls 1.5 Plumbing 2.0 Supports 33.0 Kg (73 lb)	The on-board pumping system requires power from the Orbiter during prelaunch; line separation system for free flyer mission (operates only during prelaunch).

NOTES:

(1) For a temperature rise of 1.73K to 2.0K (3.1R to 3.6R)

(2) The ground hold period can be extended with an equivalent loss of orbital life as shown.

(3) The first vapor-cooled shield is shorted to the torus tank; consequently, the heat rate into the primary tank is extremely low due to the 4.2K (7.6R) boundary. Also, the PODS supports are not shorted out in one-g.

(4) The higher heat rate is due to the higher warm boundary temperature of 300K (540R) as compared to orbit.

(5) Leybold Heraeus D2A pump.

Since holding the tank non-vented did not provide an adequate ground hold time, two other ground hold concepts were examined.

5.1.5.1 Concept 1: Normal Helium Tank. To extend the ground hold period and reduce the orbit weight penalty, a one atmosphere pressure, 4.2K (7.6R) helium torus tank plus one additional valve was added to the dewar as shown in Fig. 5.11. The tank is thermally shorted to the first vapor cooled shield to intercept the ground hold parasitic heat load. During ground hold, the normal helium vapor is vented through all of the vapor cooled shields. The tank can be located inside the 1.7K (3.1R) enclosure because the radiation heat transfer is negligible between the torus and the superfluid helium tank. The subatmospheric pressure superfluid helium tank is non-vented during ground hold. Table 5.3 shows the added bottle, helium and plumbing weight, 8.8 kg (19 lb), for a 12-day prelaunch ground hold.

5.1.5.2 Concept 2: Onboard Pumping System. To keep the superfluid helium tank at 1.7K (3.1R), a pumping system is located onboard the Orbiter to maintain the appropriate low pressure in the tank as shown in Fig. 5.11. The pumping system flies with the Orbiter but is operated only during the prelaunch phase. In orbit, the dewar vent line is separated from the pumping system prior to dewar ejection from the cargo bay; the pumping system remains in the Orbiter. This system has a higher heat rate into the superfluid helium tank by a factor of 10 over Concept 1, and the added system weight is higher, 33 kg (73 lb) vs. 8.8 kg (19 lb). For orbital altitudes higher than the Orbiter is capable of achieving, i.e., requiring the use of the IUS, the added dewar weight becomes more important. Comparison of Concepts 1 and 2 shows Concept 2 is 4.3 kg (9.5 lb) lighter.

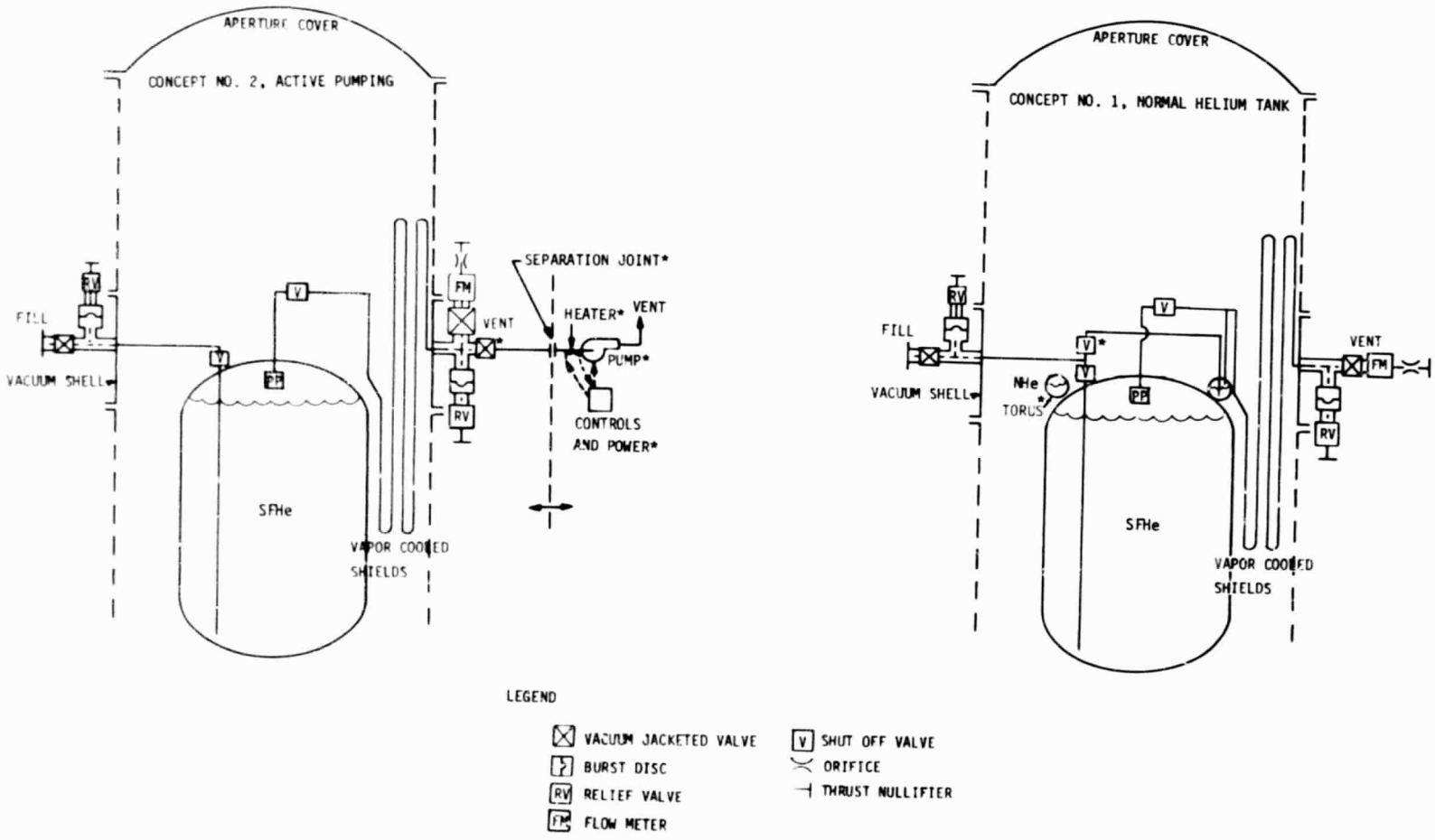

Fig. 5.11 Ground Hold Candidates

Concept 1	5.3 kg	(11.7 lb)	(tank, plumbing)
Concept 2	1.0 kg	(2.2 lb)	(one valve)
Δ	4.3 kg	(9.5 lb)	

5.1.5.3 Selected Concept. Concept 1 has been selected for the reference design for the following reasons:

1. A nonvented tank without cooling or pumping does not provide adequate ground hold times with acceptable weight penalties.
2. Concept 1 is lighter by ~ 24 kg (53 lb), has a lower heat rate into the superfluid tank by a factor of 10 and has simpler orbiter interfaces than Concept 2.
3. The slight dewar weight advantage for Concept 2, 4 kg (8.8 lb), at higher orbital altitudes is not significant enough to justify selection of Concept 2.

5.1.6 Vacuum Shell Analysis

The vacuum shell is divided into four parts: 1) the center invar ring to which the 12 PODS supports are attached; 2) the aft cylinder/dome; 3) the forward cylinder; and 4) the aperture cover. Analyses were performed on the cylinder/dome and cylindrical sections to determine which material should be used and the ring and membrane dimensions required. The required buckling pressure capability of the shell is set at

$$1.03 \times 10^5 \text{ N/m}^2 \; (1.5)/(0.7) = 2.21 \times 10^5 \text{ N/m}^2$$

or

$$(15 \text{ psi}) \; (1.5)/(0.7) = 32 \text{ psi}$$

where 1.5 is a safety factor and 0.7 is a knockdown factor to account for manufacturing imperfections.

Of the two cylindrical segments, the longer one (cylinder only) is the buckling-critical one. A preliminary analysis (Baruch-Singer) indicated that this cylinder buckles in 4 circumferential waves. Based on this, a STAGS model was set up and subjected to a bifurcation buckling analysis. Figure 5.12 shows the STAGS model and the buckling mode shape.

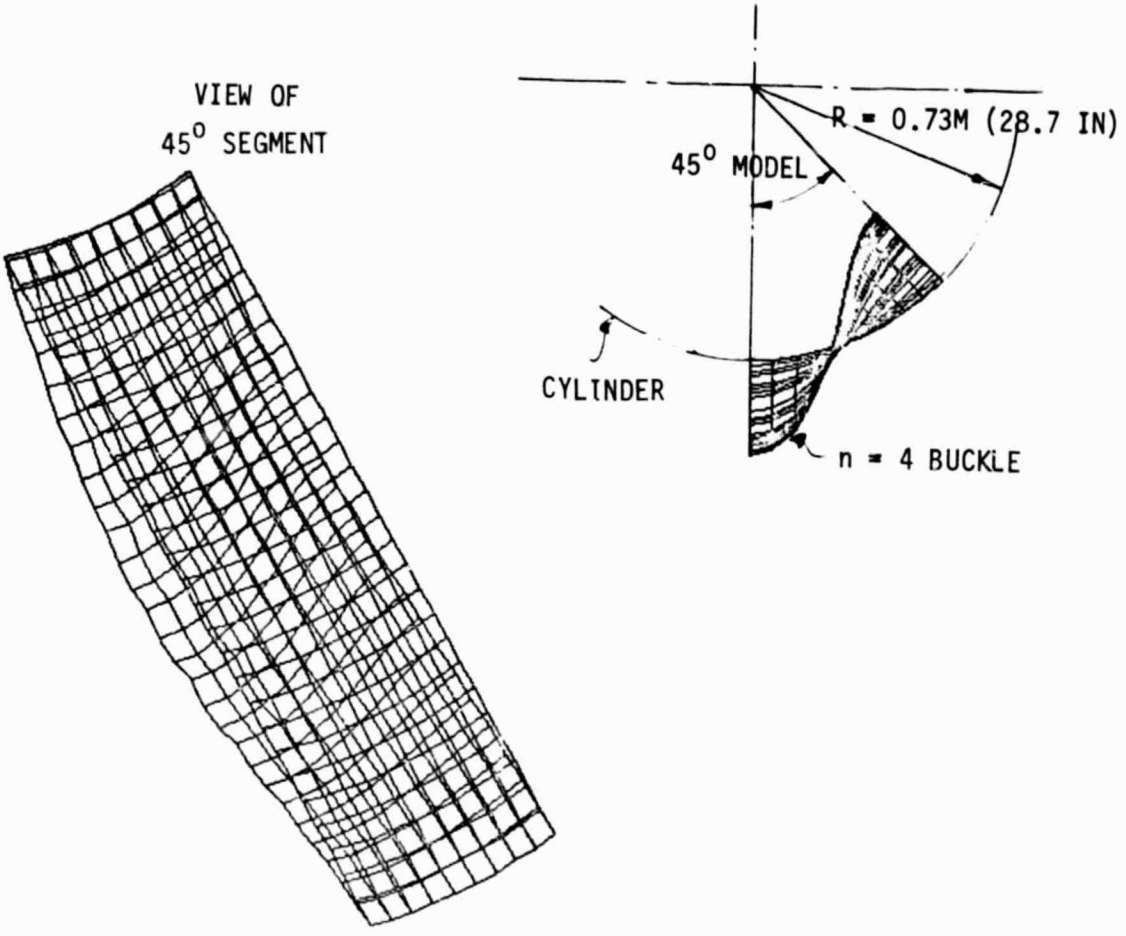

Fig. 5.12 Vacuum Shell Buckling Mode Shape

A weight analysis was then performed on the cylinder only section for Invar, 6Al 4V titanium and 6061 aluminum. Using PANDA, the buckling pressure was set at

1.03×10^5 N/m^2 (32 psi) in a general instability mode with four circumferential waves. The ring thickness was set and the ring spacing was varied. The optimum ring height, membrane thickness and cylinder weight was calculated and plotted in Figs. 5.13 and 5.14. Note a substantial weight penalty is incurred going to an all Invar shell.

The aluminum vacuum shell is the lightest weight and is also the lowest cost shell to build. Consequently, a design concept was developed where an Invar flange transitions into an aluminum vacuum shell as shown in Fig. 5.15.

A simplified model with a symmetry plane replacing the ring is shown in Fig. 5.16. Versions of this model were used for preliminary analyses of the joint.

The joint is fabricated at 300K (540R), and subsequently baked out at 350K (630R) and cooled to 100K (180R) in orbit. The worst case is the cooling. During the cooling, the aluminum contracts in the radial direction about 0.25 cm (0.1 in) while the Invar section only wants to contract some 0.06 cm (0.025 in). But the twain must meet, so forces are applied which create stresses. There is no way to avoid these stresses by beefing up the material, a thickness increase in one material will result in a stress increase in the other.

There are two stress problems in the joint which are addressed here.

Assuming that the bond between the Invar and aluminum is intact, the structure behaves as a shell structure with variable thickness layered skin (the skin is layered Invar-aluminum-Invar in the joint area). This problem is solved by thin-shell analysis, in this case with the help of the STAGS finite element

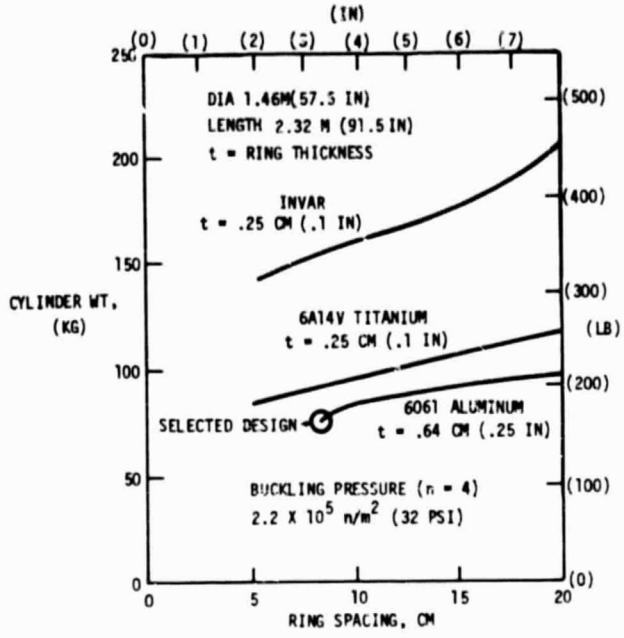

Fig. 5.13 Vacuum Jacket Weight vs. Materials

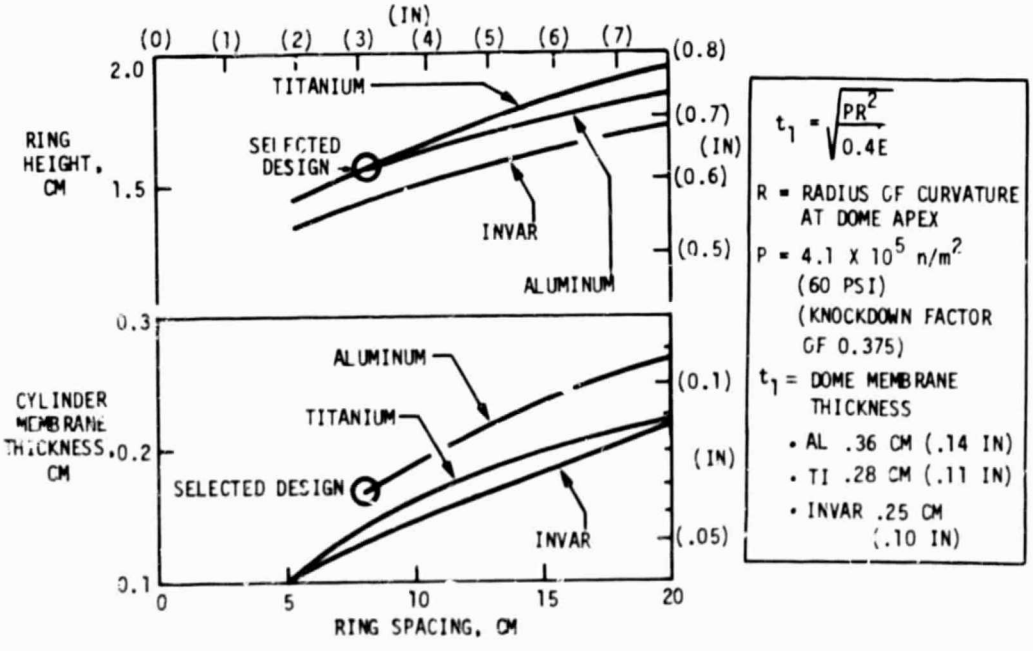

Fig. 5.14 Vacuum Jacket Dimensions

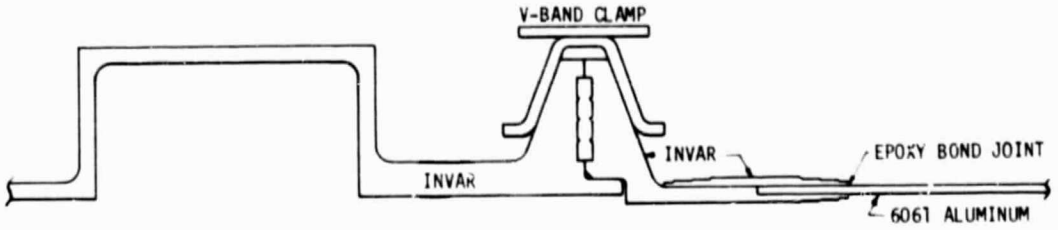

Fig. 5.15 Vacuum Jacket Invar/Aluminum Joint

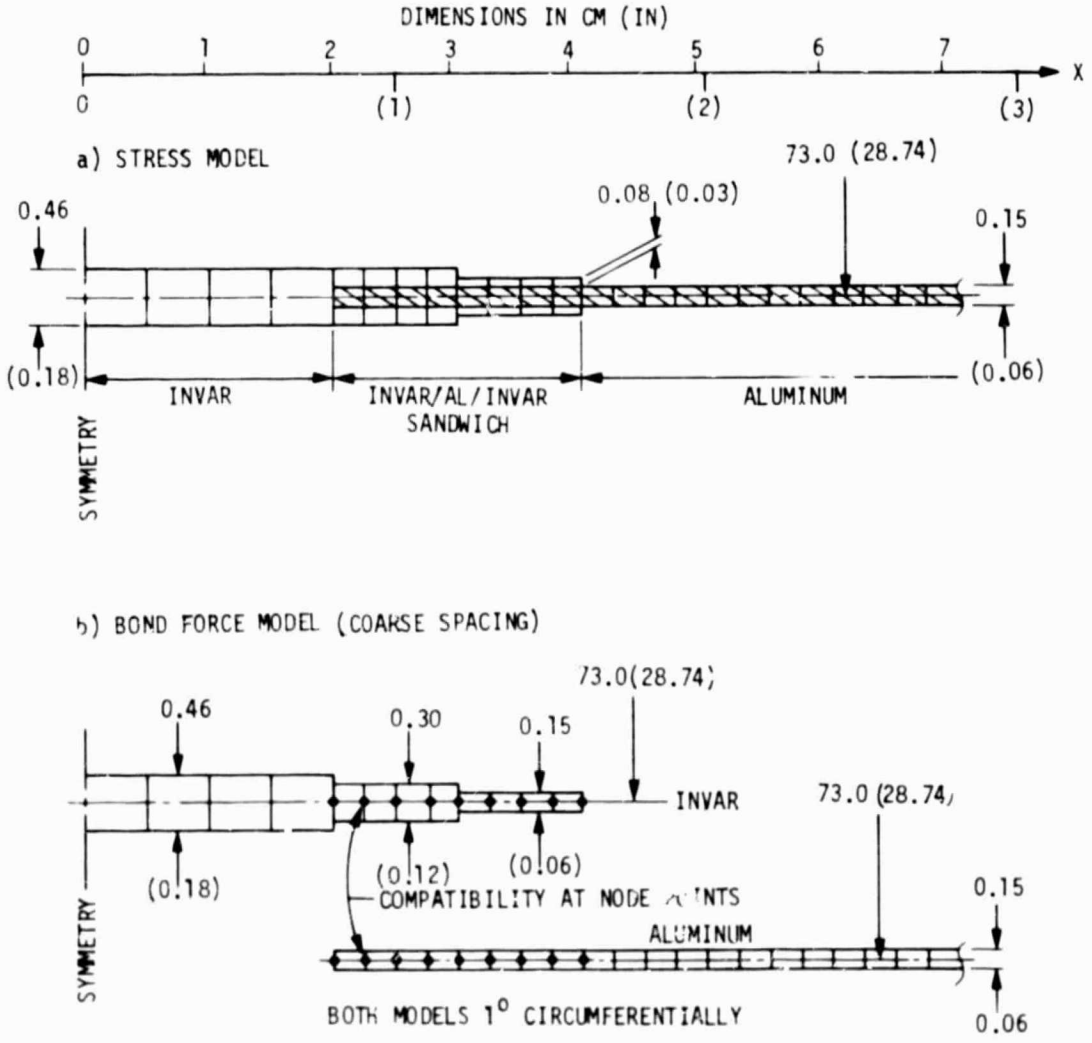

Fig 5.16 Vacuum Jacket Invar/Aluminum Joint, STAGS Models, Thick Joint

code. The STAGS stress model configuration is shown in Fig. 5.16a. Fig. 10.4 gives the thermal contraction values.

The problem of forces, particularly peeling or normal forces in the bond layer, is a particularly difficult problem, since the strength of the bond in peel is not a well-defined quantity. The approach here is to minimize the peel forces at the edge of the joint as much as possible. The analysis of this problem is most accurately made with a three-dimensional finite element code, but this is time-consuming and expensive. The peel force analysis used here employs a novel approach, again with the aid of STAGS. The invar section is modeled as a continuous layer, as shown in Fig. 5.16b. The thickness is the combined thickness of the face plates of the stress model. The centerline of the Invar section is tied to the centerline of the aluminum section withhin the bond area. In this model, the overall stiffness of the joint is somewhat underestimated, while the stiffness of the individual Invar overlaps is overestimated. The normal forces between the two shells are computed as equilibrium forces in the STAGS code. Due to the design of the model, these forces are probably over-estimated somewhat, but this is not of much concern, since we only want to study their distribution in different geometry models. (A more exact analysis could be had if the two shell segments were defined as eccentric to each other.)

Two different versions of the joint were analyzed, one with the Invar thicknesses varying as shown in Fig. 5.17 (thick joint) and one with the Invar thickness varying as shown in Fig. 5.18 (thin joint). From the results shown in Figs. 5.17 and 5.18, the maximum stresses for the two cases are:

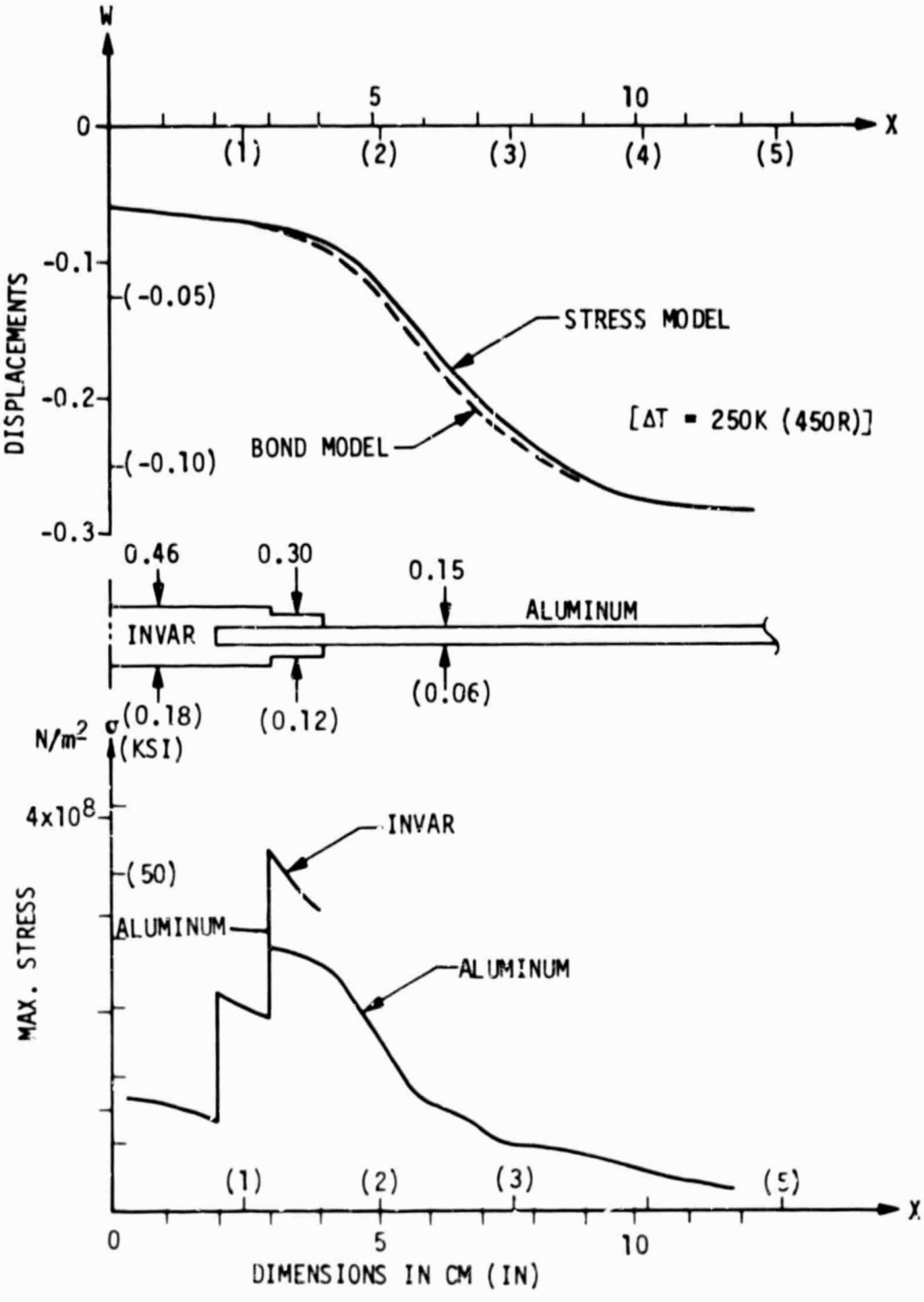

Fig. 5.17 Invar/Aluminum Joint, Temperature Stresses and Displacements, Thick Joint

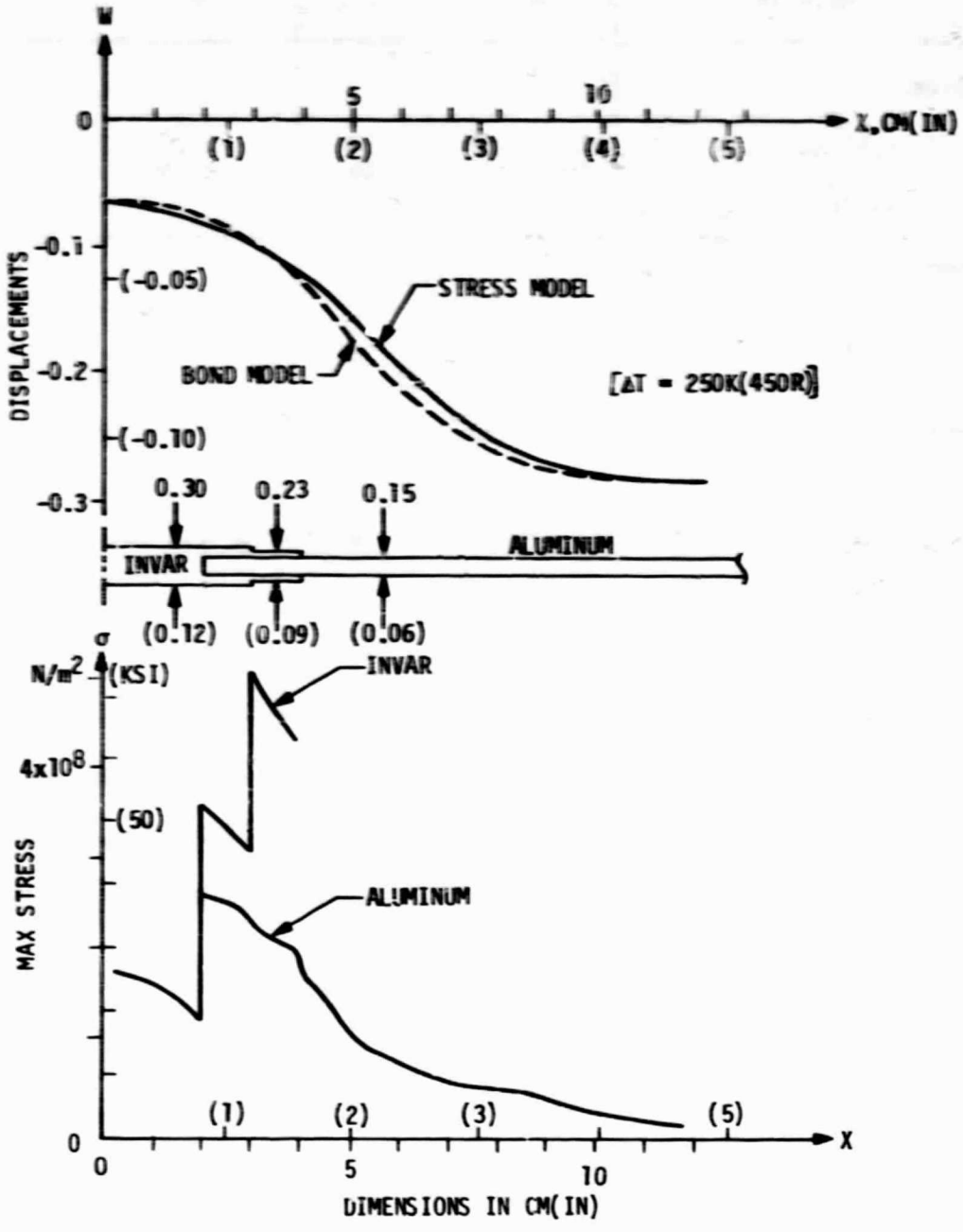

Fig. 5.18 Invar/Aluminum Joint, Temperature Stresses and Displacements, Thin Joint

C-2

	Thick Joint		Thin Joint	
Material	N/m^2	(KSI)	N/m^2	(KSI)
Invar				
Applied	3.7×10^8	54	5.1×10^8	74
Yield (Annealed)	2.3×10^8	40	2.8×10^8	40
Ratio (Yield/Appl.)	0.74		0.54	
6061-T6 Aluminum				
Applied	2.9×10^8	42	2.6×10^8	38
Yield	2.5×10^8	36	2.5×10^8	36
Ratio (Yield/Appl.)	0.86		0.95	

As can be seen, neither joint is acceptable; in both cases, the yield strength is exceeded in both materials.

Titanium has thermal expansion properties part way between Invar and aluminum as shown in Fig. 10.4 plus a much higher yield strength than either material, as shown in Table 10.1. Consequently, a new joint configuration, shown in Fig. 5.19, was analyzed that consists of a short titanium flange section and a bonded titanium to aluminum joint.

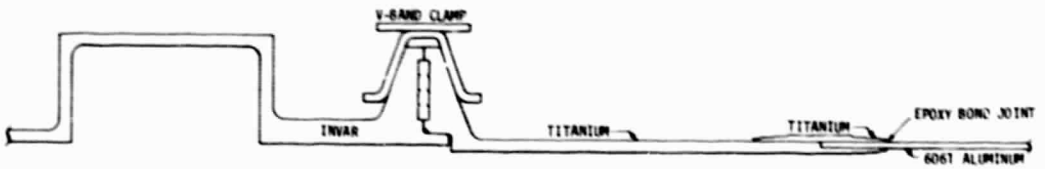

Fig. 5.19 Vacuum Jacket, Titanium/Aluminum Joint

The short titanium section moves the joint away from the stressed Invar/titanium seal area. In the seal area, the maximum temperature induced stresses in the mating Invar/titanium flanges are on the order of:

	N/m^2	(KSI)
Titanium	1.4×10^8	(20)
Invar	$< 1 \times 10^8$	(< 14)

well within their elastic limits.

At the bonded titanium/Invar joint, the maximum stresses are (ratioed from the invar/aluminum data based on the lower differential expansion values):

	Thick Joint		Thin Joint	
Material	N/m^2	(KSI)	N/m^2	(KSI)
6Al 4V Titanium				
Applied	1.8×10^8	26	2.5×10^8	36
Yield	8.2×10^8	128	8.2×10^8	120
Ratio (Yield/Appl.)	4.9		3.6	
6061-T6 Aluminum				
Applied	1.4×10^8	20	1.2×10^8	18
Yield	2.5×10^8	36	2.5×10^8	36
Ratio (Yield/Appl.)	1.8		2.0	

Ratioing the values is not quite accurate since titanium's modulus is 20% lower than Invar's, but the conclusion reached about the joint acceptability is valid because of the large margin of applied to yield stresses. Again, the stresses are within the elastic limits for both the titanium and the aluminum.

The bond force model shown previously in Fig. 5.16b yielded the results shown in Fig. 5.20 for the Invar/aluminum joint. These analyses were completed before the titanium/aluminum bond joint was selected and represents a more severe case than the selected design. Since the forces in the Invar/aluminum thin joint design appear to be reasonable, the analyses were not repeated for the titanium/aluminum bond joint since the differential temperature-induced stress is less.

Three models were analyzed: two "thick" ones (one with coarse and one with fine mesh), and one "thin". Fig. 5.20a and b gives the force distribution in the "thick" models. The forces represented in the figure are the normal forces applied to the node points. We see that the total force in the two cases is the same and the distribution similar: uniform in the interior (note that the force per unit area is the same) and spikes at the discontinuities in thickness. Of interest is the spike at the end of the joint, 36 N (8.06 lb_f) and 34 N (7.63 lb_f). This spike is the peeling force that tries to open the end of the joint. Note that this spike is practically identical in the two models. This indicates that the spacing is too coarse, even in the fine model, to define the force variation in the edge zone; all we can say there is a rapid increase of peeling force at the end of the joint.

The analysis of the "thin" joint (Fig. 5.20c) yields a much smaller spike; the total force on the edge node is less than three times the force on interior nodes, compared to almost nine times in the "thick" model. Since peel strengths of typical epoxy adhesives are on the order of 35 N/cm (20 lb/in), only the thin joint appears to be a safe design.

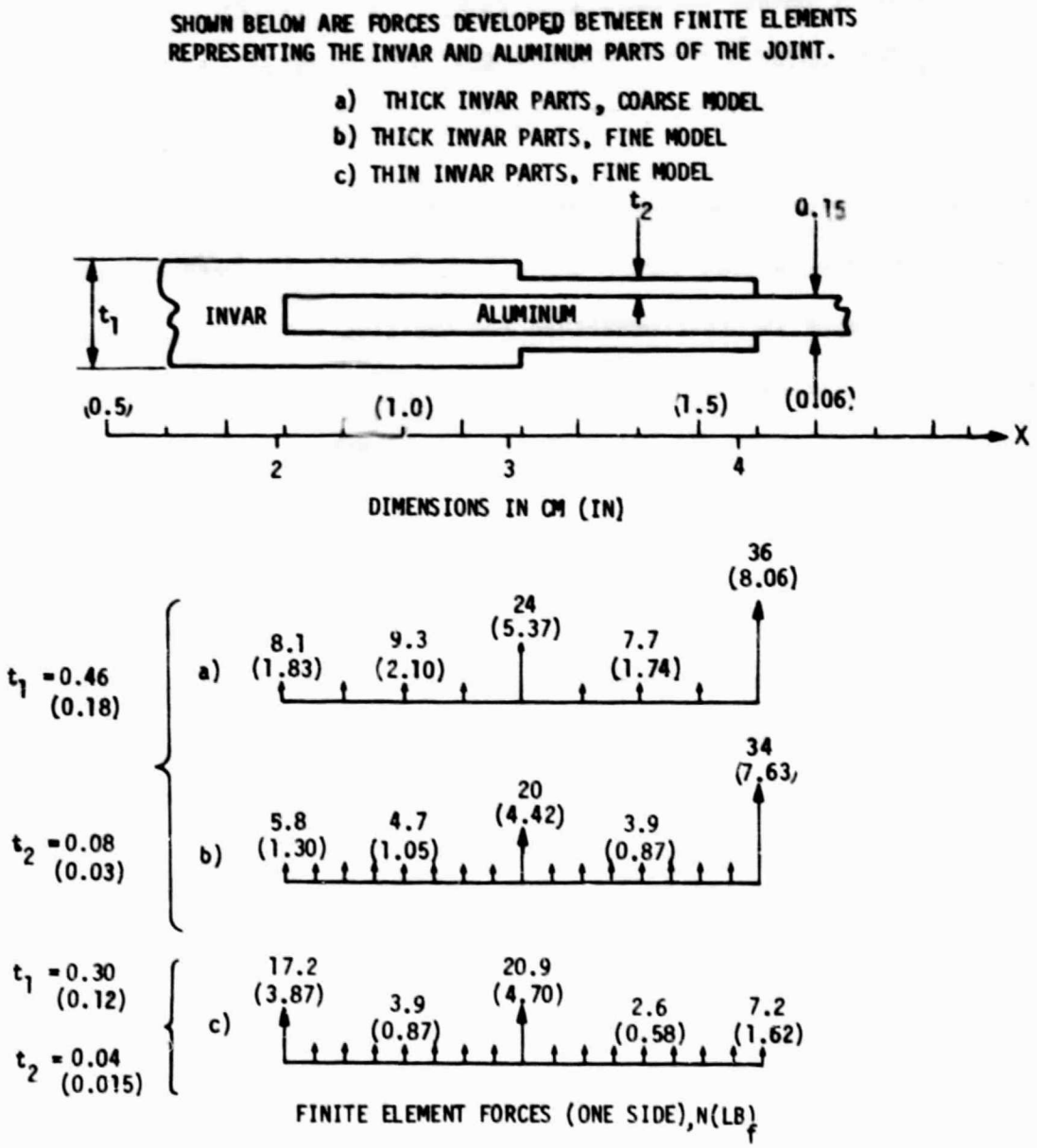

Fig. 5.20 Vacuum Jacket, Invar/Aluminum Joint Bond Forces, Thick and Thin Joints

	Peel Force at Joint End	
	N/cm	(lb_f/in)
Thick Joint	28.0	(15.2)
Thin Joint	5.7	(3.2)

The ideal situation would be if the edge node force is one half of the interior node force, then the peeling forces would be uniform in the entire joint. With a more gradual change in thickness than the two-step configurations used here, it should be possible to come close to this ideal. Consequently, a thin joint design with a smooth taper was selected for the titanium/aluminum joint.

5.1.7 Tank Analyses

The helium tank configuration is shown later in Fig. 5.23. The tank is designed by a variety of loading conditions:

External pressure, -1×10^5 N/m^2 (-15 psi) operating
Internal pressure, 4.1×10^5 N/m^2 (60 psi) operating
Accelerations, 10 "g" axial, radial

Of the two pressure loadings, the external pressure is the worst condition. An initial design was selected by comparison with the vacuum shell discussed in Section 5.1.6. This design was analyzed in the same fashion as the vacuum shell. The results are shown on the next page.

RING-STIFFENED CYLINDER

Weight kg (lb)	Cylinder Thickness cm (in)	Ring Spacing cm (in)	Ring Thickness cm (in)	Ring Height cm (in)	Buckling Pressure N/m^2 (psi)
12.4 (27.3)	0.14 (0.055)	7.6 (3.0)	0.38 (0.15)	0.79 (0.31)	2.2×10^5 (32) (n=6)*
13.3 (29.3)	0.16 (0.063)	10.2 (4.0)	0.38 (0.15)	0.81 (0.32)	2.2×10^5 (32) (n=6)
14.1 (31.1)	0.18 (0.070)	12.7 (5.0)	0.38 (0.15)	0.86 (0.34)	2.2×10^5 (32) (n=6)
14.9 (32.9)	0.19 (0.076)	15.2 (6.0)	0.38 (0.15)	0.89 (0.35)	2.2×10^5 (32) (n=6)

* Selected design

The end dome thickness is 0.28 cm (0.110 in).

5.2 DEWAR LAYOUT

Using the results of the analyses obtained in Section 5.1 plus the plumbing schematic in Fig. 5.21, the dewar preliminary design was developed on CADAM. Fig. 5.22 provides the overall dewar layout, while Figs. 5.23 through 5.26 provide details of the design. Dewar characteristics are summarized in Table 5.4.

A description of key features of the design and assembly sequences are discussed first followed by a typical operational sequence. Refer back to these figures and table while reading the following material.

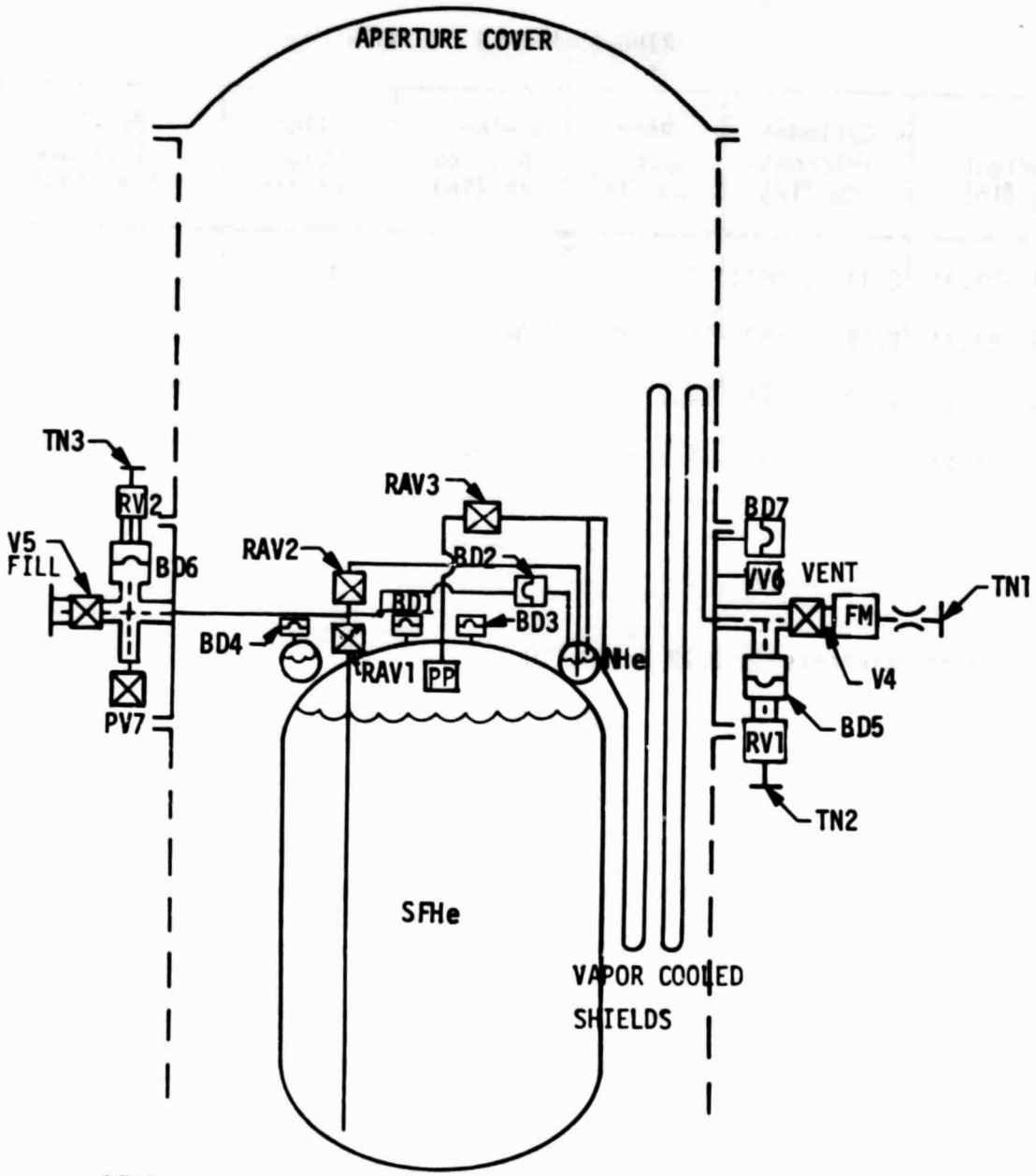

LEGEND

BD - BURST DISC

FM-FLOW METER

PP-POROUS PLUG

PV-PYROTECHNIC VALVE, NC

RAV-REMOTE ACTUATION VALVE

RV-RELIEF VALVE

TN-THRUST NULLIFIER

V-VACUUM JACKETED MANUAL VALVE

VV-VACUUM PUMPOUT VALVE

Fig. 5.21 Dewar Plumbing Schematic

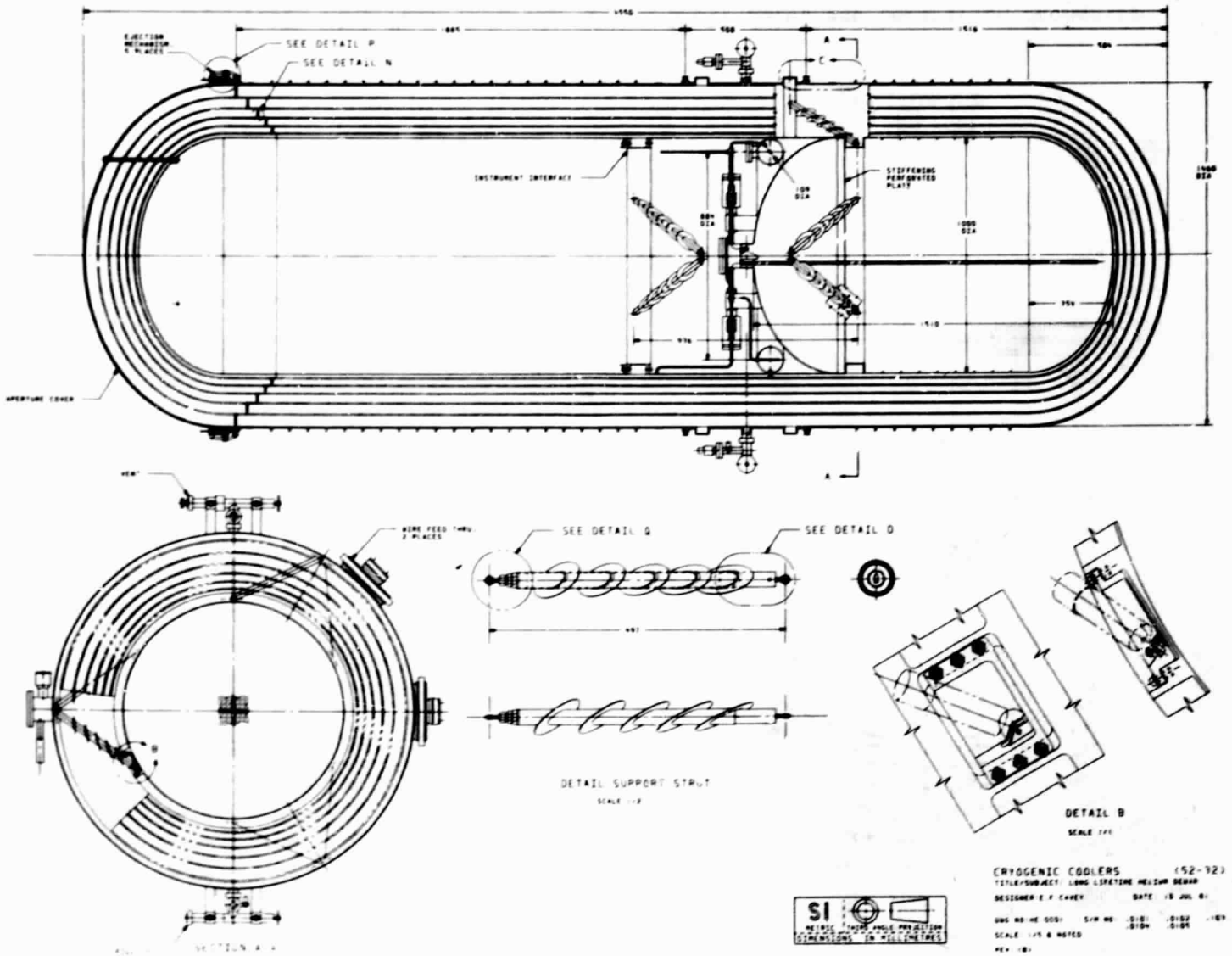

Fig. 5.22 [illegible]out

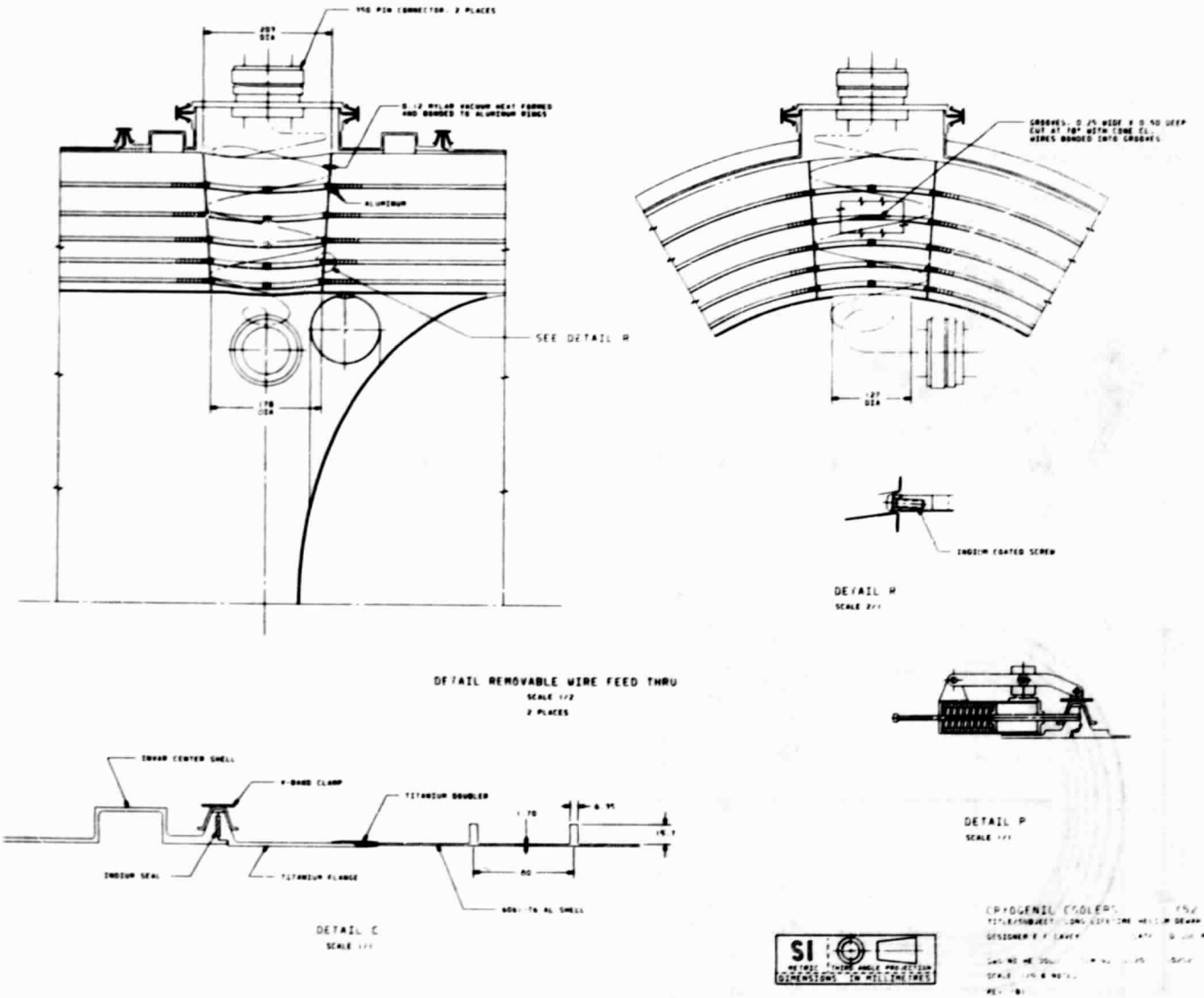

Fig. 5.23 Wire Feed Through, Vacuum Shell Joint and Separation Mechanism

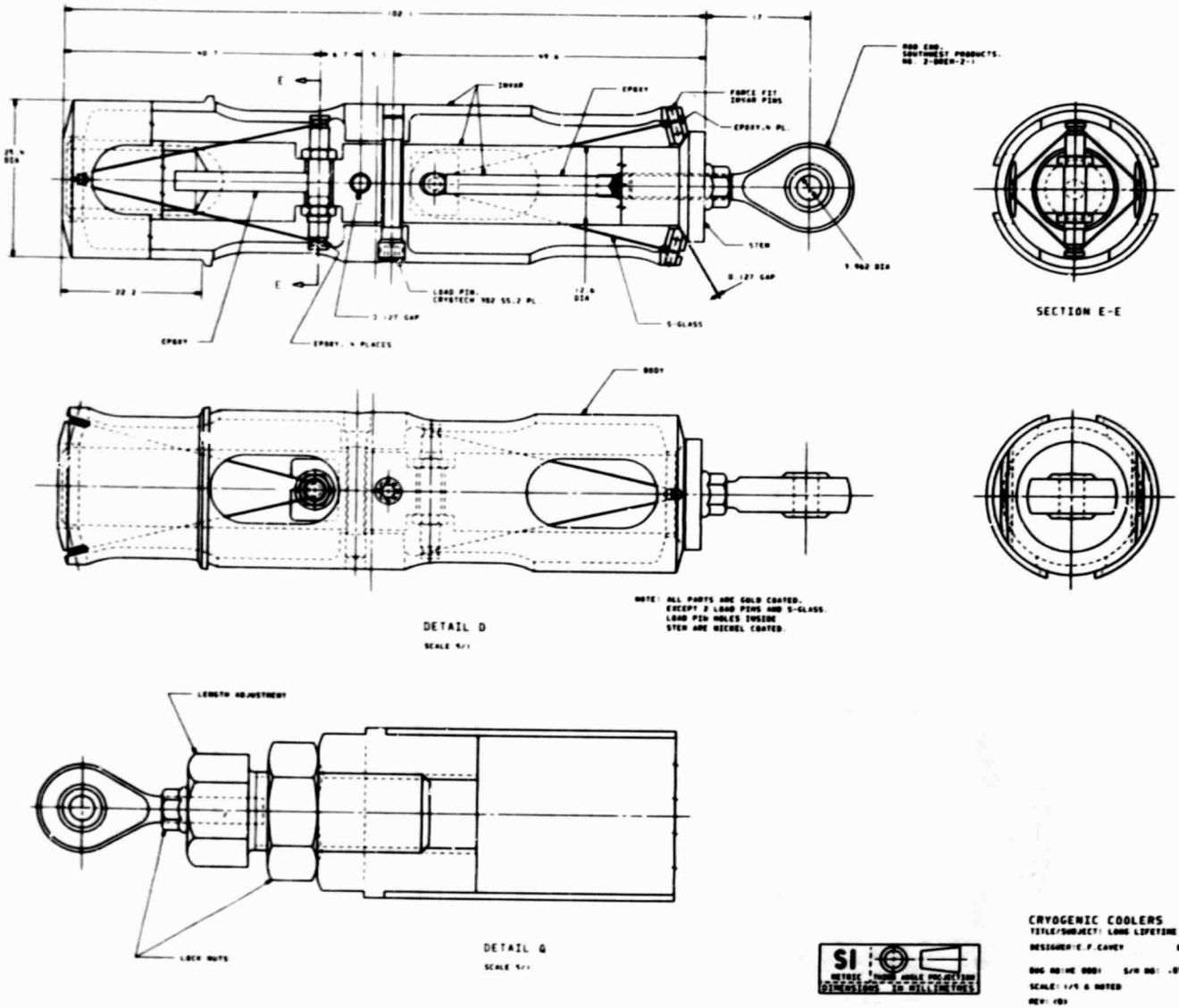

Fig. 5.24 PODS Support

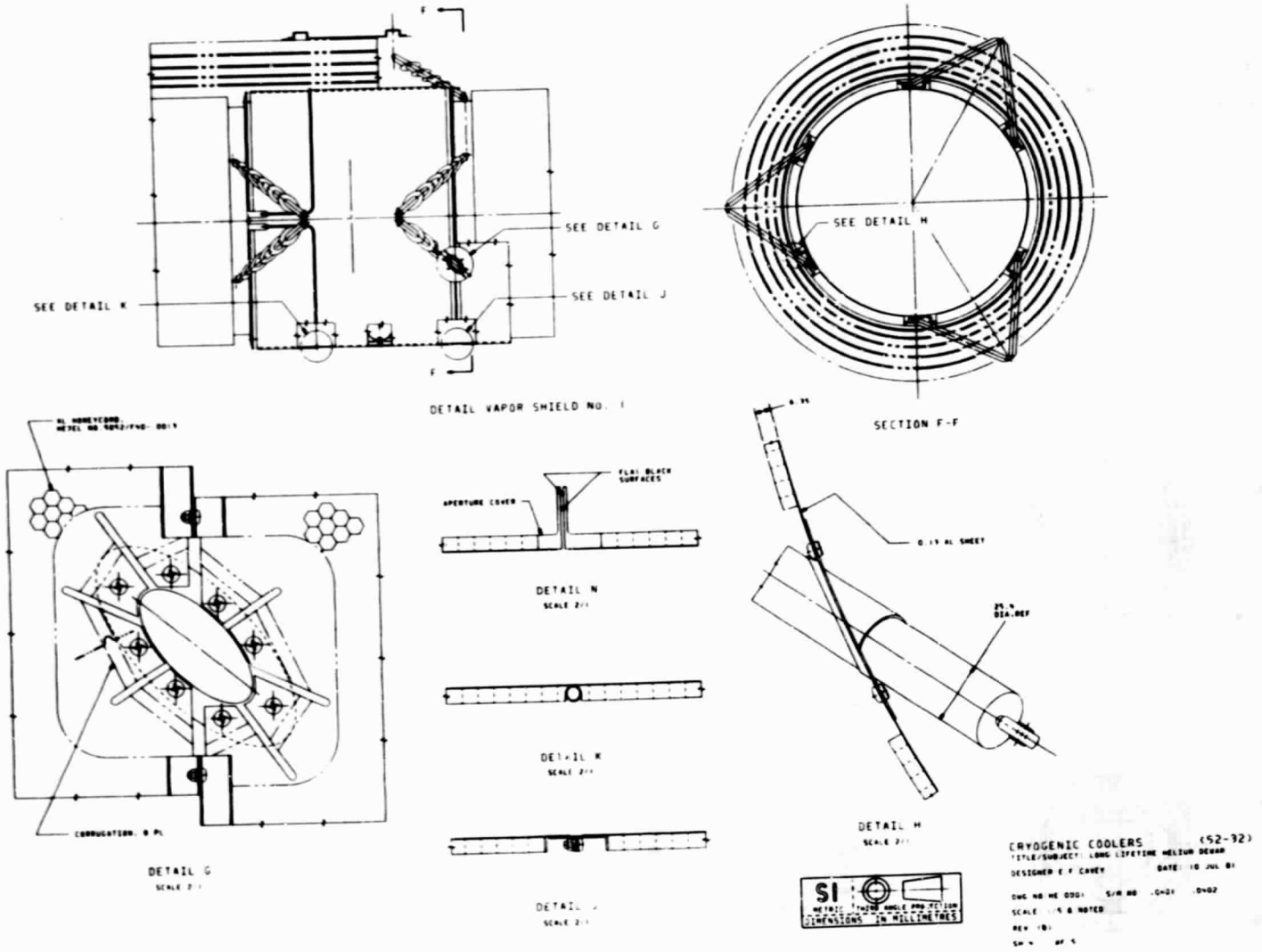

Fig. 5.25 Vapor-Cooled Shields

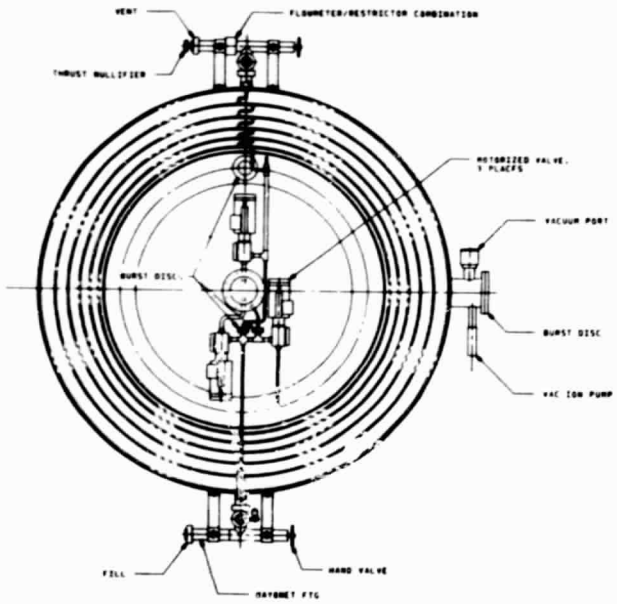

SECTION L-L

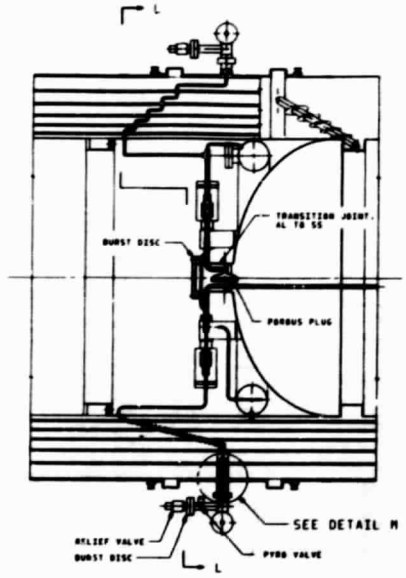

PLUMBING DETAIL

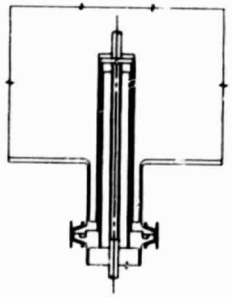

DETAIL M
SCALE 1:1

SI METRIC THIRD ANGLE PROJECTION DIMENSIONS IN MILLIMETRES

CRYOGENIC COOLERS (52-92)
TITLE/SUBJECT: LONG LIFETIME HELIUM DEWAR
DESIGNER:E.F.CAREY DATE: 10 JAN 91
DWG NO:ME 0001 S/N NO: .0501 .0502 .0503
SCALE: 1/5 & NOTED
REV: (B)
SH 5 OF 5

Fig. 5.26 Plumbing Installation

Table 5.4 DEWAR DESIGN CHARACTERISTICS

1. SUPERFLUID HELIUM TANK	
Temperature:	1.73K (3.11R)
Operating Pressure:	9.4 Torr (0.18 psi)
Material:	6061-T6 Aluminum
Volume:	1.0 m^3 (35.3 ft^3)
Ullage:	4%
Dome Thickness:	0.28 cm (0.110 in)
Cylinder Thickness:	0.14 cm (0.055 in)
Ring Thickness x Height x Spacing:	0.38 x 0.79 x 7.6 cm (0.15 x 0.31 x 3.0 in)
Ground Hold Heat Rate:	3.2 mW (0.01 Btu/hr)
Temperature Rise Rate (Ground Hold):	0.0009 K/day (0.0016 R/day)
Orbit Lifetime:	> 3 years
2. NORMAL HELIUM TORUS TANK	
Temperature:	4.2K (7.6R)
Operating Pressure:	760 Torr (14.7 psi)
Material:	6061-T6 Aluminum
Volume:	0.026 m^3 (0.92 ft^3)
Ullage:	4%
Thickness:	0.15 cm (0.061 in)
Ground Hold Lifetime:	11.1 days

Table 5.4 (continued)

3. VAPOR-COOLED SHIELDS (5 ea)	
Face Sheet:	6063 Aluminum, 0.013 cm (0.005 in)
Honeycomb:	5052/F40 - 0.0013 Aluminum, 33.7 kg/m^3 (2.1 lb/ft^3)
Shield Locations:	(X/X_{TOTAL}) 0.12,0.25,0.40,0.57,0.78
4. INSULATION	
Radiation Shields:	Double Aluminized Mylar
Spacer:	Silk Net (2 ea)
Thickness:	18.4 cm (7.25 in)
Layers/cm:	14
Bulk Density:	30.8 kg/m^3 (1.92 lb/ft^3)
5. PODS SUPPORTS (12 EA)	
Rod End to Rod End Length:	44.7 cm (17.6 in)
Fiberglass Tube Length:	31.0 cm (12.2 in)
Fiberglass Wall Thickness:	0.107 cm (0.042 in)
Fiberglass Tube ID:	2.5 cm (1.0 in)
Area of one S-Glass Strand:	5.1 x 10^3 cm^2 (7.96 x 10^{-4} in^2)
Length of S-Glass Strand:	4.6 cm (1.82 in)
Weight Supported Before Support's Short:	600 kg (1322 lb)

Table 5.4 (continued)

6. VACUUM SHELL (4 SECTIONS)

Aft Dome/Cylinder	
• Material:	6Al4V Titanium Flange, 6061-T6 Aluminum Cylinder/Dome
• Dome Thickness:	0.36 cm (0.14 in)
• Cylinder Thickness:	0.17 cm (0.067 in)
• Ring Thickness x Height x Spacing:	0.64 x 1.57 x 8.3 cm (0.25 x 0.62 x 3.26 in)
Center Cylinder	
• Material:	Invar
• Thickness:	0.25 cm (0.10 in)
Forward Cylinder	
• Material:	6Al4V Titanium Flange, 6061-T6 Aluminum
• Cylinder Thickness:	0.17 cm (0.067 in)
• Ring Thickness x Height x Spacing:	0.64 x 1.57 x 8.3 cm (0.25 x 0.62 x 3.26 in)
Aperture Cover	
• Material:	6061-T6 Aluminum
• Dome Thickness:	0.36 cm (0.14 in)

7. PLUMBING COMPONENTS

Burst Discs	Diameter cm (in)	Pressure Differential N/m^2 (psia)
BD 1	1.3 (0.5)	1.7×10^5 (25)
BD 2	1.3 (0.5)	1.7×10^5 (25)
BD 3	10.0 (4.0)	2.4×10^5 (35)
BD 4	5.0 (2.0)	2.4×10^5 (35)
BD 5	1.3 (0.5)	1.4×10^5 (20)
BD 6	1.3 (0.5)	1.4×10^5 (20)
BD 7	10.0 (4.0)	2.1×10^5 (30)

Shutoff Valves	
RA V1	Tank fill, motor driven (cold)
RA V2	Torus fill, motor driven (cold)
RA V3	Tank vent, motor driven (cold)
V4	Tank vent, manual, vac jacketed
V5	Tank fill, manual, vac jacketed
VV6	Vacuum shell evacuate/relief
PV7	Fill line evacuate in orbit, pyro, NC

Relief Valves	Pressure Differential	
	N/m^2	(psi)
RV 1	1.4×10^5	20
RV 2	1.4×10^5	20

Table 5.4 (continued)

7. PLUMBING COMPONENTS (continued)

Line	Mat'l	Diameter cm (in)	Wall Thickness* cm (in)	Length** m (in)
Fill	321 SS	.64 (1/4)	.015 (.006)	0.76 (30)
Primary Tank to 1st Shield	321 SS	.32 (1/8)	.015 (.006)	0.76 (30)
1st Shield	6061 Al	.32 (1/8)	.015 (.006)	3.23 (127)
2nd Shield	6061 Al	.32 (1/8)	.015 (.006)	3.38 (133)
3rd Shield	6061 Al	.64 (1/4)	.015 (.006)	3.56 (140)
4th Shield	6061 Al	.95 (3/8)	.020 (.008)	3.81 (150)
5th Shield	6061 Al	.95 (3/8)	.020 (.008)	4.01 (158)
5th Shield to Vent	321 SS	.95 (3/8)	.020 (.008)	0.46 (18)

* 321 Stainless Steel transition sections between shields
** 6061 Aluminum tubing length

Porous plug 2-5μ 7.6 cm (3.0 in) diameter

8. INSTRUMENTATION

Sensor Type		Qty	Location	Range
Mass Flow Meter		1	Vent line exit	Up to 50 g/hr (0.1 lb/hr)
Differential Chromel-Constantan T.C.		5	Tank-instrument fill line	0-0.5K (0-0.9R) 0-200K (0-360R)
Temperature	Germanium	2	Porous Plug	1.5-3K (2.7-5.4R)
	Germanium	3	Main Tank	1.5-3K (2.7-5.4R)
	Germanium	2	Torus Tank	3-6K (5.4-10.8R)
	Platinum	10	Vapor-cooled shields and supports	15-300K (27-540R)
	Platinum	5	Vacuum shell & flow meter	100-250K (180-450R)
Open Circuit		12	Struts	0 or infinite resistance
Ion Pump (pressure)		1	Vacuum Shell	10^{-4} to 10^{-8} Torr
Accelerometers		3	Instrument	---

Table 5.4 (continued)

8. INSTRUMENTATION (continued)

NUMBER OF WIRE FEED THROUGH LEADS

	Coaxial Wires	Manganin Wires		
		Gage		
		#40	#32	#24
Instrument	400	200	40	10
Valves				6
Instrumentation	---	104	---	4

	Material	Cross-sectional Area (per wire)	
		m^2	(in^2)
Coaxial Wires			
• Sheath	304 SS	4.1×10^{-8}	6.3×10^{-5}
• Insulator	Teflon	3×10^{-8}	4.7×10^{-5}
• Wire	304 SS	2×10^{-9}	3.1×10^{-6}
Manganin			
• #40	Manganin	5×10^{-9}	7.5×10^{-6}
• #32	Manganin	3.2×10^{-8}	5×10^{-5}
• #24	Manganin	2×10^{-7}	3.2×10^{-4}

5.2.1 Design Features

The large superfluid helium tank shown in Fig. 5.22 maintains the instrument at < 2K (< 3.6R) for the required three-year orbit lifetime. The instrument is thermally connected and mounted to the tank through an aluminum barrel extension and mounting flange. The smaller normal helium torus tank, mounted off the first vapor-cooled shield, is used to minimize the ground hold heat rate so the servicing interval in the Orbiter can be extended to 11.1 days; that is, under a normal launch sequence, no servicing is required once the dewar is located inside the cargo bay. The vented normal helium from the torus tank (ground hold) or the vented superfluid helium from the primary tank (orbit) is routed around the circumference of five vapor-cooled shields in series starting at the inner shield; the vented gas is passed through a flow meter and then exits through a thrust nullifier nozzle. Multilayer insulation is interspersed between the shields.

The vapor-cooled shield consists of a thin aluminum sheet epoxy bonded to aluminum honeycomb on one side. The shields are attached to the supports in multiple sections using indium coated screws and nuts as shown in Fig. 5.25, Details G, H, and J. The corrugation and slots shown around the strut permits the axial and circumferential movement required of the vapor-cooled shields during temperature changes to prevent shorting of the struts. Diaphragm action of the thin sheet plus corrugations around the strut allows the required radial movement.

The tank and instrument are supported off the vacuum shell with 12 PODS supports, six each end as shown in Figs. 5.22 and 5.24. The support rod ends are attached to fittings inside channels on both the tank/instrument barrel and the vacuum shell in order to position the strut so the cold end of the PODS mechanism is located at the first vapor-cooled shield and the warm end of the fiberglass tube is positioned at the outside layer of the insulation. A perforated plate is attached across the tank channel to stiffen the tank, distribute the point loads and raise the resonant frequency. The instrument flange is assumed to be stiffened by attachment of the instrument. Note in Table 5.4 that the struts will support a fully-loaded tank plus instrument weighing 431 kg (950 lb) in one-g without shorting out. Consequently, "orbit" performance can be demonstrated in one-g thermal tests and ground hold heat rates into the primary tank will be very low.

The tanks and lines are protected against overpressure with burst discs as shown in Figs. 5.21 and 5.26. BD1, 2, 5 and 6 protect the lines against trapped liquid and the tanks against overpressure. Burst discs BD3, 4 and 7 are protection of the tanks against a catastrophic accident, i.e., a large hole in the vacuum jacket permitting air to solidify onto the tanks. If this happens, burst discs BD3 and 4 rupture, dumping helium into the instrument cavity; BD7 then ruptures (in case the hole in the vacuum jacket is not large enough to handle this vent rate), venting the vacuum shell. This design was chosen because the required line sizes were too large (from a thermal viewpoint) to vent the tank directly outside of the vacuum shell.

All plumbing components and lines will have adequate support bracketry to survive the dynamic load environment. The plumbing clusters external to the vacuum shell are connected through bayonnet fittings as shown in Fig. 5.26, Detail H. This feature permits rapid field replacement of faulty components. A description of an actual usage sequence is the easiest way to explain why the plumbing is laid out as shown so this discussion is deferred to Section 5.2.3.

The design of the wire feed through is shown in Fig. 5.23. The feed through consists of a heat-formed Mylar cone with five bonded aluminum rings located at the five vapor-cooled shields. The wires are wrapped in a spiral on the outside of the cone and bonded into grooves cut into each aluminum ring to effect good heat transfer at the vapor-cooled shield locations. The assembly/removal procedure of the feed through is described in Section 5.2.2.

The bonded titanium/aluminum joint in the vacuum shell is shown in Fig. 5.23, Detail C. This type of bond joint has been used successfully on all aluminum vacuum shells on previous cooler programs, i.e., Teal Ruby. (This cooler has been qualified but not yet flown.)

The aperture cover separation mechanism shown in Fig. 5.23, Detail P, is activated with explosive bolts around the circumference of the V-band clamp. The clamp diameter is expanded by the compression spring/lever arm shown. The compressed spring/plunger then pushes the aperture cover away from the dewar. Note the inclined seal surface traps the O-ring and prevents it from dislodging over the aperture upon cover separation.

5.2.2 Assembly Sequence

Once the various component parts are fabricated, the dewar is assembled in the following manner.

The center Invar section of the vacuum shell is slipped over the tank/instrument barrel section with the torus tank and all the internal plumbing installed and leak checked. "Zero clearance" load pins (two each) are installed in each PODS support and the strut length is adjusted at the warm end for all 12 struts using the mechanism shown in Fig. 5.24, Detail Q. The locking nuts are tightened and the six forward struts are removed. The flight load pins are then substituted for the "zero clearance" pins on all struts.

The fill line plumbing connection is made from the primary tank to the vacuum shell and leak checked. Insulation is installed from the forward strut area (struts now removed) around the aft struts and back over the tank. The first vapor-cooled shield is installed next in two sections, a dome/cylinder section, up to the six aft struts and a cylinder section that fits between the struts (see Fig. 5.25, Detail G). This cylinder may be split in half for ease of installation. The torus tank is attached to the first vapor-cooled shield. The next insulation layers plus second vapor-cooled shield sections are installed in the same manner, brazing and leak checking the vent line connections as the assembly proceeds until all vapor-cooled shields and insulation are installed up to the forward strut area.

The six forward struts are installed next and bolted to the vacuum shell, instrument channel and the vapor-cooled shields. Insulation is then laid on the instrument barrel, butting up to the blanket already installed. Ticks of aluminized Mylar tape are used periodically to prevent the tapered joint from opening. The first cylindrical vapor-cooled shield (again split in two halves for ease of assembly) that covers the instrument section is slipped on and bolted to itself and to the mating shield already installed. The remaining vapor-cooled shields and insulation in the instrument section are installed in a similar manner. The aft (cylinder/dome) and forward (cylinder) vacuum shell are then slipped on and clamped to the Invar shell. The external plumbing modules, assembled and leak checked separately, can now be installed using the bayonnet connection shown in Fig. 5.26, Detail M.

The removable wire feed throughs (Fig. 5.23) are installed after the experiment is installed and bolted to the interface flange. The installation method is to reach in the hole through the insulation and vapor-cooled shields and make the electrical connection, then slip the cone-shaped connector into the hole. Discs of insulation are laid inside the cone and an aluminum disc is placed inside the cone. The disc and cone are attached to the first vapor-cooled shield with indium-coated screws (Fig. 5.23, Detail R). This process is repeated until all five aluminum discs are attached to the five vapor-cooled shields with insulation discs in between the aluminum. The cone is made of clear Mylar to aid in the assembly. The flange cover seal is then made.

The aperture cover is installed and leak checked to complete the assembly.

5.2.3 Operational Sequence

A typical operational sequence is described to provide additional insight into the design. Refer to Fig. 5.21. The vacuum shell is evacuated at a controlled rate (to prevent insulation damage) through valve VV6 and baked out at ~ 350K (630R) for four to six weeks to outgas the dewar.

Both the primary tank and torus tank are evacuated and back filled with helium gas several times. Both tanks are then cooled down to near helium temperature at a controlled rate and the primary tank is nearly filled with superfluid helium through valve RAV1. Valves RAV3 and V4 are open for this operation. The vacuum-jacketed transfer lines will probably have to have a LN_2-cooled shield plus multilayers to allow transfer of superfluid helium. The end of the vented line is connected to a vacuum pump to maintain a low pressure in the tank for the fill operation. Tank pressure can be controlled by changing valve setting V4. Pressure is inferred from tank temperature. Top off of the tank is performed as many times as required until the tank is full (4% ullage) as determined by continuous weighing of the dewar.

Valves RAV1, RAV3 and V4 are closed and the pump shut off. Valve RAV2 is opened and normal liquid helium is introduced into the torus tank through valve V5 until flow stops. Valve V4 is then opened and flow continued until the torus tank is full. The vent line inlet is positioned so a 4% ullage always remains in the tank. Flow is continued until temperature sensors on the second vapor-cooled shield show liquid helium is exiting the torus tank.

Valve RAV2 is closed and the line back to V5 is evacuated. Valve V5 is then closed. Helium continues to vent out of the torus tank through valve V4 for the prelaunch hold and launch. Once in orbit outside the cargo bay, pyro valve PV7 is opened to vent the fill line to space in case valve RAV1 has a slow leak. The aperture cover is then ejected. When the flowmeter shows the torus tank is empty, valve RAV3 is opened and the primary tank is vented through the vapor-cooled shields to space for the remainder of the mission. The flowmeter provides data for an extrapolation of the mission lifetime.

The operation of the PODS supports is of interest during the launch and orbit phase. Under launch loads, the S-glass strands shown in Fig. 5.24 stretch elastically until the Invar stem seats against the two load pins (tension) or the stem conical section seats against the Invar body (compression). Once orbit is achieved, the stem recenters itself inside the body, passively disconnecting the stem from the body. Heat is then transferred by radiation between the gold-coated stem and body and by conduction along the S-glass strands. Electrical resistance measurements indicate whether this passive disconnect did occur on all 12 struts.

5.3 DEWAR PERFORMANCE

The dewar ground hold interval where no servicing is required is 11.1 days with the current size torus tank; the heat rate into the non-vented superfluid helium tank for the same period is 3.2 mW (0.009 Btu/hr), 13% of the

200K (360R) orbit case. The temperature rises only 0.01K (0.02R) during this 11.1 day period. The reason for the extremely low ground hold heat rate is as follows. The 4.2K (7.6R) torus tank is shorted to the first vapor-cooled shield; consequently, the heat rate into the tank is lower than in orbit where the first shield floats and is nearer 15K (27R). Also, the PODS supports do not short in one g, minimizing the support heat leak. The heat map for the ground hold case is shown in Fig. 5.27 for a warm boundary temperature of 300K (540R).

The dewar orbital lifetime is plotted as a function of the vacuum shell temperature in Fig. 5.28. The vapor-cooled shield temperatures are shown in Fig. 5.29. These calculations assume a 40% degradation factor over flat plate data for the installed multilayer insulation (see Fig. 10.1). No attempt was made to calculate the insulation degradation in the region of supports, wiring, plumbing or joints. A much more detailed thermal model would be required to make these calculations of radiation tunneling and insulation shorting that occurs in actual installations. The conductivity used assumes the insulation is installed one layer at a time.

The orbital heat map for T_H = 200K (360R) case is shown in Fig. 5.30. Note a substantial amount of energy is being radiated to space off the flanged ends of vapor-cooled shields 4 and 5. In an actual flight system, this radiated flux will be lower because of the radiation coupling between these flanges and a Sun shade, i.e., with a configuration such as shown in Fig. 5.31. (No orbit or pointing requirements were defined for this study so this type of systems analysis was not performed.) Note in the Fig. 5.30 heat map, the Mylar cone plus the wires are treated separately for the wire feed throughs. The

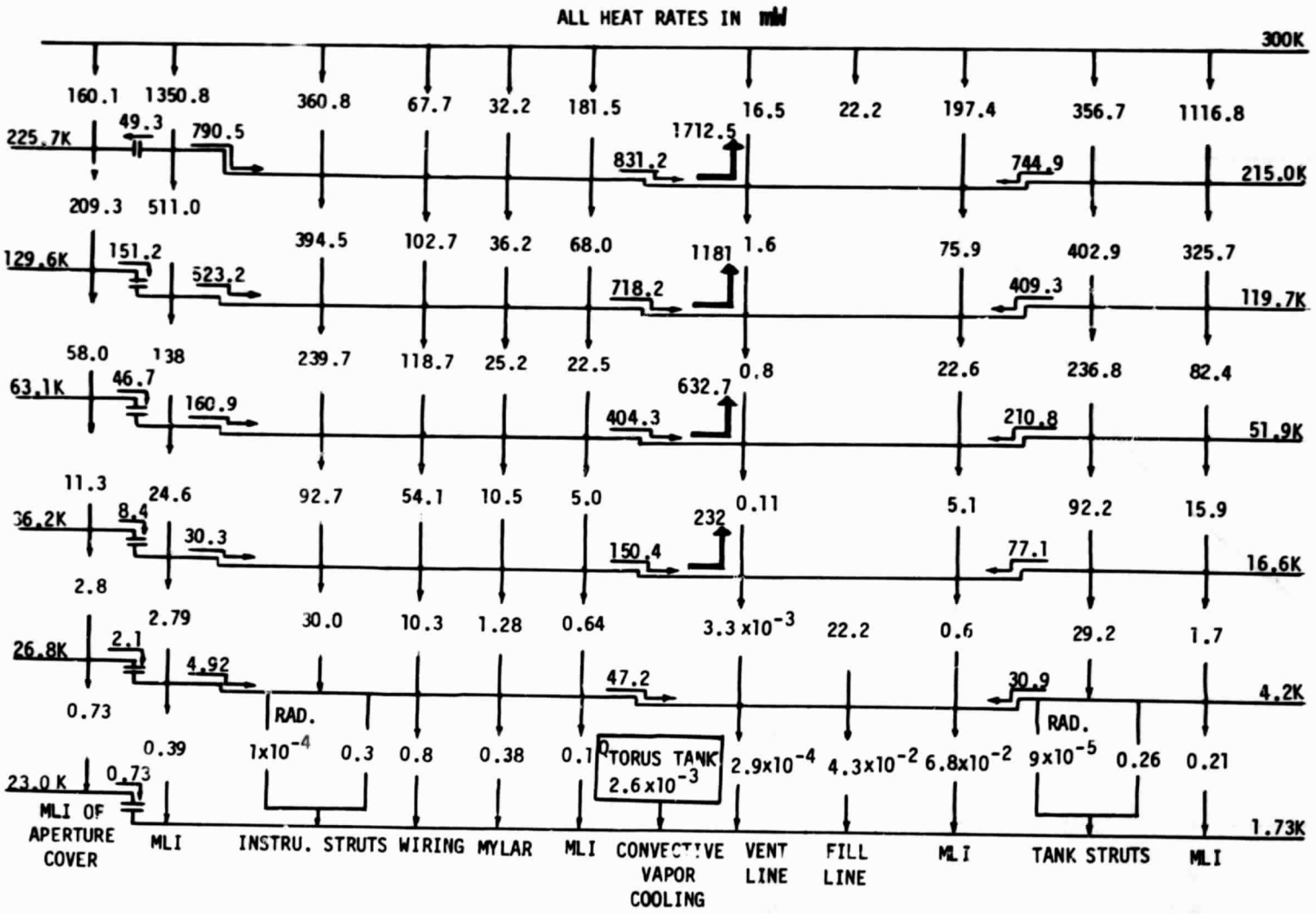

Fig. 5.27 Ground Hold Heat Map for T_H = 300K (540R)

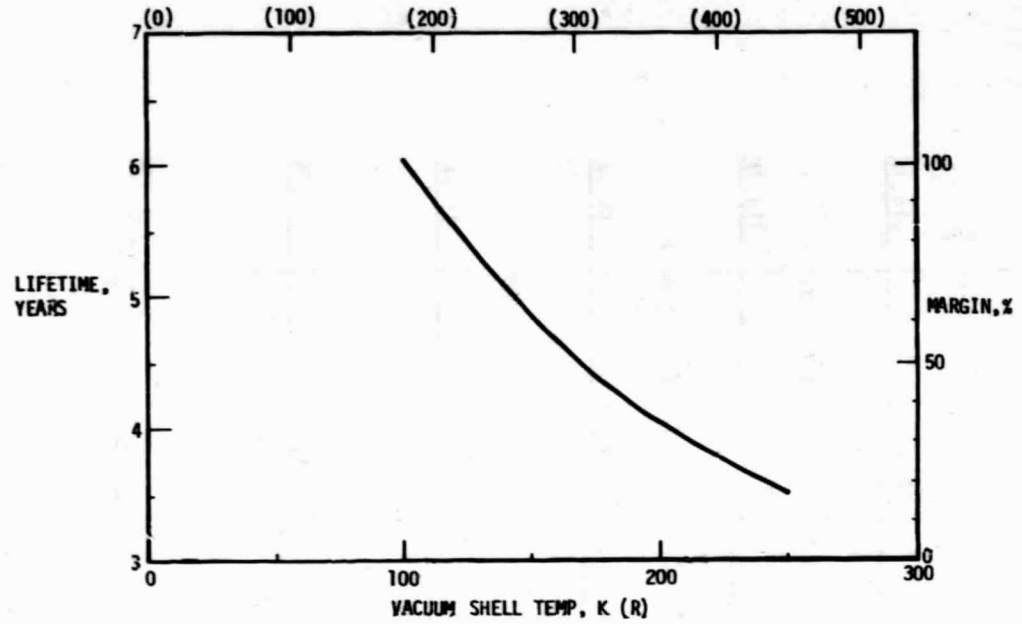

Fig. 5.28 Dewar Orbital Lifetime as a Function of Vacuum Shell Temperature

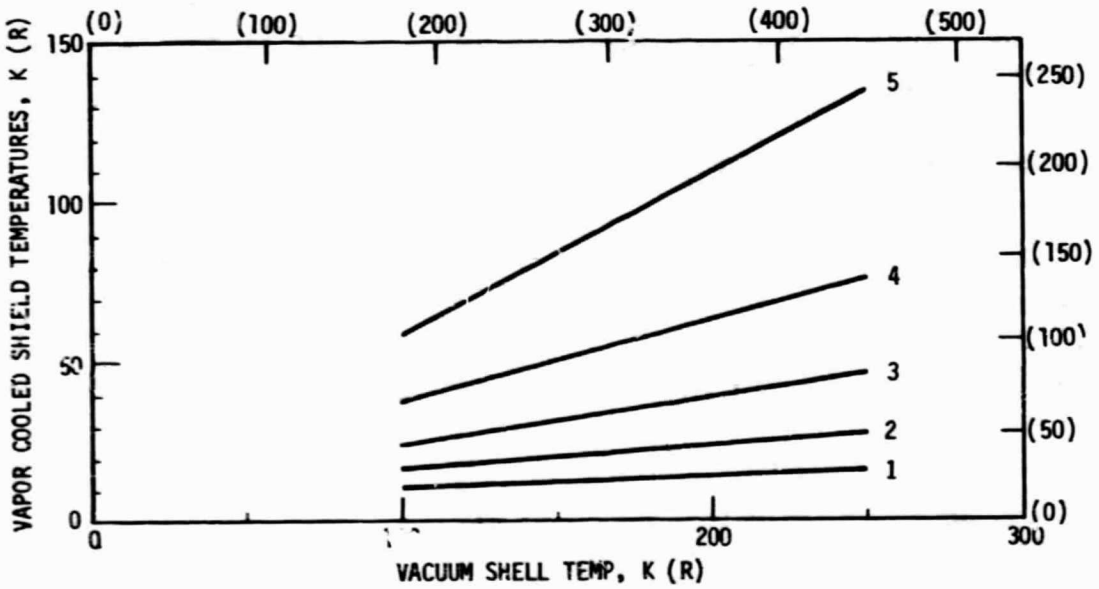

Fig. 5.29 Vapor-Cooled Shield Temperatures as a Function of Vacuum Shell Temperature

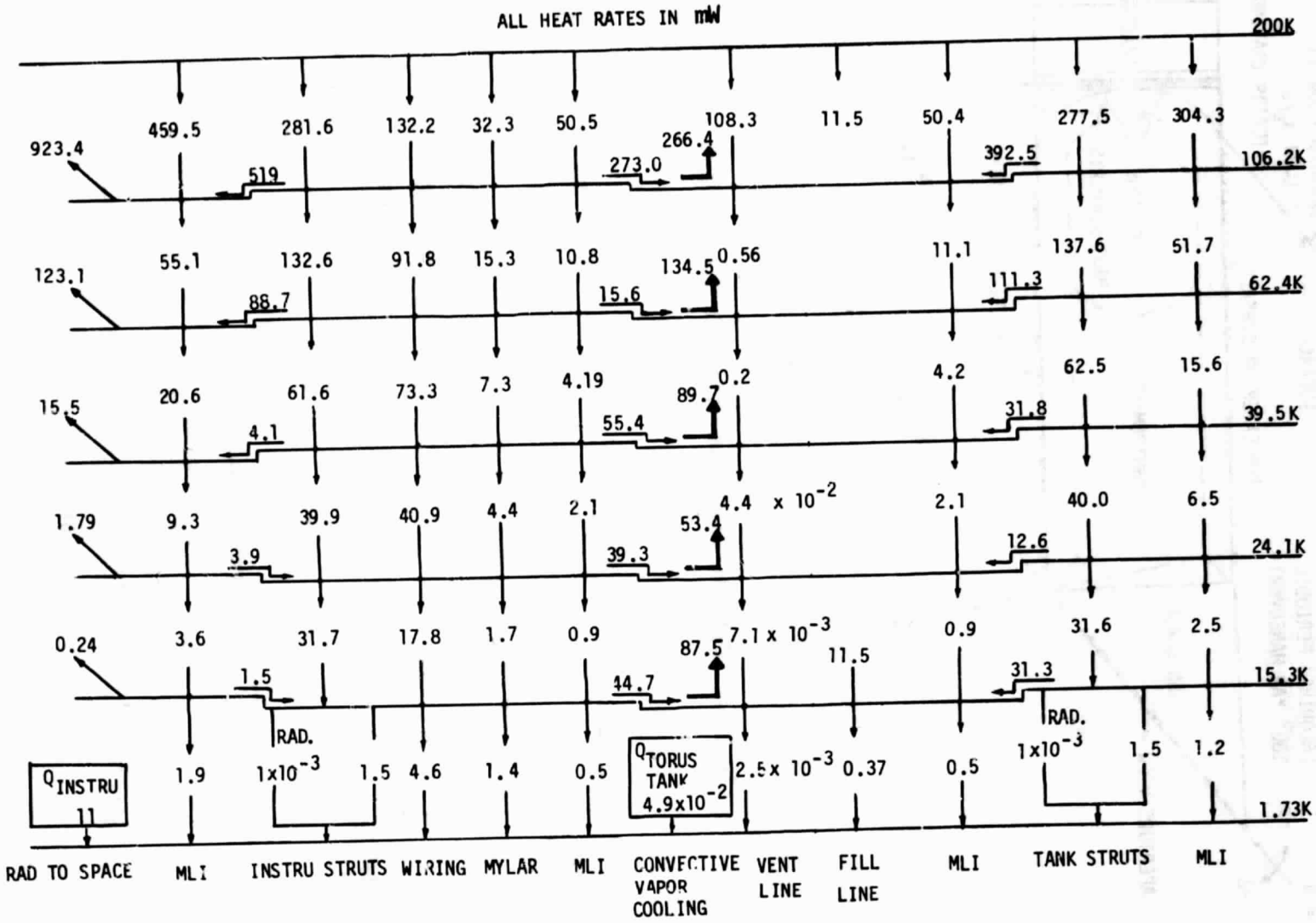

Fig. 5.30 Orbital Heat Map for T_H = 200K (360R)

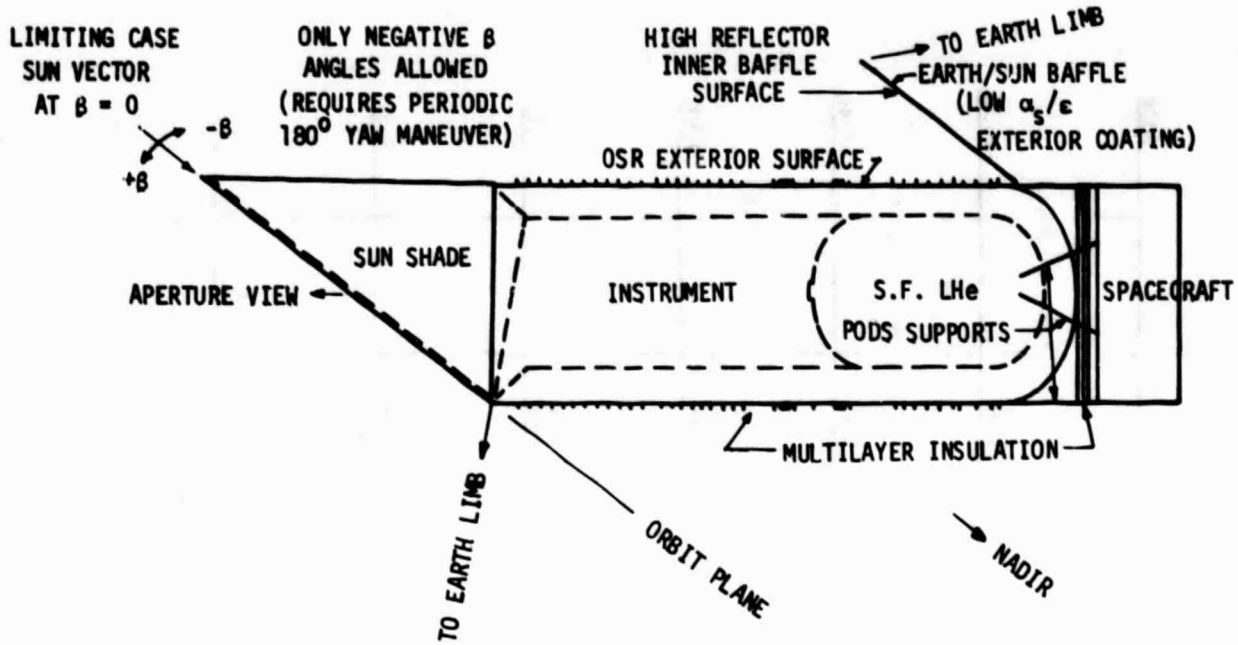

Fig. 5.31 Typical Dewar/Spacecraft Configuration

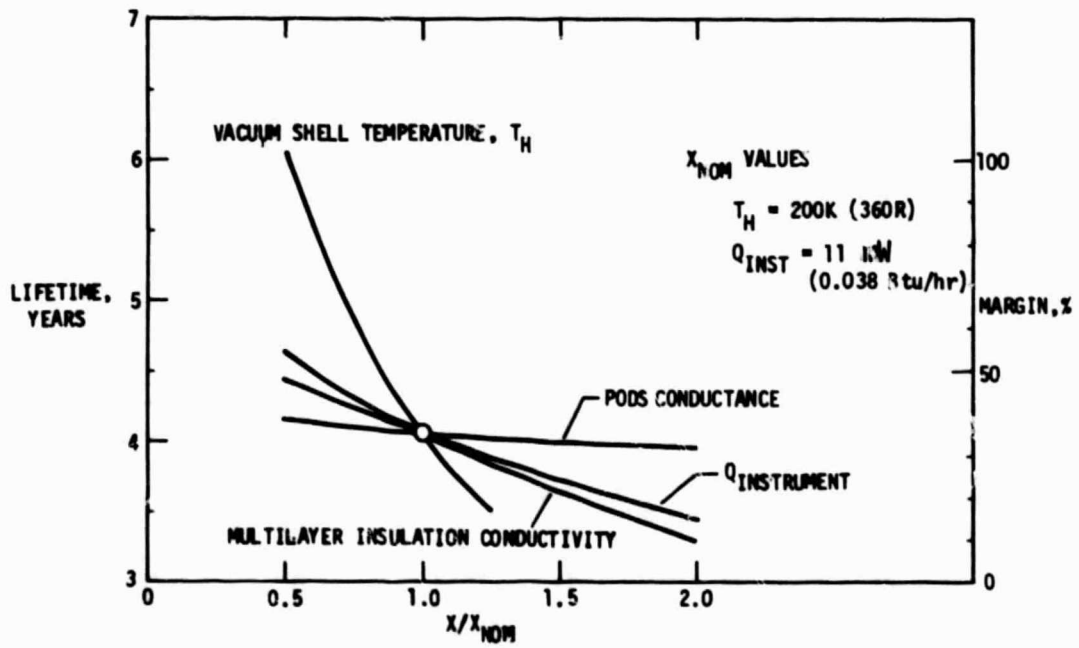

Fig. 5.32 Orbital Performance Sensitivities

number of wires were increased to account for the motor-operated valves and instrumentation as well as the instrument as shown previously in Table 5.4.

Fig. 5.32 (on the previous page) provides dewar orbital lifetime sensitivity to changes in the vacuum shell temperature, multilayer insulation conduct-tivity, instrument heat load and PODS conductance. The lifetime is the most sensitive to vacuum shell temperature changes and least sensitive to changes in the PODS conductance.

5.4 DEWAR WEIGHT SUMMARY

A preliminary weight statement of the dewar design described in Section 5.2 is provided in Table 5.5. The dry weight includes a 10% margin. The center of gravity (CG) of the mass supported by the 12 PODS supports falls midway between the supports. This mass includes both tanks plus helium, inner instrument barrel, vapor-cooled shields, insulation, PODS supports, cold plumbing and tne instrument. The CG of the instrument is 0.55 m (21.6 in) forward of this CG point.

Table 5.5 PRELIMINARY DEWAR WEIGHT STATEMENT

	kg		lb	
Primary Tank (1.0 m^3)		38.7		85.3
Inner Instrument Barrel		27.3		60.1
Torus Tank (0.026 m^3)		5.0		11.0
Vapor-Cooled Shields		57.9		127.6
#1	9.8		21.6	
#2	10.7		23.5	
#3	11.4		25.2	
#4	12.5		77.5	
#5	13.5		29.8	
Insulation		77.1		170.0
PODS Supports (12 ea)		5.8		12.8
Vacuum Shell		241.0		531.3
Aft Cyl/Dome	61.4		135.4	
Invar Cyl	72.6		160.0	
Forward Cyl	107.0		235.9	
Plumbing and Wiring		29.2		64.3
Burst Discs	3.1		6.8	
BD1	0.2		0.5	
BD2	0.2		0.5	
BD3	0.7		1.6	
BD4	0.3		0.7	
BD5	0.4		1.0	
BD6	0.4		1.0	
BD7	0.7		1.5	
Shutoff Valves	4.5		10.0	
V1	0.9		2.0	
V2	0.9		2.0	
V3	0.9		2.0	
V4	0.5		1.0	
V5	0.5		1.0	
V6	0.7		1.5	
V7	0.2		0.5	

Table 5.5 (continued)

	kg		lb	
Relief Valves	0.45		1.0	
RV1	0.2		0.5	
RV2	0.2		0.5	
Mass Flowmeter	1.8		4.0	
Vac Ion Pump (8 l/s)	4.5		10.0	
Thrust Nullifiers	0.7		1.5	
TN1	0.2		0.5	
TN2	0.2		0.5	
TN3	0.2		0.5	
Plumbing Lines and Bayonnets	6.8		15.0	
Wire Feed Throughs (2 ea) including flanges	7.3		16.0	
Instrument		200.0		440.9
10% Margin		68.0		150.0
Dry Weight Minus Aperture Cover		750.0		1653.0
Aperture Cover (with Ejection Mech, Shields, Insul.)		99.0		218.0
Dry Weight with Aperture Cover		849.0		1871.0
Superfluid Helium		137.0		302.0
Normal Helium		3.2		7.2
LAUNCH WEIGHT		989		2180

Section 6

TECHNOLOGY DEVELOPMENT PLAN

Prior to designing, building and qualifying a three-year superfluid helium flight dewar, it is necessary to perform a series of development tasks to reduce the technical and cost risks to an acceptable level. These tasks consist of a series of component and subsystem developments culminating in a series of full-scale helium dewar tests as shown in Fig. 6.1. These tasks were selected based on their criticality to system performance (Table 6.1) and their current level of development. In the following sections, the major objectives plus the recommended approach is provided for each of these tasks. A schedule plus ROM costs concludes the development plan.

6.1 TASK DEFINITIONS

6.1.1 System Requirements Definition and Design Update (Task 1)

6.1.1.1 Objective. The objective of the task is to increase the level of design detail to the point component and subsystem development items can be fabricated.

6.1.1.2 Approach. More detailed system requirements provided by the customer (including experiment definition and operational mode) will be incorporated into the dewar design. The level of structural and thermal analysis and design detail will be increased to permit component and subsystem test items to be fabricated in each of the tasks.

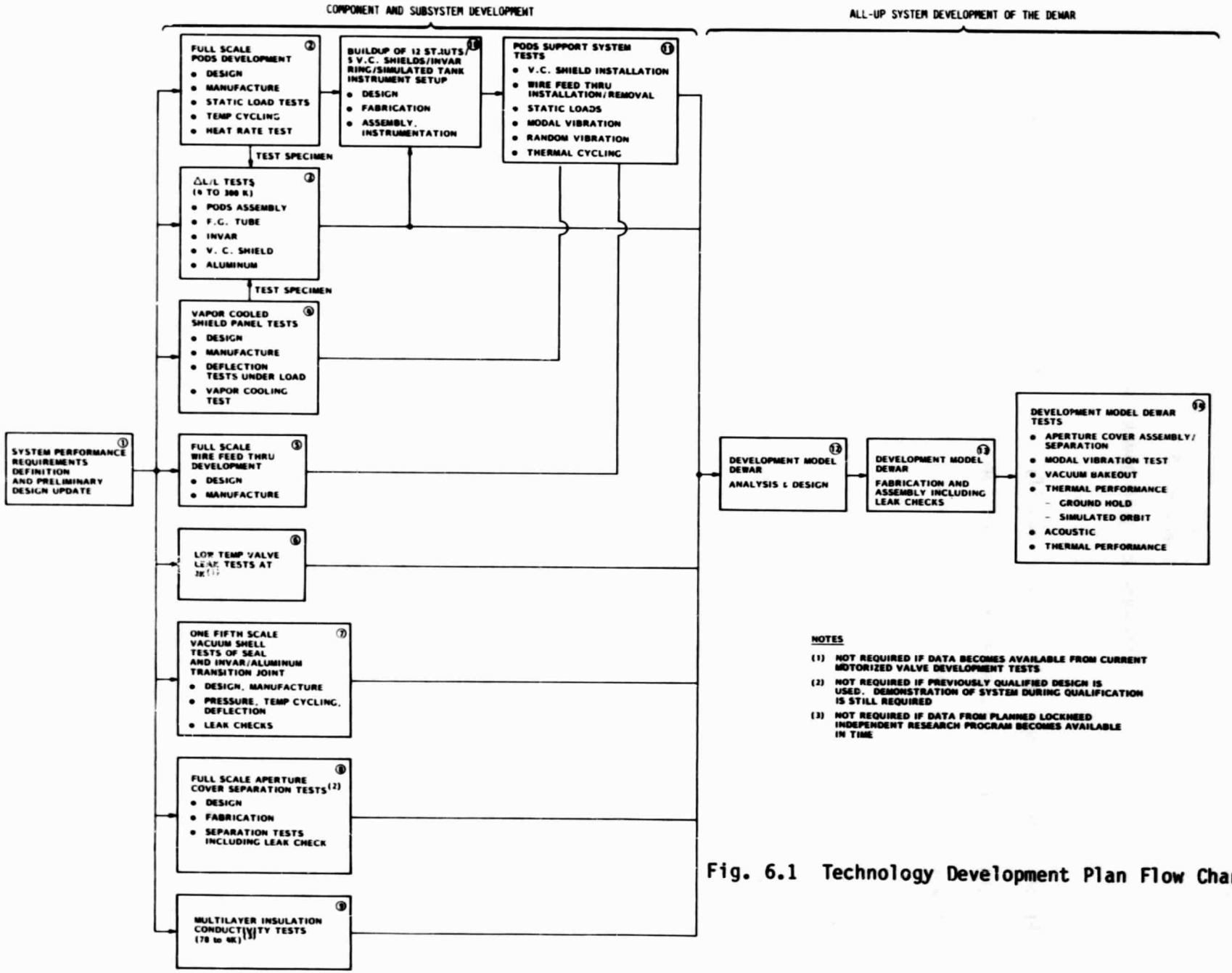

Fig. 6.1 Technology Development Plan Flow Chart

Table 6.1 PRIORITY RANKING OF COMPONENT AND SUBSYSTEM DEVELOPMENT TASKS

Task No.	Priority Ranking	Task	Ranking Criteria
2 10 11	1* 1 1	PODS tests PODS support system buildup PODS support system tests	The support system thermal performance is the key to meeting the dewar 3-year life-time goal. If the supports don't perform as designed and state-of-the-art supports are used, the dewar lifetime is cut by approximately two thirds.
3	1	ΔL/L Tests	These data are required to design the support system. Data are currently available from different sources. These tests will provide comparable data on actual materials in the same test setup.
4	1	Vapor-cooled shield tests	The current design is based on 100% heat exchanger efficiency. These tests will determine how closely the design approaches this value. Delaying the tests until the full dewar is assembled may necessitate expensive redesign if the heat exchanger performance is inadequate.
7	1	Vacuum shell tests	Vacuum leaks are a major problem, historically, on flight dewars. These 1/5 scale tests will demonstrate the Invar/Aluminum transition joint plus the flange seal remain leak tight over the required operating temperature range, prior to incorporating them into the full-scale vacuum shell design.
9	1	Multilayer insulation conductivity	Multilayer insulation consitutes 30% of the parasitic heat load to the dewar. To date, no experimental data are available in the lower temperature region, i.e., 78 to 2K. The current performance is based on test data over a broader temperature range, i.e., 278 to 20K. In addition, improved multilayer performance may be obtained by changing the spacer/shield combinations to minimize the dominant conduction term at these low temperatures.
5	2	Wire feed-through development	This modular design provides easy removal/installation plus wiring changes and ensures efficient vapor cooling of the wires. Demonstration of the design prior to system testing is not as critical, thermally, as PODS, vapor shields or multilayer insulation testing, however, since changes can be made at the system test level.
6	3	Low-temperature valve leak tests	The evacuated fill line heat leak will increase in orbit if it fills with leaking helium. This problem can be eliminated by opening the external fill line valve in orbit. However, the leak rate of the cold valve must be low enough to prevent excessive loss of helium over three years.
8	3	Full-scale aperture cover separation tests	Ejection of the aperture cover is critical to operation of the experiment. However, these tests can be delayed until system testing without too large a technical risk since a flight-qualified system will have been tested on the IRAS program.

* 1 is the highest priority

6.1.2 Full-Scale PODS Development (Tasks 2, 10, 11)

6.1.2.1 Objectives. The objectives of these tasks are sixfold.

- Demonstrate the support system can be manufactured within tolerances and installed with vapor-cooled shields and a wire feed through without the load pins shorting.
- Measure the load it takes to short the load pins on individual struts and as installed.
- Demonstrate the load pins will not short with T_C = 4K (7.2R) and T_H varied over 300 to 100K (540 to 180R).
- Measure the thermal performance of the strut over its operational temperature range.
- Demonstrate the structural load capability of the struts individually and installed (12 each) both statically and dynamically.
- Measure the modal vibration frequencies of the support system both for the launch and orbit conditions (full to empty tank).

6.1.2.2 Approach. Initially, one PODS support will be manufactured. The change in length of the strut with temperature will be measured in Task 3. The strut will be loaded in tension and compression to determine the load required to thermally "short" the load pins. The loads will then be increased to design loads. The strut will be thermally cycled between 300 and 4K (540 to 7.2R) and the design load tests repeated. The strut will then be tested to destruction in compression.

The heat rate for a second PODS support will be measured between T_H = 300K (540R) to T_C = 4K (7.2R) with the load pins shorted to simulate the launch condition. The simulated orbit heat rate will be measured with the stem at T_C = 2K (3.6R) and T_1 (Invar body) varied from 10 to 40K (18 to 72R).

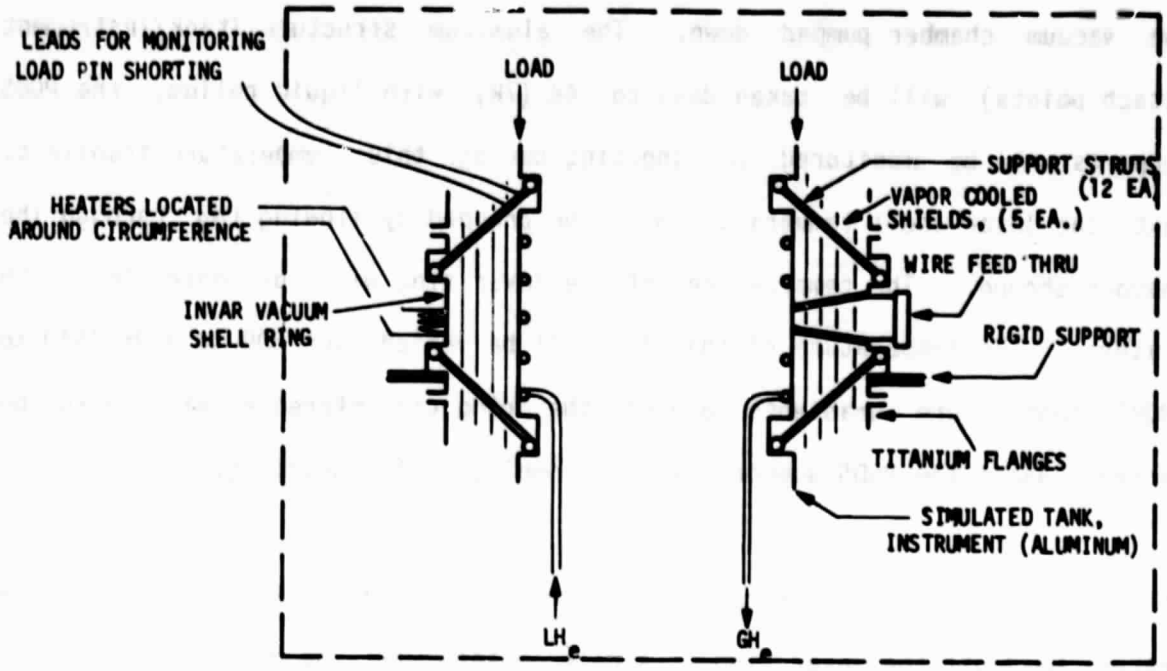

Fig. 6.2 Support System Test Setup

Using the thermal expansion/contraction data from Task 3, a test setup will be designed and fabricated to test the installed struts as shown in Fig. 6.2 above. The setup consists of the Invar vacuum ring, mating titanium flanges, 12 PODS supports, five vapor-cooled shields, one wire feed through, plus an aluminum inner structure that simulates the tank and instrument attach points. The installation/removal procedure of the supports, vapor-cooled shields and wire feed through will be demonstrated including ohmmeter measurements to demonstrate the load pins don't short. Loads in first the axial and then the lateral direction will be applied to the support system until the load pins "short out". The axial load will then be increased to the design load for a series of cyclic load tests.

The test setup will be moved into a LN_2 shrouded vacuum chamber. Helium heat exchange coils will have been welded to the aluminum structure previously and

the vacuum chamber pumped down. The aluminum structure (tank/instrument attach points) will be taken down to 4K (7R) with liquid helium; the PODS supports will be monitored for shorting during this temperature transient. Next the Invar shell temperature will be dropped by flowing LN_2 through the chamber shroud. The temperature of the Invar ring will be controlled with heaters. The temperature of the ring will be varied over 300 to 100K (540 to 180R); temperature gradients around the ring circumference will also be varied. Again the PODS supports will be monitored for shorting.

The test article will be removed from the vacuum chamber and supported on a shaker head off the Invar ring. Accelerometers will be mounted on the test article as required. A low-level modal resonance survey will be performed in three axes with the load pins shorted by adding weights to simulate the dewar launch (condition) and removing the weights so the load pins are not shorted (simulated orbit condition). The measured orbit resonances can be corrected to the design mass, depending on the weights used in the test.

The weights will again be added to simulate the dewar launch weight and a random vibration test performed in three axes.

6.1.3 $\Delta L/L$ Tests (Task 3)

6.1.3.1 Objective. To properly design the support system, accurate thermal expansion/contraction data are needed for the PODS supports, Invar vacuum ring material, and titanium and aluminum (used in the helium tank, vacuum shell and the aluminum/honeycomb vapor-cooled shield) over the temperature range 300 to 4K (540 to 7R).

6.1.3.2 Approach. The PODS support $\Delta L/L$ measurements will be performed separately on the PODS cold end assembly, fiberglass tube and warm end assembly. This approach is necessary in order to fit the specimens into an existing test apparatus. Specimens of Invar, titanium, aluminum and the aluminum honeycomb will also be measured. The contraction will be measured going from high to low temperature followed by expansion going from low to high temperature. The data will be used to calculate the optimum support spacing of the opposing six strut assemblies. 6.1.4 Vapor-Cooled Shield Tests (Task 4)

6.1.4.1 Objectives. The objectives are threefold: First, demonstrate the manufacturing techniques for the honeycomb panels and tube heat exchangers; Second, determine the load-bearing capability of the honeycomb panel; and third, measure the thermal efficiency of the heat exchangers with and without joints over their operating temperature and pressure range.

6.1.4.2 Approach. Representative honeycomb panels will be fabricated and load deflection tests performed to demonstrate their structural capability. Next a thermal efficiency test will be performed using the test setup shown in Fig. 6.3. Scale test samples of the heat exchanger will be fabricated using different size vent tubing and a simulated joint. Heat flux will be varied by changing boundary temperature T_2. The inlet pressure and temperature of helium flowing through the heat exchanger will be varied around the predicted values and the outlet pressure controlled. The enthalpy change in the gas and the temperature gradients along the shield and the joint will be measured.

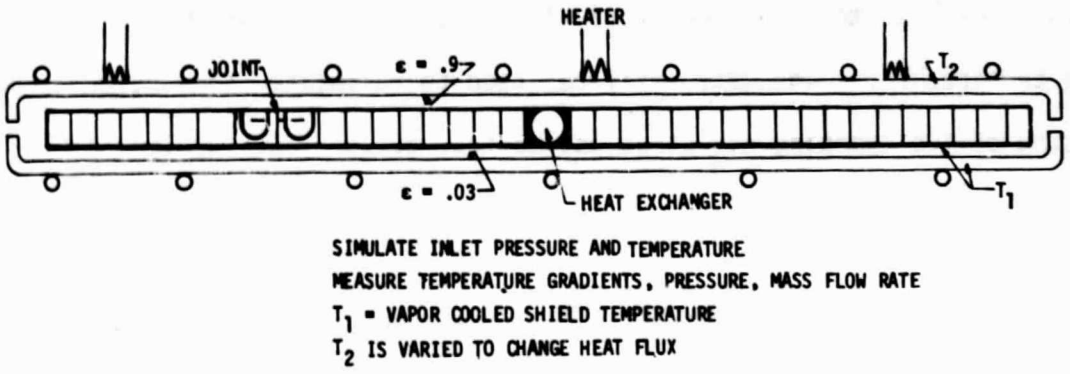

Fig. 6.3 Vapor-Cooled Shield Thermal Efficiency Test

6.1.5 Wire Feed Through Development (Task 5)

6.1.5.1 Objective. The objective of this task is to demonstrate the manufacture and assembly of the wire feed through.

6.1.5.2 Approach. The fabrication plus the heat forming assembly techniques will be developed for the Mylar cone and aluminum rings. (In Task 11, the installation/removal of the feed through in the dewar is demonstrated; the thermal performance of the feed through is monitored in Task 14.)

6.1.6 Low-Temperature Valve Leak Tests (Task 6)

6.1.6.1 Objective. Measure the valve leak rate as a function of the number of openings/closings with < 2K (3.6R) superfluid helium on one side and high vacuum on the other.

6.1.6.2 Approach. A motor-operated superfluid liquid helium valve is currently under development. These tests in a vacuum chamber will be required only if the program does not adequately test this valve under the desired operating conditions or if the measured leakage rates are too high. In that case, additional valve development may be required.

6.1.7 One-Fifth Scale Vacuum Shell Tests (Task 7)

6.1.7.1 Objectives. Demonstrate the vacuum shell flange seal plus the titanium/aluminum transition joints will not leak after repeated temperature and pressure cycling.

6.1.7.2 Approach. A one-fifth scale model of the vacuum jacket flange seal plus titanium/aluminum bond joint will be fabricated and installed in a vacuum system as shown in Fig. 6.4. The scale model will be evacuated with a helium mass spectrometer; the vacuum bell will be evacuated separately and back filled with helium to 0.9 atmospheres. Leak checking will be performed continuously during these sequences. The helium pressure will be decreased to zero to see if a decreased line load on the seal will initiate a leak. The helium pressure will be increased back to 0.9 atmospheres and the shroud enclosure cooled down gradually from 300 to 100K (540 to 180R). Once the test

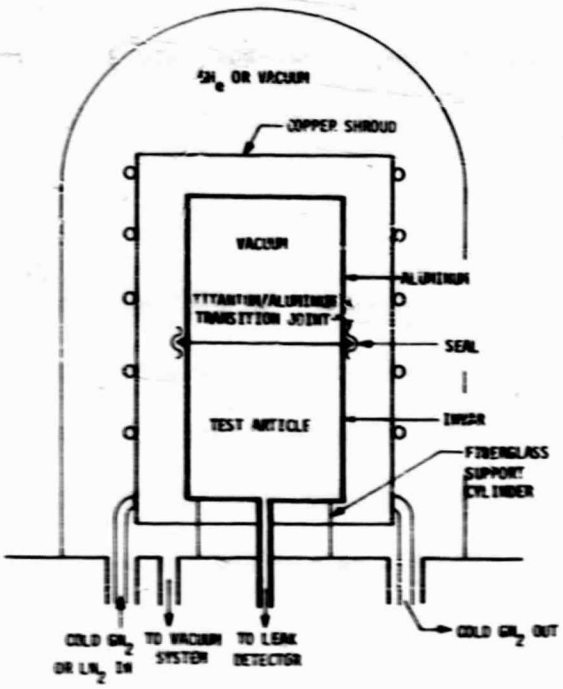

Fig. 6.4 One-Fifth Scale Model Test of the Vacuum Jacket Flange Seal and Bond Joint

setup reaches 100K (180R), the helium pressure will be decreased again to zero. This cooldown, pressure cycling sequence will be performed enough times to simulate twice the number of pressure/temperature cycles the vacuum shell would experience in use.

6.1.8 Full-Scale Aperture Cover Separation Tests (Task 8)

6.1.8.1 Objective. Demonstrate the aperture cover seal is vacuum tight (leak rate less than a specified amount) yet will separate reliably from the vacuum shell on command.

6.1.8.2 Approach. Prior programs such as IRAS eject the aperture cover in orbit once it is outside the Oribter cargo bay. Assuming this design works reliably, it will be incorporated into this program and demonstrated only on the qualification model. If for any reason designs from other qualified systems are not suitable for this dewar, then the following development tests will be conducted.

A full-scale aperture cover will be designed and built including a mating vacuum shell hat section. The aperture cover seal will be leak checked by evcuating the cover and bagging and flooding the exterior seal area with helium. The cover is returned to ambient pressure, the bag removed and the aperture cover installed in a vacuum chamber. The cover will be connected to a counter-balanced weight using a pulley system to permit separation under simulated zero-g conditions in vacuum. The aperture cover separation mechanism will be fired, separating the cover. Movies will be taken of the tests. This test will be repeated a number of times to demonstrate the reliability of the seal and separation mechanism.

6.1.9 Multilayer Insulation Conductivity Tests (Task 9)

6.1.9.1 Objectives. The objectives of this task are twofold: 1) Measure the conductivity of the selected multilayer insulation over the temperature range 78 to 4K (140 to 7R); and 2) develop and measure new combinations of radiation shields and spacers that are more efficient thermally over this temperature range.

6.1.9.2 Approach. These tests are currently planned to be performed on the Lockheed Independent Research Program. They consist of measuring the conductivity of selected multilayer insulations over the temperature range 78 to 4K (140 to 7R) and then varying the number of spacers used between radiation shields to reduce the dominant conduction term. The tests are to be performed in a flat plate test apparatus with and without simulated joints. These data should be available in time for use on this program. If they are not, these tests should be conducted on this program.

6.1.10 Development Model Dewar Analysis and Design (Task 12)

6.1.10.1 Objective. Perform sufficient analyses and design work to allow a full-scale, flight-weight, development dewar system to be fabricated.

6.1.10.2 Approach. Using the data from Tasks 2 through 11, update and expand the stress analysis, thermal model analysis and design developed in Task 1 to a level of detail needed to fabricate the complete full-scale, flight-weight development dewar.

6.1.11 Development Model Dewar Fabrication and Assembly (Task 13)

Using the drawings from Task 12, fabricate, assemble and leak check one complete, full-scale flight-weight superfluid helium dewar including the aperture cover. Perform extensive leak checks as the dewar is assembled. Internal instrumentation such as temperature sensors and accelerometers will be installed as the assembly progresses. The following parts will be

available from prior tasks assuming no changes are required based on the tests performed.

Quantity	Part	Task No.
12	PODS Supports	10
1	Invar Vacuum Shell Ring	10
5	Vapor-Cooled Shields (partial)	10
1	Wire Feed through	5
2	Low-Temperature Valves	6
1	Aperture Cover	8

6.1.12 Development Model Dewar Tests (Task 14)

6.1.12.1 Objective. Demonstrate the dewar will meet all the system perform-ance requirements defined in Task 1.

6.1.12.2 Approach. Following assembly and leak check of the dewar, a series of tests will be performed to demonstrate the dewar meets all performance requirements defined in Task 1. Periodic leak checks will be performed throughout the test program. The following series of tests will be performed.

- Aperture Cover Separation Test. The test described in Task 8 will be repeated only this time it will be installed on the complete dewar that includes insulation and shields.

- Modal Vibration Test. The modal vibration tests described in Task 11 will be repeated in three axes on the evacuated, full-scale dewar. A

200 kg mass will be installed to simulate the instrument weight and the helium tank will be partially filled with water to simulate the helium mass. Accelerometers will be installed as required. The results will be compared with the test data obtained in Task 11.

- Vacuum Bakeout. The 200 kg mass simulating the experiment will be removed prior to the bakeout. The dewar insulation will be evacuated at a controlled rate and baked out at as high a tempera-ture as allowed by the materials used in the construction. Based on prior programs, this temperature should be in the area of 350K (630R). The high vacuum pumping system will be connected to the dewar and operated during the entire bakeout cycle. Prior program experience shows the bakeout time will probably be on the order of 4-6 weeks before the rate of pressure decrease will be less than 5% per week.

- Thermal Performance. The dewar will be installed in a LN_2 shrouded vacuum chamber for the following tests as shown in Fig. 6.5. The superfluid helium tank plus the ground hold torus tank will be evacuated and then purged with GHe several times. A normal helium storage dewar located outside the chamber will be converted to superfluid helium by pumping on the dewar. A vacuum pump will be attached to the development dewar vent line and superfluid fluid helium transferred from the storage dewar to the primary tank. The helium fill level will be on the order of 20% for the initial tests. The primary tank is then locked up and the torus filled with normal liquid helium. Ground hold tests will measure the temperature

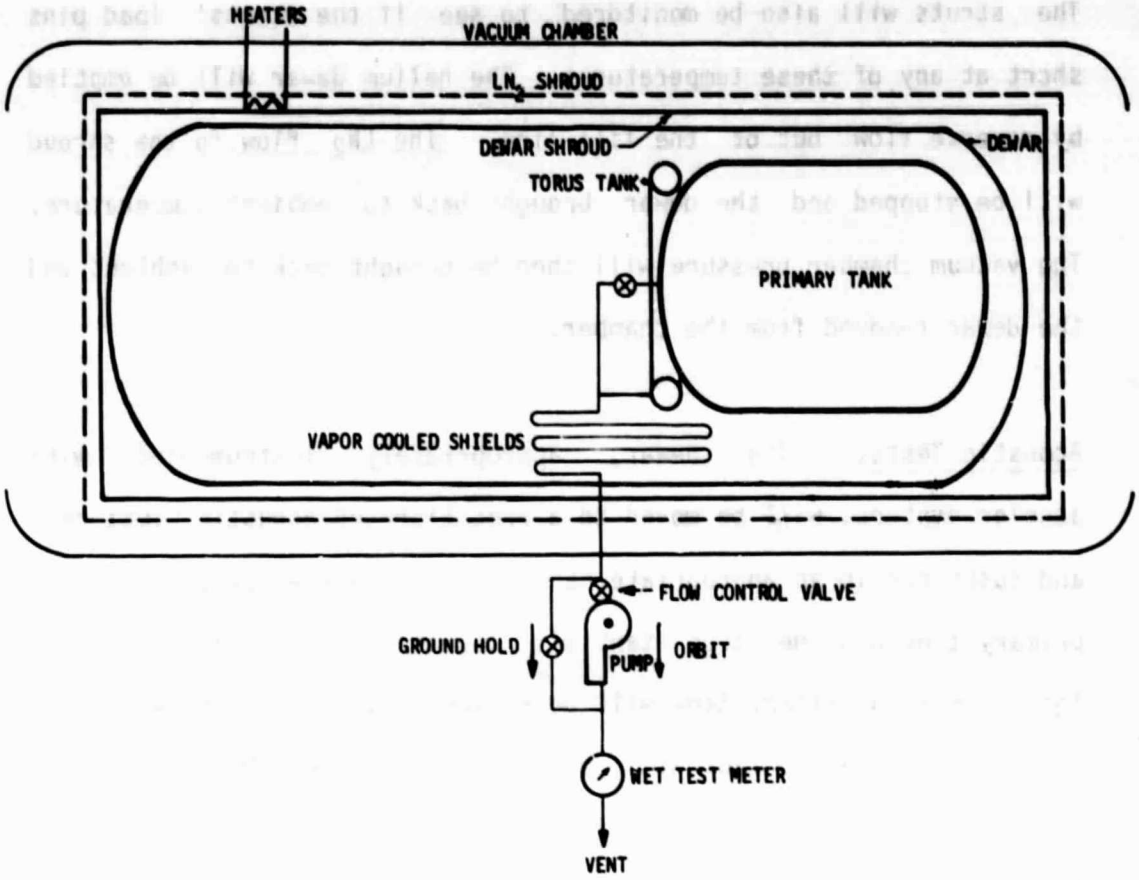

Fig. 6.5 Dewar Thermal Test Setup

distributions throughout the dewar, the rate of pressure rise in the primary tank and the boiloff rate in the torus tank.

Once the torus tank is emptied, the primary tank will be vented through the vapor-cooled shields and a pump on the vent line to maintain the tank temperature constant. The boiloff rates will be measured and then the vacuum shell temperature will be dropped in increments to 250, 200, 150 and 100K (450, 360, 270 and 180R) by flowing LN_2 through the chamber shroud and adjusting the heater power levels on the dewar shroud. Dewar temperatures plus the boiloff rate will be measured at each of these temperature levels.

The struts will also be monitored to see if the struts' load pins short at any of these temperatures. The helium dewar will be emptied by reverse flow out of the fill line. The LN_2 flow to the shroud will be stopped and the dewar brought back to ambient temperature. The vacuum chamber pressure will then be brought back to ambient and the dewar removed from the chamber.

- Acoustic Tests. The dewar, appropriately instrumented with acceler-ometers, will be moved to a precalibrated acoustic test cell and suspended in an appropriate manner, i.e., bungee cord. Both the primary tank and the torus tank will be filled with liquid helium. The superfluid primary tank will be nonvented for this test while the normal helium torus tank will be venting through the vapor-cooled shields. The acoustic levels will be demonstrated in short 10-second bursts before the full duration test is conducted at the required decibel level. The temperatures, pressures and accelera-tion levels will be monitored throughout the test.

- Repeat Thermal Performance. The dewar will be moved back to the vacuum chamber and the thermal performance tests repeated for ground hold and at T_H = 200 and 100K (360 and 180R) for the simulated orbit test. These data will be compared to the pre-acoustic test data to see if any degradation has occurred.

6.2 PRELIMINARY DEVELOPMENT SCHEDULE

The Technology Plan Schedule is provided in Fig. 6.6. As can be seen from the schedule, the subsystem and development tasks are complete after two years; the fabrication, assembly and test of the full-scale development dewar takes another year and one-half for a total development span of three and one-half years. This schedule could be compressed to three years without undue technical problems.

6.3 ROM DEVELOPMENT COSTS

Based on the task definitions in Section 6.1, the Schedule in 6.2 and the costing ground rules in Table 6.2, an ROM cost estimate was prepared for the program, task by task, as shown in Table 6.3.

Table 6.2 COSTING GROUND RULES

- 1981 dollars
- Program Manager (no cost to program)
- No Quality Assurance coverage (development program)
- Fee not included
- LHe $2.30 per liter
- LN_2 $0.27/ft^3$ (bulk)
- CADAM $56/hour
- 1110 computer $500/hr
- No GSE costed
- $43/hour labor (except manufacturing)
- $46/hour manufacturing
- Use flight-weight hardware

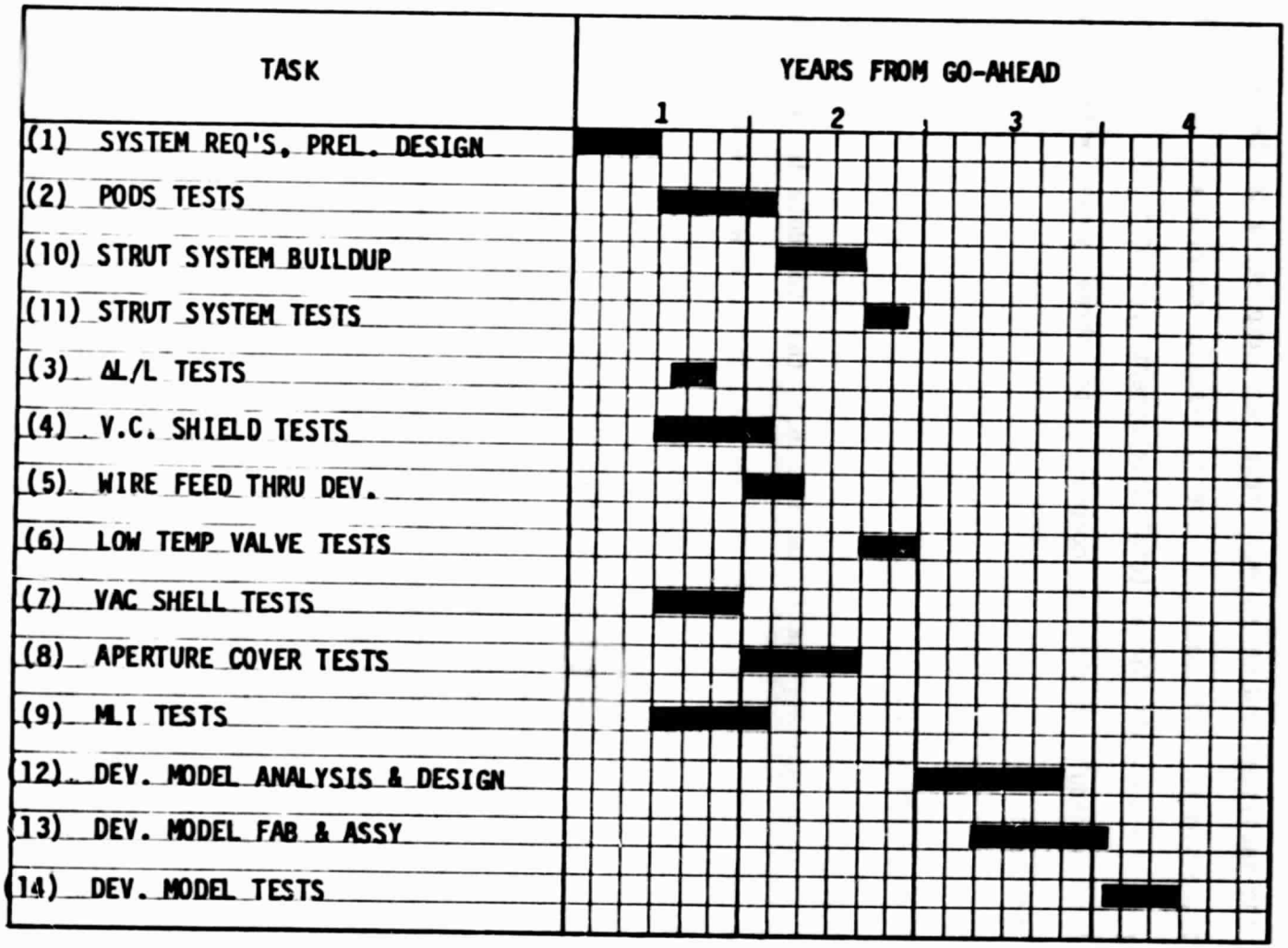

Fig. 6.6 Technology Development Plan Schedule

Table 6.3 ROM COST BREAKDOWN FOR THE FULL-SCALE, FLIGHT-WEIGHT, DEVELOPMENT DEWAR

LITERS LH_2	LITERS LN_2	HTL SUB CONTRACT DOLLARS $ 1000		CADAM HRS	1110 HRS	TASK	MAN HOURS TALEI (LABOR CATEGORY/CLASSIFICATION) SUBTOTAL	DESIGN	THERMAL ANALYSIS	STRUCTURAL ANALYSIS	TEST	MANUFACTURING	TECHNICAL PUBLICATIONS	TECHNICAL MANAGEMENT	SYSTEMS ANALYSIS	$ 1000 MANHOURS COST	SUBCONTRACT, COMPUTER, MATL, CRYOGEN COSTS	TOTAL COSTS
				960	10	1. SYSTEM PERFORMANCE REQUIREMENTS AND DESIGN UPDATE	3,040	1,200	640	400			160	640	640	165	53	218
300	1,000	0		120	3	2. PODS DEVELOPMENT	2,000	160	120	120	800	560	80	320		88	17	105
900		.5				3. △L/L TESTS	376				320		16	40		16	3	19
600	2,000	10		100	3	4. VAPOR COOLED SHIELD PANEL TESTS	1,960	160	200	80	800	200	40	320		85	17	102
		2		90		5. WIRE FEED THRU DEVELOPMENT	560	160	40			320		40		25	7	32
200		10				6. LOW TEMP VALVE LEAK TESTS	696				160	480	16	40		31	11	42
	600	2		70	2	7. ONE-FIFTH SCALE VACUUM SHELL TESTS	1,000	120		160	320	320	80	80		47	7	54
		10		190		8. FULL SCALE APERTURE COVER SEPARATION TESTS	1,320	320			320	480	80	120		58	21	79
1200	1200	3				9. MULTILAYER CONDUCTIVITY TESTS	1,240		320		640		120	160		53	6	59
		40		190		10. STRUT SYSTEM BUILDUP PLUS INVAR SHELL	2,680	320			320	1,880		160		121	51	172
		0				11. PODS SUPPORT SYSTEM TESTS	2,000				1,200		160	640		89	10	99
				1,700	20	12. DEVELOPMENT MODEL ANALYSIS AND DESIGN	7,620	2,900	960	660			320	960	1620	319	105	424
		95				13. DEVELOPMENT MODEL FAB AND ASSEMBLY	10,420				960	8,500		960		476	95	569
8,000	100,000	12			3	14. DEVELOPMENT MODEL TESTS	5,820				4,900	640	720	960		295	33	328
11,100	139,000	200.5		3,400	61		62,492	5,420	2,360	1,500	10,700	13,460	1,352	5,000	2260	1,866	435	2,301

This total program cost of 2.3 million dollars is for a full-scale development dewar using flight-weight equipment and hardware.

The costs were also re-examined for a half-scale development dewar. The cost reduction amounted to only 8%, with most of those cost savings coming in Tasks 13 and 14. The reason for this small reduction is as follows.

A smaller dewar does not reduce design, analysis, technical publications or management costs. In fact, small-scale models increase analysis costs slightly because of uncertainties and difficulties in scaling the test results. Some lower material costs plus lower fabrication costs are possible for a smaller dewar. However, these cost-reductions are not large because the fabrication and assembly process is highly labor-intensive and depends more on the number of process steps than the part size. Test costs are only slightly affected by the decreased cryogen costs. Basically, the same number of fabrication and assembly steps are required for a half-scale dewar as a full-scale dewar; consequently, the cost savings are not large.

This type of analysis shows why it is more cost effective to build a slightly larger and heavier single-stage helium dewar than a slightly smaller and lighter-weight dual-stage dewar (with a larger number of parts and consequently more fabrication and assembly steps.)

Some of the development tasks shown in Table 6.3 stand along (such as 2, 3, 4, 5, 6, 7 and 9) and could be accomplished through individual research programs, and accomplished in the order shown in Table 6.1 based on the priority rankings.

Section 7

CONCLUSIONS

The major conclusions reached in this study are as follows.

1. A three-year lifetime superfluid helium dewar is feasible at one-half the maximum weight specified in the contract, 989 kg (2180 lb) vs. 2000 kg (4409 lb).

2. Demonstration of the PODS support system is the key technology item required to achieve the predicted performance.

3. The achievable warm boundary temperature in orbit has a strong effect on system performance and selection of cryogens. Below ~ 150K (270R), a single-stage helium dewar is the best overall choice when both weight and manufacturing complexity are considered. Between 150 and 200K (270 and 360R), the single-stage helium dewar is still the best overall choice although dual-stage He/Ne and He/N_2 dewars are ~ 20% lighter. Above 200K (360R), the dual-stage concepts should be seriously considered because of their increasingly larger weight advant-ages. Warm boundary temperatures predicted for current dewar flight programs are 150K (270R)--Teal Ruby (Ne/CH_4)--and 170K (306R)--IRAS (SF He). These temperatures are achieved using thermal control coatings, insulation, radiators and active orientation systems.

4. The SF He cylindrical tank with ellipsoidal ends chosen for this study may not be the optimum geometry for other systems depending on their specific requirements. For example, a toroidal tank surrounding the instrument cavity shows a lower CG shift as the tank is emptied, decreases the dewar length by 40% and improves the PODS thermal performance (since the shorter length decreases the tilt loads now designing the supports). Altering the tank geometry changes dewar dimensions but does not alter the basic development tasks recommended in Section 6.

5. The support resonances were calculated assuming the tank/instrument and vacuum shell attach points were infinitely rigid. More detailed analyses are required to determine the actual stiffening required at these attach points to achieve the desired resonances.

6. More than adequate ground hold times can be obtained using a secondary normal helium tank with a minimal weight penalty. The ground hold heat rate into the nonvented superfluid helium tank is extremely low, 3.2 mW (0.009 Btu/hr) or approximately 13% that of the 200K (360R) orbit case. The reason for the extremely low ground hold heat rate is as follows. The first vapor-cooled shield is shorted to the torus tank at 4.2K (7.6R); in orbit, the shield temperature is allowed to float. Secondly, the PODS supports do not short in one-g, minimizing the support heat leak and finally, the instrument is not operating.

7. Sensitivity analyses show the dewar lifetime is affected by the following parameters listed in order of increasing sensitivity: PODS conductance, instrument heat load, multilayer insulation con ductivity and vacuum shell temperature.

8. A development program can be accomplished in three and one-half years.

9. Development program costs of 2.3 million dollars are reduced only 8% going to a half-scale dewar.

Section 8

REFERENCES

1.1 Proceedings of the Seventh International Cryogenic Engineering Conf., ICEC 7, p. 132, London, 4-7 July 1978.

3.1 Nast, T.C., Barnes, C.B., and Wedel, R.K., "Development and Orbital Operation of a Two-Stage Solid Cryogen Cooler," J. Spacecraft and Rockets, Vol. 15, pp. 85-91, 1978.

3.2 Proceedings of the Seventh International Cryogenic Engineering Conf., ICEC 7, p. 132, London, 4-7 July 1978.

3.3 "Teal Ruby Cryostat Critical Design Review," LMSC-D057954, 11,12 Jan 1978.

4.1 Proceedings of the Seventh International Cryogenic Engineering Conf., ICEC 7, p. 132, London, 4-7 July 1978.

4.2 Cryogenic Tank Support Evaluation, Interim Report, NASA CR-72538, 15 April 1969.

4.3 Fiberglass Supports for Cryogenic Tanks, NASA CR-120937, 10 Oct. 1972.

4.4 Proceedings of Cryogenic Workshop, G.C. Marshall Space Flight Center, March 29-30, p. 15, 169, 1972.

4.5 Bushnell, D., "PANDA--Interactive Computer Program for Preliminary Minimum Weight Design of Composite, Stiffened Cylindrical Panels and Shells Under Combined Loads," Lockheed Missiles & Space Co., Rept. No. LMSC-D767794, March 1981.

4.6 Vanderplaats, G.N., and Moses, F., "Structural Optimization by Methods of Feasible Directions," Computers & Structures, Vol. 3, pp 739-755, 1973.

4.7 Vanderplaats, G.N., "CONMIN--A FORTRAN Program for Constrained Function Minimization; User's Manual," NASA TM X-62,282, Ames Research Center, Moffett Field, CA, Aug. 1973; version updated in March 1975.

4.8 Zoutendijk, G., Methods of Feasible Directions, Elsevier Publ. Co., Amsterdam, 1960.

5.1 Lockheed Independent Research and Development Program, LMSC-D630733, Vol. II, pp. 7-137, 1978 Report, 1979 Plan.

5.2 Lehmann, W., and Zahn, G., Safety Aspects for LHe Cryostats and LHe Transport Containers, IPC Business Press, 1978.

9.1 Vanderplaats, G.N., and Moses, F., "Structural Optimization by Methods of Feasible Directions," Computers & Structures, Vol. 3, pp. 739-755, 1973.

9.2 Vanderplaats, G.N., "CONMIN-A FORTRAN Program for Constrained Function Minimization; User's Manual," NASA TM X-62,282, Ames Research Center, Moffett Field, CA, Aug. 1973; version updated in March 1975.

9.3 Zoutendijk, G., Methods of Feasible Directions, Elsevier Publ. Co., Amsterdam, 1960.

9.4 Bushnell, D., "PANDA--Interactive Computer Program for Preliminary Minimum Weight Design of Composite, Stiffened Cylindrical Panels and Shells Under Combined Loads," Lockheed Missiles & Space Co., Rept. No. LMSC-D767794, March 1981.

9.5 Almroth, B.O., and Brogan, F.A., "The STAGS Computer Code," NASA CR 2950, NASA Langley Research Center, Feb. 1978.

10.1 Bell, G.A., Nast, T.C., and Wedel, R.K., "Thermal Performance of Multilayer Insulation Applied to Small Cryogenic Tankage," Advances in Cryogenic Engineering, Vol. 22, 1977.

10.2 Hurst, J.G., and Arvidson, J.M., "Thermal Conductivity of Glass Fiber/ Epoxy Composite Support Bands for Cryogenic Dewars," Report 275.03-78-2, Cryogenics Division, NBS, Feb. 1978.

10.3 Keller, C.W., "Fiberglass Supports for Cryogenic Tanks," NASA CR-120937, Lockheed Missiles & Space Company, 10 October 1972.

10.4 Childs, Ericks and Powell, "Thermal Conductivity of Solids at Room Temperature and Below," NBS Monograph 131, Sept. 1973.

10.5 "Handbook of Thermal Design Data for Multilayer Insulation Systems," LMSC-A742593-VI, Lockheed Missiles & Space Company, 11 August 1965.

10.6 Johnson, V.J., "A Compendium of the Properties of Materials at Low Temperature (Phase 1)," WADD Tech. Rept. 60-56, Part II, NBS Cryogenic Engineering Laboratory, Oct. 1960.

10.7 "Invar Technical Data Sheet," Carpenter Steel Company, Reading, Pa.

10.8 1979 Materials Selector, Materials Engineering, December 1978.

10.9 "Comparative Data E, S and S2 Glass," Owens Corning Fiberglass Data Sheet, Toledo, Ohio.

10.10 Cryogenic Materials Data Handbook ML-TDR-64-280, Wright-Patterson Air Force Base, August 1964.

Section 9

COMPUTER PROGRAMS

Eight computer programs were used in this study. A description of each program is provided here along with the sections of the report where it was required.

9.1 CRYOP (Sections 3 and 4)

CRYOP is a UNIVAC 1110 computer program that sizes single-or dual-stage dewars. This program was initially developed in 1973 and has been continuously refined and improved over the years until it is now a generalized cryogenic dewar optimization program.

The inputs to the program are number of cryogens, wire penetrations and plumbing lines, MLI type, number of vent-cooled shields and the type of vent cooling (supports, MLI, wiring, plumbing), required lifetime, boundary temperatures, experiment heat loads and an initial geometry.

The solution provides a breakdown and summary of the heat load to each cryogen, the temperatures and locations of the vent-cooled shields, the volumes of the tanks, the overall dimensions of the tanks and the dewar, the optimum MLI thickness and a weight breakdown and summary of the dewar.

The program modifications made specifically for this study are:

- The PODS are now a support option with a heat leak that is both cryogen weight and temperature dependent.
- Up to six shields for each cryogen are available for vent cooling of the supports, insulation, plumbing, and lead wires.
- The primary helium tank is 1 m (39.7 in) in diameter with ellipsoidal ends and a cylindrical section. The secondary tank for dual-stage applications is a torus.
- Weights are included for the MLI, vent-cooled shields and vacuum jacket surrounding the 1 m (39.4 in) diameter by 2 m (78.7 in) long instrument. Aperture cover weight and length are not included. (These values were added in manually for this study.)
- The thermal conductivity is input as a function of temperature for coax wires (stainless steel and Teflon) and the manganin wires. The wire length was assumed to be 0.5 m (19.7 in).

The method of solution is to first calculate the heat load and thereafter the tank size for the primary cryogen. The secondary cryogen sizing is done after the primary cryogen sizing is completed since the net heat load to the secondary consists of the secondary heat load inputs less the primary heat loads due to the MLI, to the supports, and to the plumbing penetrations. Also, if vent gas cooling is considered, the primary vent gas effects on the secondary are included. The amount of cryogen to match the required lifetime for the calculated heat load is then calculated.

9.2 VENTCOOL (Section 3)

A computer program that is used to optimize the location of vent-cooled shields. The cryogen flow rate, boundary temperatures, and polynomial of a material's thermal conductivity vs. temperature and the number of vent shields are input. A Rosenbrock function minimization technique is used to locate the shields in the insulation to give the minimum heat flow. The output is the heat flow, the

shield locations, and their temperatures. This program is used as a subroutine in CRYOP or can be used separately.

9.3 PRESS (Section 5)

A computer program that determines the cryogen temperature and vapor pressure for a given flow system. The inputs are flow rate, molecular weight, and mathematical curve fits for the vapor pressure and viscosity versus temperature of the cryogen, the outlet (minimum) pressure in the system, and the dimensions of the tubes and boundary temperatures. Any number of tubes and temperature boundaries can be input. An iterative process is used to obtain the vapor pressure of the cryogen at a corresponding temperature by calculating the pressure change through each tube section assuming an ideal gas with Poiseuille-type flow. This program defines the required line sizing for proper cryogen temperature control.

9.4 THERM (Sections 4 and 5)

Detail design analyses are done with the Lockheed thermal analyzer computer program, THERM, on the UNIVAC 1110 computer. The configuration is arbitrarily divided into nodes by the designer, and THERM uses a finite difference solution for the three-dimensional heat transfer equation at each node. Programs with well over 1000 nodes have been run with no difficulty. Steady state occurs when the largest temperature difference of any node between consecutive iterations is less than a value specified in the program. Subroutines for THERM can be performed at many places in the calculation. Two examples are: 1) at each iteration, the temperature-dependent properties can be recalculated; and 2) heat maps can be obtained for different nodes.

9.5 PODS (Sections 4 and 5)

A thermal model (9 nodes) was setup for the PODS support. The THERM program is used to perform the analyses. Program inputs include the boundary temperatures, emittance of all surfaces, length and area of S-glass strands, fiberglass tube area and effective length, diameter and length of the stem, body, load pin and load pin hole, and epoxy areas where the S-glass strands are bonded. Program outputs include temperature distributions along the strut and a heat map between nodes.

9.6 FTS (Section 4)

A thermal model (7 nodes) was setup for the FTS support. The THERM program is used to perform the analyses. Program inputs include the boundary temperatures, all three fiberglass tube diameters, areas and effective lengths and emittance and dimensions of the end fittings. Program outputs include temperature distributions along the strut and a heat map between nodes.

9.7 STAGSC1 (Section 4)

The program performs stress, buckling, modal vibration, and transient response analyses of general shells with stiffeners, elastically and plastically. Complex wall construction is permitted. The method uses discrete variational analysis; local two-dimensional power representations of the displacement components; modified Newton method for solution of the nonlinear algebraic equations and automatic correction of load or time steps with restart capability.

Free-field input with 11 standard geometries is defined by their dimensions or data cards. Non-standard geometries require user-written subroutines. No element or node numbering is required for standard geometries. Automatic mesh is generated for geometries defined analytically in user-written subroutines. Loads are defined on data cards, or if varying with location on shell, are defined in user-written subroutines. Loads can be forces or displacements.

The output includes displacements, stress resultants, stresses, strains, equilibrium forces, eigenvalues, eigenvectors, lists and plots.

9.8 PANDA-DEWAR (Sections 4 and 5)

The objective of this support thermal/structural optimization program is to minimize the flow of heat from the vacuum shell to which they are attached, while maintaining enough structural rigidity to keep the lowest frequencies at launch and during orbital conditions above certain specified values, and stresses due to assembly and launch loads below those that would cause buckling or material failure.

In the analysis, the vacuum shell and the tank/instrument structure to which it is attached are assumed to be rigid and the supports to be massless. It is also assumed the tank, vapor-cooled shields, insulation and payload are rigid, supported by elastic struts or tension bands which carry loads only along their axes (pinned ends).

In the PODS and FTS concepts, the effective axial stiffness $(EA)_{eff}$ and heat flow conductance $(KA/L)_{eff}$ change abruptly from the launch condition to the

orbital condition due to certain "disconnect" features within each strut, so the design of each of these support systems involves the solution of two optimization problems, one corresponding to the launch phase and the other corresponding to the orbital phase. The tension band concept involves solution of one optimization problem, corresponding to the launch condition only, since the nature of this support system does not change for the orbital phase and the launch phase represents the more severe environment.

The program inputs include weights and dimensions of supported equipment, launch and orbital frequency constraints, Young's modulus and the maximum allowable stress of the fiberglass tube or band and thermal conductivities of the tube, band and S-glass filaments. Program outputs include: 1) center of gravity locations and polar and tilting moments of inertia of supported equipment; 2) design margins at launch of maximum stress, tube column (Euler) buckling, tube shell (local) buckling, and tube or band thermal stress; 3) strut length and diameter, strut spacing and angles; cross-sectional area and wall thickness and pretension load (tension band only); 4) launch and orbital frequency margins in lateral, tilt, axial and torsional modes; and 5) the axial length and cross-sectional area of the S-glass filaments for the PODS support.

Optimization is carried out by a nonlinear programming algorithm called CONMIN [9.1,9.2]. This program, wirtten by Vanderplaats in the early 1970's, is based on a nonlinear constrained search algorithm due to Zoutendijk [9.3]. The basic analytic technique used in CONMIN is to minimize an objective function (heat flow, for example) until one or more constraints, in this case vibration frequencies, buckling loads, maximum stress or strain, and upper and lower bounds on design variables, become active. The minimization process then

continues by following the constraint boundaries in design variable space in a direction such that the value of the objective function continues to decrease. When a point is reached such that no further decrease in the objective function is obtained, the process is terminated. The analyses that make up this program are described in the following sections.

General Case

The kinetic energy of the body shown in Fig. 9-1 is

$$\text{K.E.} = \tfrac{1}{2}M\sum_{i=1}^{3}\dot{u}_{c_i}^2 + \tfrac{1}{2}\sum_{i=1}^{3}I_i\,\dot{\alpha}_{c_i} \qquad (1)$$

in which M is the mass; I_i, i = 1,2,3 are the principal moments of inertia; $\dot{u}_{c_i}$ are the velocity components along the principal axes; and $\dot{\alpha}_{c_i}$ are the angular velocity components about the principal axes.

If the N identical pinned structural members supporting the body are under initial tension, the strain energy in all of the members (or straps) due to modal vibrations or loading from the prestressed state is

$$\text{Strain Energy} = \tfrac{1}{2}(EA)_{eff}\,L\sum_{j=1}^{N}(e_j^2 - e_{j_o}^2) \qquad (2)$$

in which $(EA)_{eff}$ is the effective axial stiffness of each strut, and e_{j_o} are the initial axial strains associated with the initial tension (prestress) in the members.

The total axial strain e in any member can be written as

$$e = u'_{TOT} + \tfrac{1}{2} u'^{2}_{TOT} \tag{3}$$

in which u_{TOT} is the total displacement along the axis of the member

$$u_{TOT} = u_o + u \tag{4}$$

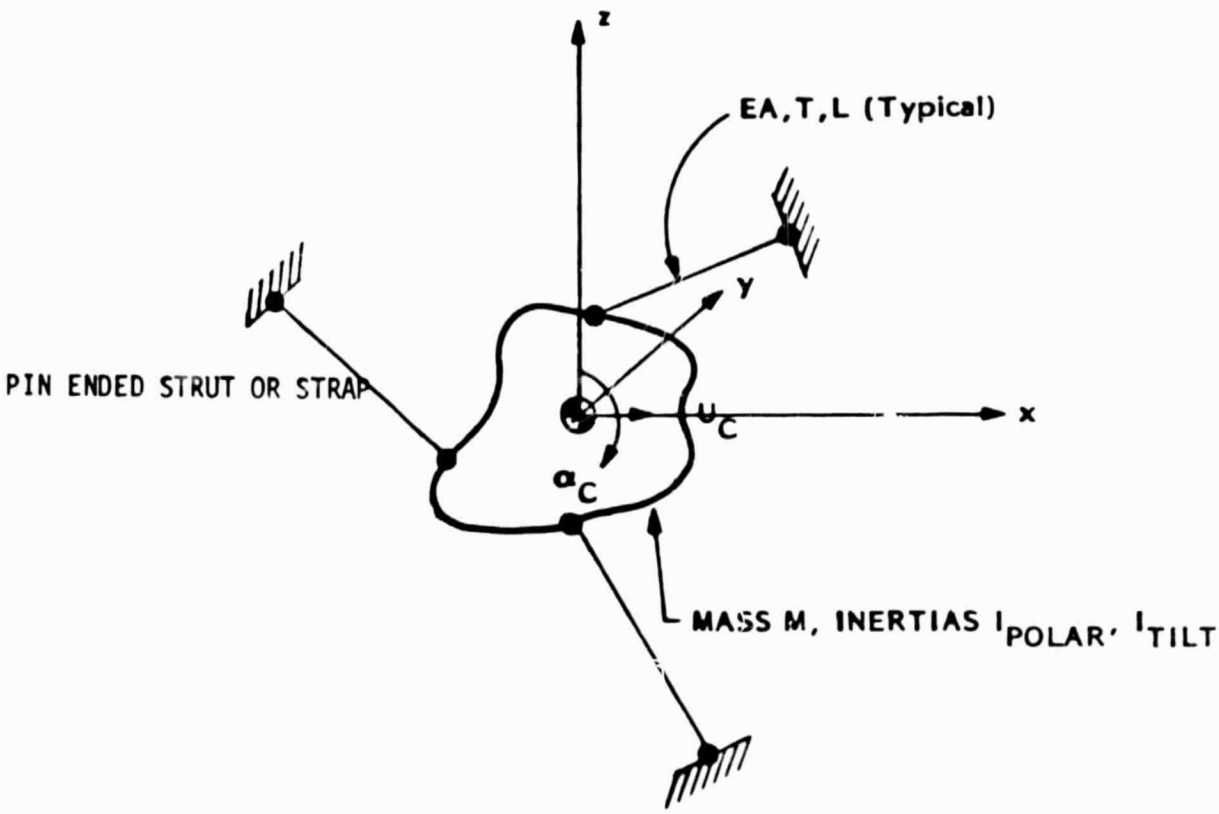

Fig. 9.1 Mass Supported By Pinned, Massless Members With Length L, Stiffness EA, Tension T

with u_o being the displacement associated with the initial tension and u being the displacement associated with infinitesimal modal vibration or static loading. The superscript ( )' represents the derivative of u_{TOT} with respect to the coordinate along the axis of the member. The total strain e can, with (4), be written in the form

$$\begin{aligned} e &= u_o' + u' + \tfrac{1}{2}(u_o' + u')^2 \\ &= e_o + u'(1 + u_o') + \tfrac{1}{2}u'^2 \end{aligned} \tag{5}$$

The strain energy U in Eq. (2) can then be written in the form

$$U = \tfrac{1}{2}(EA)_{eff} L \sum_{j=1}^{N} \left[e_{j_o}^2 + 2e_{j_o} u_j' (1 + u_{j_o}') + e_{j_o} u_j'^2 + u_j'^2 (1 + u_{j_o}')^2 + \text{h.o.t.} - e_{j_o}^2 \right] \tag{6}$$

The second term on the right-hand-side of Eq. (6) drops out when the work done to provide the initial tension is considered to be part of the total energy of the system. This term is equal and opposite in sign to the work done on the system to provide the initial tension. (It is assumed, of course, that the initially tensioned system is in equilibrium!) The "h.o.t." represents cubic and quartic terms in u_j', which can be dropped if we consider vibrations or static deflections of infinitesimal amplitude. With use of the approximation $u_o' \approx e_o$, Equation (6) can be expressed in the form

$$U = \tfrac{1}{2}(EA)_{eff} L \sum_{j=1}^{N} \left[u_j'^2 (1 + 3e_{j_o}) \right] \tag{7}$$

or, with use of the stress-strain relation,

$$(EA)_{eff} e_{j_o} = T_j \tag{8}$$

in which T_j is the tension in the jth member, Eq. (7) becomes

$$U = \tfrac{1}{2} L \sum_{j=1}^{N} \left[(EA)_{eff} + 3T_j \right] u_j'^2 \qquad (9)$$

With equal tension in all members, we have

$$U = \tfrac{1}{2} L \left[(EA)_{eff} + 3T \right] \sum_{j=1}^{N} u_j'^2 \qquad (10)$$

Special Case: Axisymmetric Dewar with Twelve Support Struts or Straps

Configuration and Mass Properties: Figure 9.2 shows an idealized representation of an axisymmetric tank supported by twelve struts or straps, six at a location $L_s/2$ forward of the overall center of gravity (C.G.) and six aft of the C.G. by the same distance. A plan view of the supports is displayed at the top of Fig. 9.2. (In general, both the support azimuthal angle θ and the declination angle γ, shown in Fig. 9.2, may be decision variables in the optimization process. However, several computer runs have demonstrated that the optimum value of θ usually corresponds to a case in which the struts pass through one another, e.g., $\theta = 90^{\circ}$. It was therefore judged practical in the optimization computer runs to express θ as a function of γ such that pairs of struts meet at the vacuum shell, as shown in Fig. 9.2. However, in this derivation θ is maintained independent of γ.

The supported mass consists of three bodies, treated here as rigid in themselves and rigidly connected to each other:

(1) the tank and cryogen;
(2) the vapor shield and insulation;
(3) the payload.

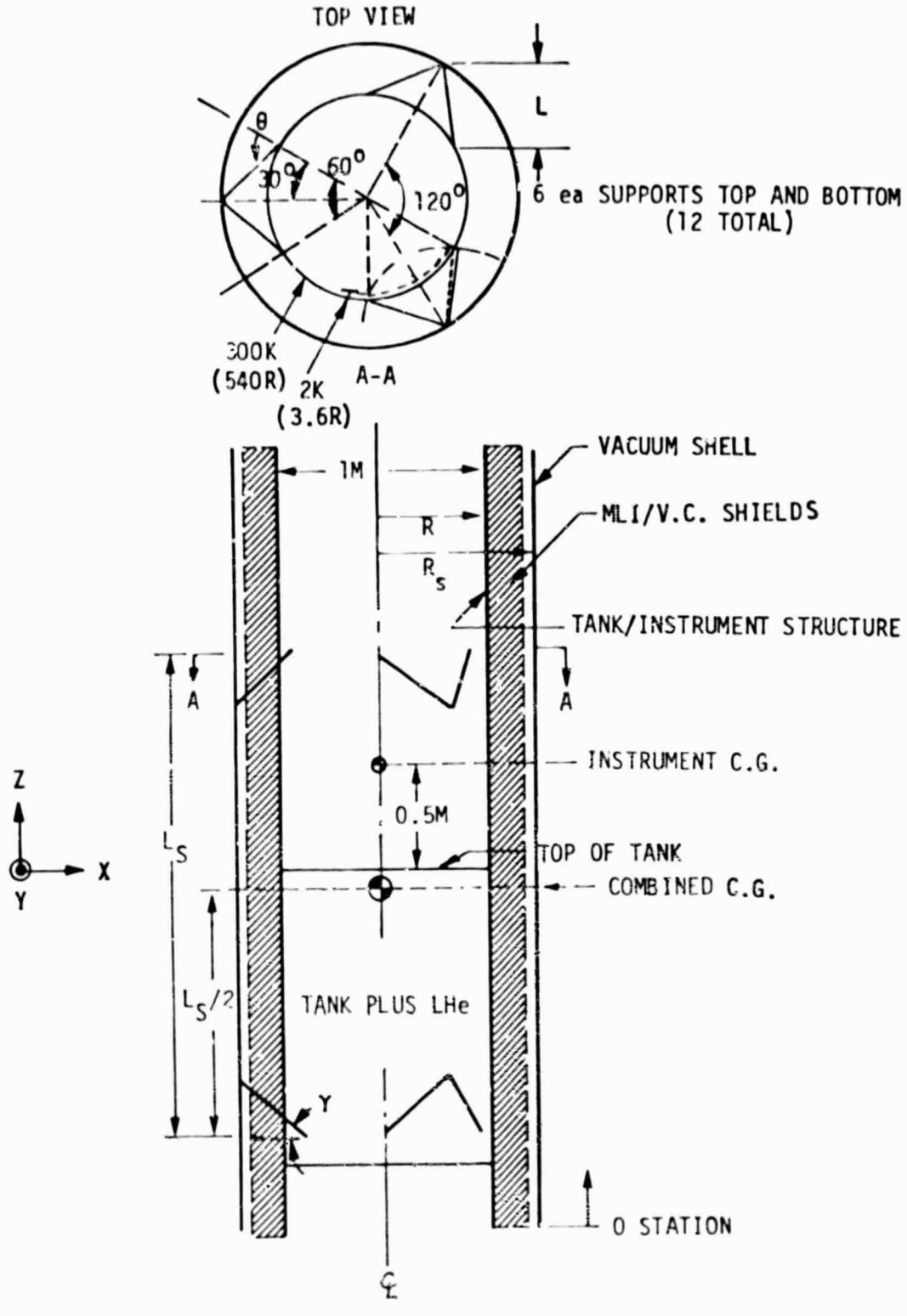

Fig. 9.2 Geometry Used in PANDA-DEWAR Analyses

The vacuum shell is treated as if it were rigid and immovable.

Optimization Strategy: The objective function of the optimization analysis, that is the quantity to be minimized, is an effective heat flow factor, $N*(KA/L)_{eff}$, in which N is the number of supports, K is the strut or strap conductivity, A is the cross-section area, and L is the length. This factor is to be minimized by variation of the design variables (decision variables) listed in Table 9.1 subject to the constraint conditions listed in Table 9.2.

In the PODS and folded tube concepts, the decision variables listed under the heading "LAUNCH CONDITION" are first allowed to vary as the heat flow factor $(KA/L)_{launch}$ is minimized. The variables listed under "ORBITAL CONDITIONS" are not part of this problem. They have no influence at all, since the nature of the PODS and folded tube designs are such as to render them inactive during launch. After optimum values of L_s, θ, γ, t (wall thickness) and IDIAM (inner diameter) have been found, they are held fixed and the decision variables listed under the heading "ORBITAL CONDITION" are allowed to vary as the heat flow factor $(KA/L)_{orbital}$ is minimized.

Variation of Dewar Geometry with Weight: It is of interest to ascertain optimum supports of the type shown in Figs. 4.1-4.4 for a range of weight of supported mass. In this parameter study, the inner diameter of the vacuum shell is held constant at 1.38 m (54.37 in), and the outer diameters of the tank and payload are held constant at 1 m (39.37 in). The vapor shield and insulation project forward from the forward end of the cryogen tank by a constant 2.0 m (78.74 in), and the payload center of gravity is located a constant 0.50 m (19.69 in) forward of the forward end of the cryogen tank.

The tank length in inches varies according to the supported weight (in pounds)

$$L_{TANK} = a_1 + b_1(\text{weight}), \tag{11}$$

TABLE 9.1

DESIGN PARAMETERS (DECISION VARIABLES) IN THE
OPTIMIZATION PROCESS FOR THE THREE DEWAR SUPPORT CONCEPTS

PODS CONCEPT (FIG. 4.1)		FOLDED TUBE CONCEPT (FIG. 4.3)		TENSION STRAP CONCEPT (FIG. 4.4)
LAUNCH CONDITION	ORBITAL CONDITION	LAUNCH CONDITION	ORBITAL CONDITION	BOTH LAUNCH AND ORBITAL CONDITIONS
1. L_s = axial spacing of supports on dewar (Fig. 9.2)	1. A_2 = cross section area of S_{glass} strands	1. same as for PODS concept	1. A_2 = cross section area of tube no. 2	1. same as for PODS concept
2. θ = azimuthal angle of strut (Fig. 9.2)	2. SGLASL = axial length of S_{glass} strands	2. same as for PODS concept	2. A_3 = cross section area of tube no. 3	2. same as for PODS concept
3. γ = declination angle of strut (Fig. 9.2)		3. same as for PODS concept	3. FOLDL = length of tubes 2 and 3 as percentage of length of tube no. 1	3. same as for PODS concept
4. t = thickness of fiberglas tube		4. t = thickness of tube no. 1		4. A = cross section area of strap
5. IDIAM = inner diameter of fiberglas tube		5. IDIAM = inner diameter of tube no. 1		5. TENSN = tension in strap

Table 9.2

CONSTRAINT CONDITIONS ON THE OPTIMIZATION PROCESS FOR THE THREE DEWAR SUPPORT CONCEPTS

	PODS CONCEPT (FIG. 4.1)	FOLDED TUBE CONCEPT (FIG. 4.3)	TENSION STRAP CONCEPT (FIG. 4.4)
PRE-LAUNCH AND LAUNCH CONDITION	1. max. stress in fiberglas tube due to launch loads (10 g axial + 10 g lateral.)	1. same as for PODS concept, tube no. 1.	1. max. stress in strap due to launch loads, as in PODS concept.
	2. buckling of fiberglas tube as a column.	2. buckling of tube no. 1 as a column.	2. tension strap must not go slack during launch.
	3. buckling of fiberglas tube as a thin shell.	3. buckling of tube no. 1 as a thin shell.	
	4. stress in tube due to differential expansion of dewar and vacuum shell during filling with cryogen.	4. same as for PODS concept, applied to tube no. 1.	3. same as for PODS concept, applied to tension strap.
	5. minimum thickness of fiberglas tube = 0.038 cm (0.015 in)	5. minimum thickness of tube no. 1 = 0.038 cm (0.015 in)	
	6. maximum inner diameter of fiberglas tube = 3.8 cm (1.5 in)	6. maximum inner diameter of tube no. 1 = 5.08 cm (2 in)	
	7. maximum values for strut angles θ and γ = 90°.	7. same as for PODS. concept.	4. same as for PODS concept.
	8. minimum vibration frequency = 35 hertz.	8. same as for PODS concept.	5. same as for PODS concept.
ORBITAL CONDITION	1. minimum cross section area of S_{glass} members = 1.3×10^{-4} cm^2 (0.00002 in^2)	1. minimum thickness of tubes 2 and 3 equals 0.025 cm (0.01 in)	
	2. maximum axial length of S_{glass} members = 3.8 cm (1.5 in)	2. maximum length of tubes 2 and 3 = 95% of length of tube no. 1; Length of tube 2 = that of tube 3.	
	3. minimum axial length of S_{glass} members = 1.5 cm (0.6 in)		
	4. minimum vibration frequency = 20 hertz.	3. same as for PODS concept.	1. same as for PODS concept.

in which a, = -27.7; b = 0.067. The weight of the tank-plus-cryogen is given by

$$W_{TANK} = c_1 + d_1(\text{weight}) \tag{12}$$

in which c_1 = -334.0; d_1 - 0.6088. The length and weight of the vapor shield-plus-insulation are

$$L_{VAPOR} = a_1 + b_1(\text{weight}) + 78.74 \tag{13}$$

$$W_{VAPOR} = e_1 + f_1(\text{weight}) \tag{14}$$

in which e_1 = -146.0; f_1 = 0.391. The weight of the payload W_{PAY} is a constant 218 kg (480 lb). The total weight to be supported, called "weight" in Eqs. (11-14) is given by

$$\text{weight} = W_{TANK} + W_{VAPOR} + W_{PAY} \tag{15}$$

and the mass is, of course,

$$M_{TOT} = \text{weight}/g = M \tag{16}$$

The mass moments of inertia required in the modal vibration analysis are I_{polar} and I_{tilt}, the moments of inertia corresponding to rotation of the dewar about its axis of revolution (rolling) and rotation of the dewar about any axis through the C.G. normal to the axis of revolution (pitching). The polar mass moment of inertia, I_{polar}, is given by

$$\begin{aligned} I_{polar} = {} & M_{TANK}\,(R^2_{OTANK} + R^2_{ITANK})\,/2 \\ & + M_{VAPOR}(R^2_{OVAP} + R^2_{IVAP})\,/2 \\ & + M_{PAY}(R^2_{PAY})\,/2 \end{aligned} \tag{17}$$

in which M signifies mass and

$$R_{OTANK} = R; \quad R_{ITANK} = 0$$

$$R_{OVAP} = R_s; \quad R_{IVAP} = R \tag{18}$$

$$R_{PAY} = R$$

where R_s and R are given in Fig. 9.2. The mass moment of inertia corresponding to tilting, I_{tilt}, is given by

$$\begin{aligned} I_{tilt} = {} & M_{TANK}\left[L^2_{TANK}/12 + (R^2_{OTANK} + R^2_{ITANK})/4 \right. \\ & \left. + (d_{c.g} - L_{TANK}/2)^2\right] + M_{VAPOR}\left[L^2_{VAPOR}/12 \right. \\ & \left. + (R^2_{OVAP} + R^2_{IVAP})/4 + (d_{c.g.} - L_{VAPOR}/2)^2\right] \\ & + M_{PAY}\left[R^2_{PAY}/4 + (L_{TANK} + 19.7 - d_{c.g.})^2\right] \end{aligned} \tag{19}$$

in which $d_{c.g.}$, shown in Fig. 9.2, is given by

$$\begin{aligned} d_{c.g.} = {} & \left[W_{TANK}\, L_{TANK}/2 + W_{VAPOR}\, L_{VAPOR}/2 \right. \\ & \left. + 480\ (L_{TANK} + 19.7)\right] /(\text{weight}) \end{aligned} \tag{20}$$

Natural Frequencies: There are six natural frequencies for the system shown in Fig. 9.2 which correspond to rigid body motion of the supported mass. Four of these are distinct. These four correspond to translation of the mass M: (1) along the axis of revolution (axial) and (2) normal to the axis of revolution (lateral), and rotation of the mass M: (3) about the axis of revolution (torsional or rolling) and (4) rotation of M about an axis through the C.G. normal to the axis of revolution (tilting or pitching). The natural frequencies are calculated from

$$\Omega_i^2 = \frac{L\left[(EA)_{eff} + 3T\right]\sum_{j=1}^{N} u_j'^2}{M\, u_{c_i}^2}\ ; \quad i = 1,2 \qquad (21)$$

for axial or lateral modes and

$$\Omega_i^2 = \frac{L\left[(EA)_{eff} + 3T\right]\sum_{j=1}^{N} u_j'^2}{I\, \alpha_{c_i}^2}\ ; \quad i = 1,2 \qquad (22)$$

for torsional (roll) or tilt (pitch) modes. The lateral and pitching modes are decoupled because it is assumed that the rigid mass M is supported symmetrically with respect to the axial coordinate on either side of the mass centroid (Fig. 9.2). For these four modes of vibration it is required to calculate u_j', j = 1,2 ...12 given unit values of u_{c_i}, i = 1,2 (corresponding to axial and lateral components of translation) and given unit values of α_{c_i}, i = 1,2 (corresponding to unit values of rotation about the axis of revolution (torsion) and rotation about an axis through the mass centroid normal to the axis of revolution.

Calculation of u_j', j = 1,2...12 for unit values of u_{c_i} and α_{c_i}

(1) Pure Axial Motion (in the z-direction, Fig.9.2): All support members experience the same absolute value of strain $|u_j'|$. This strain is defined as

$$e_{strut} = (L_{new} - L)/L = u' \qquad (23)$$

which, from Fig. 9.2 and for small u_c, can be written

$$u' = u_c \sin\gamma/L \tag{24}$$

in which L is the length of the support member. From Eqs. (21) and (24) the frequency corresponding to the axial mode is

$$\Omega^2_{axial} = N\left[(EA)_{eff} + 3T\right]\sin^2\gamma/(LM) \tag{25}$$

in which N is the number of support members (12) and M is the supported mass.

(2) Pure Lateral Motion: In this section an expression for the frequency corresponding to motion in the (x,y) plane is desired. (See Fig. 9.2) Unlike the case for pure axial motion the support members each have different strains due to motion of the center of gravity (C.G.) in a given direction in the (x,y) plane.

Table 9.3 gives the strains in each of the six forward support members corresponding to a unit displacement in the x-direction or in the y-direction. The strains in the six aft support members are identical. With use of Eq. (21) and Table 9.3, one can write for the frequency corresponding to motion of the C.G. in the x and y directions

$$\begin{aligned}\Omega^2_x &= 4\left[(EA)_{eff} + 3T\right]\cos^2\gamma\left[\cos^2\theta + \cos^2(60-\theta) + \cos^2(60+\theta)\right]/(LM)\\ \Omega^2_y &= 4\left[(EA)_{eff} + 3T\right]\cos^2\gamma\left[\sin^2\theta + \sin^2(60-\theta) + \sin^2(60+\theta)\right]/(LM)\end{aligned} \tag{26}$$

The three terms involving θ in Eqs. (26) sum to 3/2, so that

$$\Omega^2_x = \Omega^2_y = 6\left[(EA)_{eff} + 3T\right]\cos^2\gamma/(LM) \tag{27}$$

Table 9.3

STRAIN IN VARIOUS SUPPORT MEMBERS DUE TO A UNIT LATERAL DISPLACEMENT IN EITHER THE X OR THE Y DIRECTION (See Fig. 9.2)

Support Member[a]	Strain due to Unit Displacement in y-Direction	Strain due to Unit Displacement in x-Direction
1	$-\cos\gamma\sin(\theta)/L$	$-\cos\gamma\cos(\theta)/L$
2	$-\cos\gamma\sin(60-\theta)/L$	$-\cos\gamma\cos(60-\theta)/L$
3	$-\cos\gamma\sin(60-\theta)/L$	$+\cos\gamma\cos(60-\theta)/L$
4	$-\cos\gamma\sin\theta/L$	$+\cos\gamma\cos\theta/L$
5	$+\cos\gamma\sin(60+\theta)/L$	$+\cos\gamma\cos(60+\theta)/L$
6	$+\cos\gamma\sin(60+\theta)/L$	$-\cos\gamma\cos(60+\theta)/L$

[a] As shown in Fig. 9.2, these correspond to the supports forward of the combined C.G. The strains in the corresponding members aft of the C.G. are identical.

The lateral modal vibration frequency is independent of θ. It is clear from the symmetries displayed in Fig. 9.2 that the frequency corresponding to lateral motion of the mass C.G. is the same for motion in the x-direction and for any motion in the (x,y) plane in 30° increments from the x-direction. Therefore, the modal vibration behavior corresponding to motion in the (x,y) plane is essentially isotropic.

(3) Pure Torsional (Rolling) Motion: As with pure axial motion, all N support members are strained identically. The absolute value of the strain in each member is given by

$$|e| = |u'| = u_c \cos\gamma \sin\theta/L \tag{28}$$

in which

$$u_c = \alpha_c R \tag{29}$$

The frequency squared, from Eq. (22), is therefore given by

$$\Omega^2_{TORSION} = R^2 N \left[(EA)_{eff} + 3T \right] \cos^2\gamma \sin^2\theta/(LI_{polar}) \tag{30}$$

in which N = 12, R is the radius shown in Fig. 9.2, and the polar mass moment of inertia, I_{polar}, is given by Eq. (17).

(4) Tilting (Pitching) Motion: Pitching of the supported mass about the x-axis or y-axis (Fig. 9.2) involves resultant motions of those ends of the support members that are attached at the radius R (Fig. 9.2) which are combinations of axial [Eq. (24)] and the lateral (Table 9.3) motions. Tables 9.4 and 9.5 show the strains due to these components of motion due to pitching about the x-axis and the y-axis, respectively. It can be shown from Eq. (22) with Tables 9.4 and 9.5, and with superposition of the

Table 9.4

STRAINS IN SUPPORT MEMBERS DUE TO PITCHING ABOUT THE X AXIS (Fig. 9.2)

SUPPORT MEMBER	Strain due to the component of motion parallel to the (x,y) plane		Strain due to the component of motion in the axial (z) direction	
	Forward Members[a]	Aft Members	Forward Members[a]	Aft Members
1	$-\Delta_1 \cos\gamma \sin(\theta)/L$	$+\Delta_1 \cos\gamma \sin(\theta)/L$	0	0
2	$-\Delta_1 \cos\gamma \sin(60-\theta)/L$	$+\Delta_1 \cos\gamma \sin(60-\theta)/L$	$-\Delta_2 \sin(\gamma)/L$	$+\Delta_2 \sin(\gamma)/L$
3	$-\Delta_1 \cos\gamma \sin(60-\theta)/L$	$+\Delta_1 \cos\gamma \sin(60-\theta)/L$	$-\Delta_2 \sin(\gamma)/L$	$+\Delta_2 \sin(\gamma)/L$
4	$-\Delta_1 \cos\gamma \sin(\theta)/L$	$+\Delta_1 \cos\gamma \sin(\theta)/L$	0	0
5	$+\Delta_1 \cos\gamma \sin(60+\theta)/L$	$-\Delta_1 \cos\gamma \sin(60+\theta)/L$	$+\Delta_2 \sin(\gamma)/L$	$-\Delta_2 \sin(\gamma)/L$
6	$+\Delta_1 \cos\gamma \sin(60+\theta)/L$	$-\Delta_1 \cos\gamma \sin(60+\theta)/L$	$+\Delta_2 \sin(\gamma)/L$	$-\Delta_2 \sin(\gamma)/L$

[a] $\Delta_1 = \alpha_c L_s/2$; $\Delta_2 = \alpha_c R(3)^{1/2}/2$; α_c = angular (pitching) rotation about C.G.

Table 9.5

STRAINS IN SUPPORT MEMBERS DUE TO PITCHING ABOUT THE Y AXIS (Fig. 9.2)

SUPPORT MEMBER	Strain due to the component of motion parallel to the (x,y)plane		Strain due to the component of motion in the axial (z) direction	
	Forward Members[a]	Aft Members	Forward Members	Aft Members
1	$-\Delta_1 \cos\gamma \cos(\theta)/L$	$+\Delta_1 \cos\gamma \cos(\theta)/L$	$-\alpha_c R \sin(\gamma)/L$	$+\alpha_c R \sin(\gamma)/L$
2	$-\Delta_1 \cos\gamma \cos(60-\theta)/L$	$+\Delta_1 \cos\gamma \cos(60-\theta)/L$	$-\alpha_c R \sin(\gamma)/(2L)$	$+\alpha_c R \sin(\gamma)/(2L)$
3	$+\Delta_1 \cos\gamma \cos(60-\theta)/L$	$-\Delta_1 \cos\gamma \cos(60-\theta)/L$	$+\alpha_c R \sin(\gamma)/(2L)$	$-\alpha_c R \sin(\gamma)/(2L)$
4	$+\Delta_1 \cos\gamma \cos(\theta)/L$	$-\Delta_1 \cos\gamma \cos(\theta)/L$	$+\alpha_c R \sin(\gamma)/L$	$-\alpha_c R \sin(\gamma)/L$
5	$+\Delta_1 \cos\gamma \cos(60+\theta)/L$	$-\Delta_1 \cos\gamma \cos(60+\theta)/L$	$+\alpha_c R \sin(\gamma)/(2L)$	$-\alpha_c R \sin(\gamma)/(2L)$
6	$-\Delta_1 \cos\gamma \cos(60+\theta)/L$	$+\Delta_1 \cos\gamma \cos(60+\theta)/L$	$-\alpha_c R \sin(\gamma)/(2L)$	$+\alpha_c R \sin(\gamma)/(2L)$

[a] $\Delta_1 = \alpha_c L_s/2$

strains due to the two components of motion, that the frequency corresponding to pitching about the x-axis is equal to that corresponding to pitching about the y-axis and is given by

$$\Omega^2_{TILT} = \left[(EA)_{eff} + 3T \right] \left[1.5\ L_s^2 \cos^2\gamma + 6R^2 \sin^2\gamma + 6RL_s \cos\gamma \sin\gamma \cos\theta \right] / (LI_{TILT}) \quad (31)$$

Stress and Buckling Constraints

In the pre-launch state and at launch, the dewar support system is subjected to thermal and mechanical loading that may cause failure of the support material or buckling of one or more of the struts. If the dewar is supported by tension straps, the tension in the straps must be sufficient at launch so that the g-loading does not cause any strap to go slack.

In general there are three conditions, any combination of which might constrain the optimum design:

(1) maximum tensile or compressive stress experienced by any support member during the launch, when peak accelerations of 10 g's axial combined with 10 g's lateral are seen by the dewar;

(2) possibility that any support member may buckle as a column (Euler buckling) or, in the case of the tension strap concept, that a strap may go slack due to dynamic launch loads;

(3) possibility, in the cases of the PODS or the folded tube concepts, that any strut tube may buckle as a thin shell.

Stress due to Launch Accelerations: During launch the dewar is subjected to peak accelerations with a 10 g's axial component and a 10 g's lateral component. The maximum stress seen by any support member due to the inertial reaction of the supported mass to the sum of these acceleration components must not exceed a specified maximum.

The strain in each support member due to either an axial or a lateral acceleration component can be computed in two steps:

(1) compute the amount u_c the C.G. of the supported mass moves relative to the vacuum shell due to its inertial reaction to the 10 g's acceleration;

(2) with this value of u_c, compute the maximum strain and hence stress in any support member.

The strain energy of the supports is

$$U = \tfrac{1}{2}L \left[(EA)_{eff} + 3T \right] \sum_{j=1}^{N} e_j \tag{32}$$

in which e_j is the strain in the jth support and N is the number of supports. Corresponding to axial and lateral motions the strain energy components are

$$U_{axial} = u_{c_{axial}}^2 \; 6 \left[(EA)_{eff} + 3T \right] \sin^2\gamma/L \tag{33}$$

$$U_{lateral} = u_{c_{lateral}}^2 \; 3 \left[(EA)_{eff} + 3T \right] \cos^2\gamma/L \tag{34}$$

in which Eq. (24) has been used to derive Eq. (33) and Table 9.3 has been used to derive Eq. (34). The C.G. displacements $u_{c_{axial}}$ and $u_{c_{lateral}}$ can be computed from the following equations:

$$F^{axial}_{inertial} = MQ_{axial}\, g = \frac{dU_{axial}}{du_{c_{axial}}} = 12u_{c_{axial}}\left[(EA)_{eff} + 3T\right]\sin^2\gamma/L \tag{35}$$

$$F^{lateral}_{inertial} = MQ_{lateral}\, g = \frac{dU_{lateral}}{du_{c_{lateral}}} = 6u_{c_{lateral}}\left[(EA)_{eff} + 3T\right]\cos^2\gamma/L$$

in which Q_{axial} and $Q_{lateral}$ are the numbers of g's seen by the dewar during launch ($Q_{axial} = Q_{lateral} = 10$).

The maximum axial and lateral strains corresponding to $u_{c_{axial}}$ and $u_{c_{lateral}}$ from Eqs. (35) are, from Eq. (24) and Table 9.3, respectively.

$$e_{axial} = u_{c_{axial}} \sin\gamma/L = \frac{MQ_{axial}\, g}{12\left[(EA)_{eff} + 3T\right]\sin\gamma} \tag{36}$$

$$e_{lateral} = u_{c_{lateral}} \cos\gamma/L = \frac{MQ_{lateral}\, g}{6\left[(EA)_{eff} + 3T\right]\cos\gamma}$$

The total strain in the most highly loaded support member is

$$e_{launch} = |e_{axial}| + |e_{lateral}| + T/(EA) \tag{37}$$

and the associated stress is

$$\sigma_{launch} = Ee_{launch} \tag{38}$$

The constraint condition to be used in the optimization analysis is

$$\sigma_{launch}/\sigma_{max} \leq 1.0 \tag{39}$$

Note that Eqs. (33-36) are valid only if the support members are arranged symmetrically with respect to the mass C.G. as shcwn in Fig. 9.2. Hence, the lateral component of acceleration produces only lateral displacement of the supported mass relative to the vacuum shell. In a nonsymmetrical arrangement of the supports, the lateral component of acceleration would of course produce a combination of lateral and pitching displacements of the supported mass M.

Column Buckling: For struts pinned at both ends (PODS and folded tube concepts) we have

$$\text{Critical Load} = \pi^2 EI/L^2 = EAe_{crit} \tag{40}$$

in which I is the area moment of inertia of the strut cross section about a diameter and L is the length of the strut between pinned ends (Fig. 9.2). The maximum compressive strain is

$$e_{crit} = \frac{T}{EA} - |e_{axial}| - |e_{lateral}| \tag{41}$$

in which the strain components e_{axial} and $e_{lateral}$ are given by Eqs. (36). The constraint condition to be used in the optimization analysis is

$$|e_{axial}| + |e_{lateral}| \leq \frac{\pi^2 I}{AL^2} + \frac{T}{EA} \tag{42}$$

or

$$\frac{|e_{axial}| + |e_{lateral}|}{\left(\frac{\pi^2 I}{AL^2} + \frac{T}{EA}\right)} \leq 1.0 \qquad (43)$$

In the case of tension straps, the bending rigidity is zero ($I = 0$) so that the buckling criterion (43) is replaced by a criterion that e_{crit} in Eq. (41) remains positive during launch. Thus, the buckling criterion (43) can be used for tension straps if the area moment of inertia I is set equal to zero.

Buckling of Strut as a Thin Shell: In the PODS concept and in the folded tube concept, each support member during the launch phase consists of a cylindrical shell which may be compressed axially according to Eq. (41). The buckling stress is given by

$$\sigma_{crit} = K^* \left[.6\ E\ t\ /R_{ave} \right] \qquad (44)$$

in which K* is a knockdown factor to account for the deleterious effect of initial imperfections in the shape or material of the strut, t is the thickness of the tube wall, and R_{ave} is the average radius of the tube. In this analysis K* is taken as 0.5, which previous experiments have demonstrated to be appropriate for axially compressed cylindrical shells with $R_{ave}/t \leq 100$.

The corresponding constraint condition for application in the optimization analysis is

$$\frac{E\left(|e_{axial}| + |e_{lateral}|\right)}{(K^*\ .6\ E\ t\ /R_{ave})} \leq 1.0 \qquad (45)$$

"Effective" Stiffness and Conductivity Factors

In the PODS concept and the folded tube concept, each support member is a compound strut with an "effective" stiffness $(EA)_{eff}$ and an "effective" conductivity factor $(KA/L)_{eff}$. In Fig. 9.3 is shown a schematic of a compound strut with three different sections, each with its own properties E_i, K_i, L_i, A_i, $i = 1,2,3$. The proper overall stiffness and conductivity factors are obtained from the following mixture formulas:

$$1/(EA)_{eff} = \left| L_1/(E_1A_1) + L_2/E_2A_2 + L_3/E_3A_3 \right| /L \qquad (46)$$

and

$$\left| L/(KA) \right|_{eff} = L_1/(K_1A_1) + L_2/(K_2A_2) + L_3/(K_3A_3) \qquad (47)$$

PODS concept: Figure 9.4 shows the geometry. In this case (L_1, E_1, A_1, K_1) can be associated with the fiberglas tube; (L_2, E_2, A_2, K_2) can be associated with the S-glass strands; and (L_3, E_3, A_3, K_3) can be associated with the rest of the length of the strut, that is, calculated from the dimensions of the end fittings and the distances at each end between each of the two sets of S-glass strands.

The S-glass strands run at angles to the axis of the strut, and there are eight strands (a "group") at each end of the strut, PODS both ends (1 "group" = 2 bundles of 4 each), that

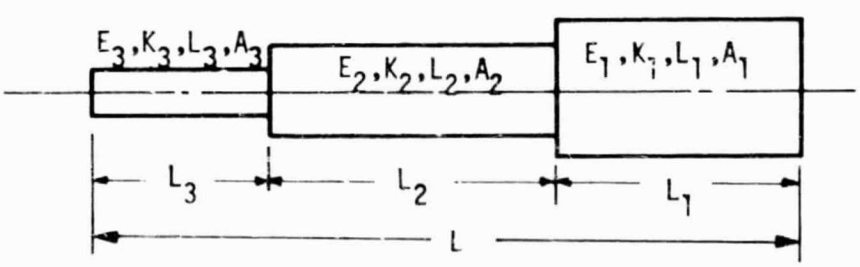

Fig. 9.3 Schematic of a Compound Strut

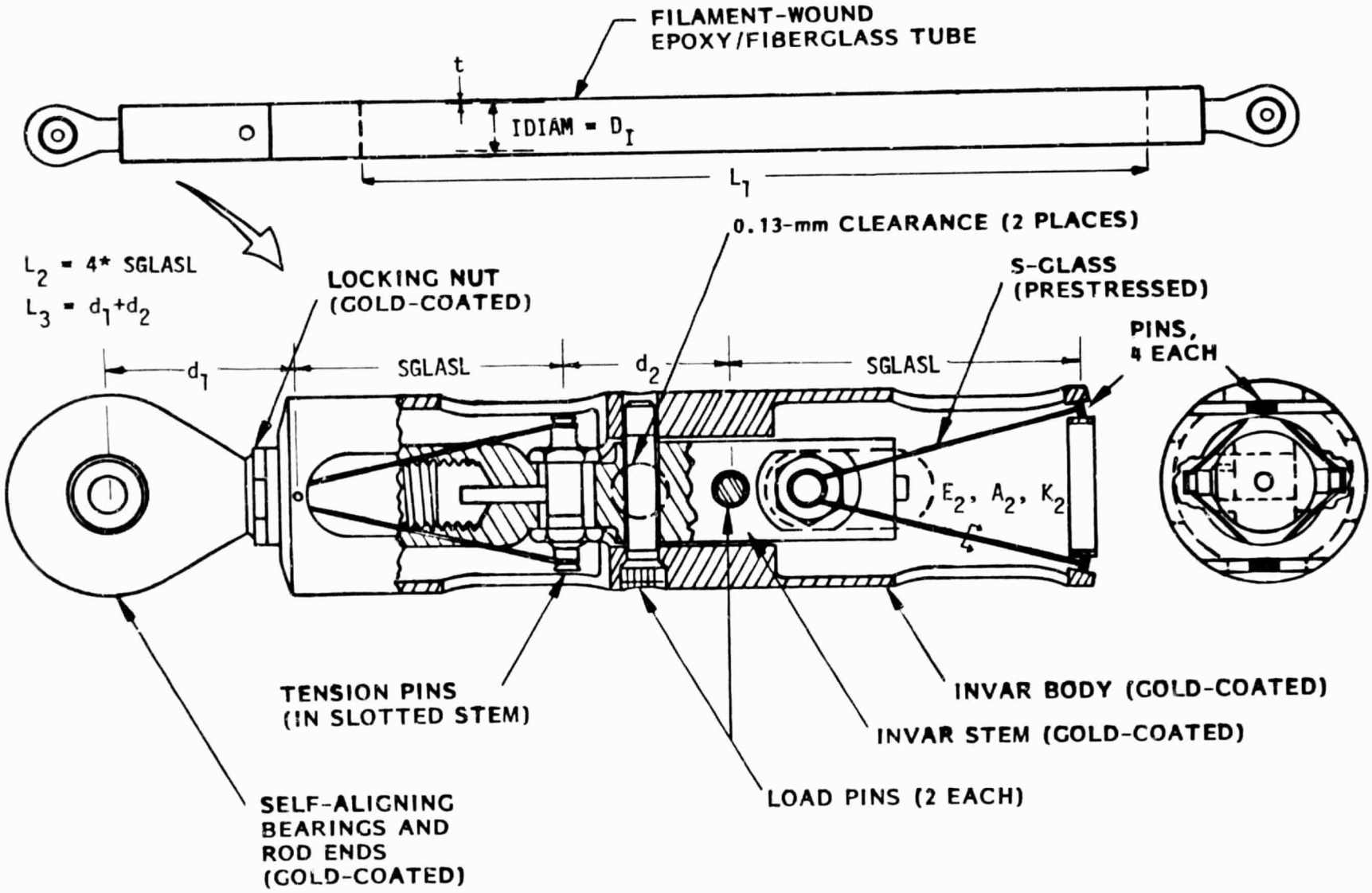

Fig. 9.4 Passive Orbital Disconnect Strut (PODS) Concept

connect the fiberglas tube to the thermally "isolated" invar body (Fig. 9.4). It can be shown that the effective axial stiffness of each group of 8 S-glass strands is

$$(EA)^{\text{s-glass}}_{\text{effective}} = 8E_sA_s\,(SGLASL)^3/\left[(SGLASL)^2 + D_I^2/2\right]^{3/2} \qquad (48)$$

in which SGLASL is the axial projection of the length of one set of 4 S-glass strands (Fig. 9.4) and D_I is the inner diameter of the fiberglas tube.

In the launch condition, the effective stiffness and conductivity factors for each support member in the PODS concept are

$$\begin{aligned}(EA)^{\text{launch}}_{\text{effective}} &= E_1A_1L/(L - 2L_3)\\ (KA/L)^{\text{launch}}_{\text{effective}} &= K_1A_1/(L - 2L_3)\end{aligned} \qquad (49)$$

in which L_3 is equal to the sum of the distance from the center of the rod end bearing to the first attachment point of the first set of S-glass strands (d_1) and the distance between the two sets of S-glass strands (d_2) (see Fig. 9.4).

In the orbital condition, the effective stiffness and conductance factors for each support member in the PODS concept are

$$(EA)^{\text{orbital}}_{\text{effective}} = L/\left\{.25\left[(SGLASL)^2 + \tfrac{1}{2}D_I^2\right]^{3/2}/\left[(SGLASL)^2E_sA_s\right] + (L - 2L_3)/(E_1A_1)\right\} \qquad (50)$$

$$(KA/L)^{\text{orbital}}_{\text{effective}} = 1/\left\{\left[(1/K_{hot}) + (1/K_{cold})\right]\left[(SGLASL)^2 + \tfrac{1}{2}D_I^2\right]^{1/2}/(8A_s) + (L - 2L_3 - 4\,SGLASL/(K_1A_1)\right\}$$

in which K_{hot} and K_{cold} are the conductivities of the S-glass strands at the "hot" and "cold" ends of each strut.

For PODS (cold end only), the effective stiffness and conductance are set at a large value for the warm end of the strut.

Folded Tube Concept: Figure 9.5 shows the geometry. In this case, (L_i, E_i, A_i, K_i) in Eqs. (49,50) can be associated with tube #1.

In the launch condition, the effective stiffness and conductivity factors for each support member in the folded tube concept are given, as in the PODS concept, by Eqs. (49), with L_3 being the length of one of the end fittings. In the orbital condition, we have

$$(KA/L)^{\text{orbital}}_{\text{effective}} = 1/\left[(L - 2L_3)/(K_1A_1) + L_{fold}/(K_2A_2) + L_{fold}/(K_3A_3)\right] \qquad (51)$$

in which L_{fold} is the length of tubes #2 and #3.

Tension Strap Concept: The effective stiffness and conductivity factors are given by Eqs. (49) with $L_3 = 0$.

Optimization

The objective of the optimization analysis for each support member concept is to derive values of the design parameters listed in Table 9.1 such as to minimize the flow of heat into the supported mass from the vacuum shell, to which it is attached, while maintaining enough structural rigidity to keep the lowest frequencies at launch and during orbital conditions above certain specified values, and stresses due to assembly and launch loads below those that would cause buckling or material failure of the support system.

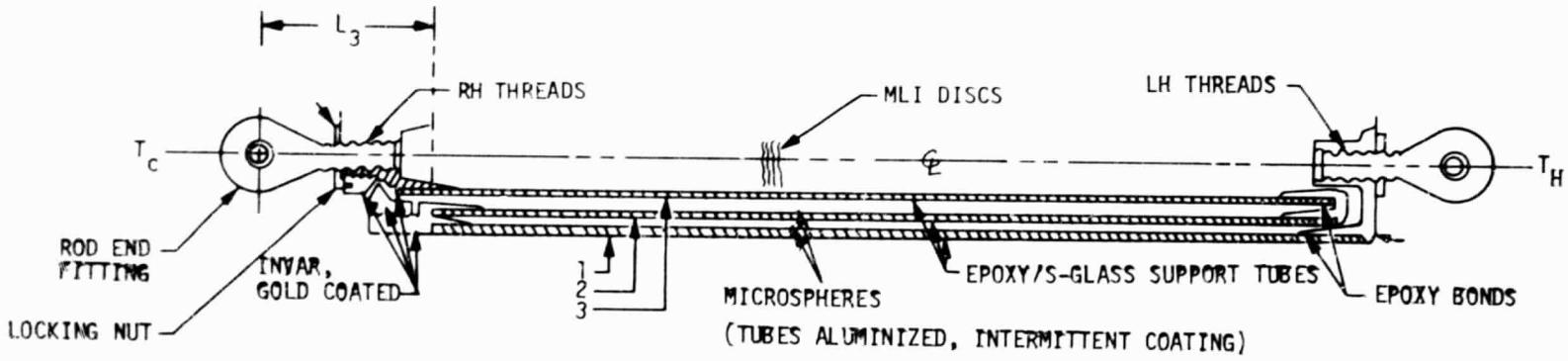

TUBE 1. DESIGNED FOR LAUNCH, ABORT LOADS AND RESONANCE
TUBES 1, 2, 3 DESIGNED FOR ORBIT RESONANCE AND MIN Q

Fig. 9.5 Folded Tube Strut (FTS) Concept

A computer program called PANDA-DEWAR has been written to solve this problem. Optimum designs have been obtained for several dewar weights for four support concepts, including two PODS concepts, a "folded tube" concept, and a simple tension strap concept. The first three concepts involve support struts the nature of which changes in a way that greatly decreases their effective conductivity for orbital conditions. Optimization of the dewar support systems involving each of these three concepts requires solution of two optimization problems, the first corresponding to launch conditions and the second to orbital conditions. In the case of the tension strap concept, the support system need be optimized only for launch conditions.

Optimization is carried out by a nonlinear programming algorithm based on the method of feasible directions [9.3]. The computer program for the dewar support design was generated by modification of a program called PANDA [9.4] for the minimum weight design of stiffened composite cylindrical panels. Application to the dewar support problem was accomplished by replacement of the expression for panel weight in PANDA with an appropriate expression for the heat conductance $N(KA/L)_{eff}$ through the support system and by replacement of certain expressions for general and local shell buckling by the appropriate expressions for frequency, stress, and buckling of the supported mass and the supports derived in the previous sections.

Figure 9.6 shows the strategy used to obtain optimum designs in PANDA-DEWAR. The starting design does not have to be close to an optimum, nor does it have to be a feasible design. For the PODS and the folded tube concepts, the strategy outlined in Fig. 9.6 is applied twice, first for the launch condition, during which parameters relative to the orbital phase (Table 9.2) have no role, and then for the orbital phase, during which the parameters varied in the launch phase are held constant.

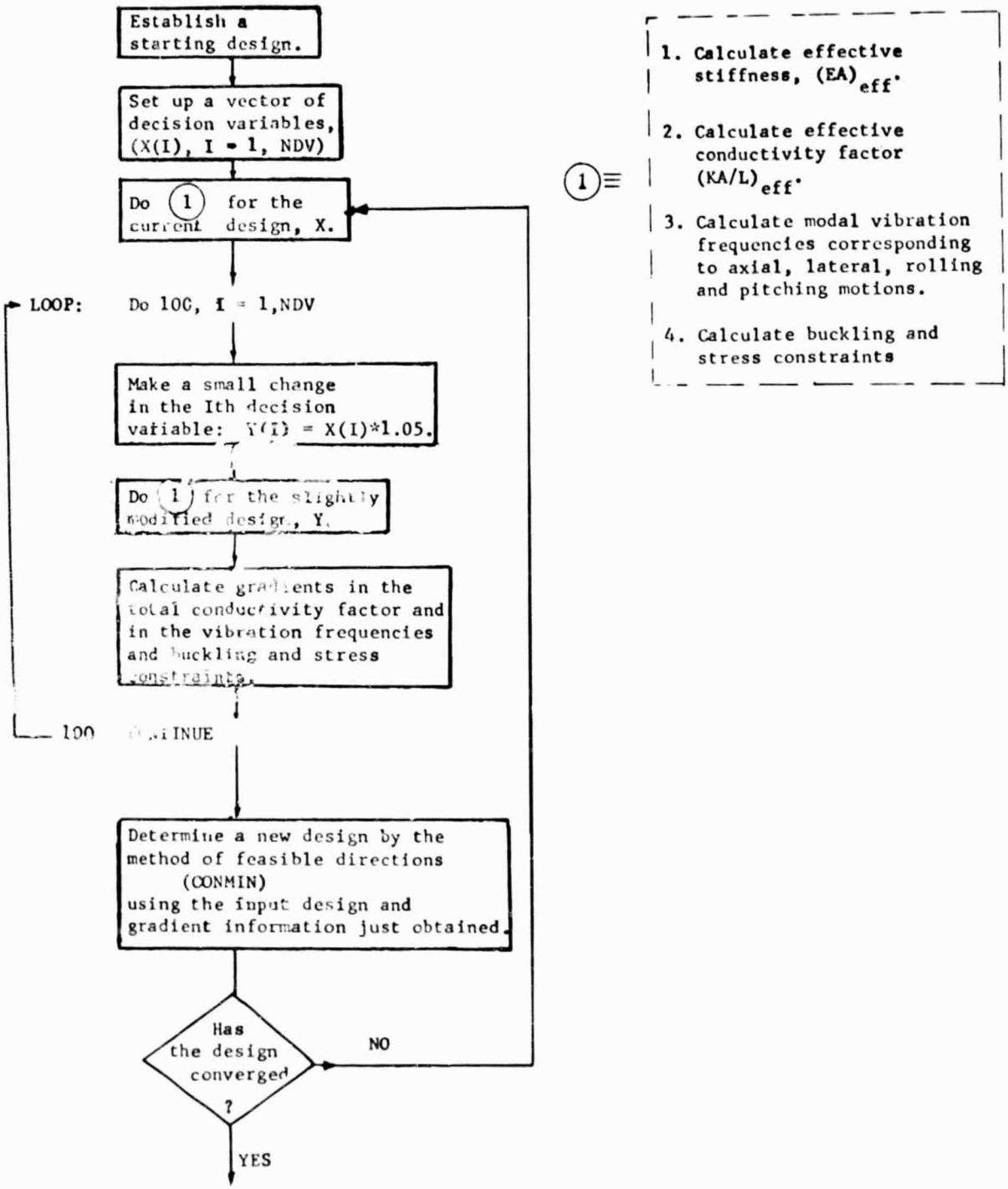

Fig. 9.6 Strategy Used in Optimization Process

STAGS Analysis for Check of Equations (25), (27), (30), and (31)

It was judged advisable to check the equations for the modal vibration frequencies by setting up a finite element model of a typical case: a 635 kg (1400 lb) mass, launch conditions, PODS concept. This was done for the geometry shown in Fig. 9.2. The STAGSC-1 computer program [9.5] was used for the analysis.

The agreement with PANDA is excellent, as listed below.

Vibration Mode	PANDA-DEWAR	STAGSC-1
Axial	35.0035	35.014
Lateral (y-axis)	35.0595	35.052
Lateral (x-axis)	35.0595	35.054
Pitching (about x-axis)	47.5755	47.311
Pitching (about y-axis)	47.5755	47.314
Rolling	54.236	53.47

Section 10

THERMAL AND MECHANICAL PROPERTY DATA

As a convenience to the reader, thermal and mechanical property data used throughout this report are provided in this section. Data references are also given.

	Property	Materials
Fig. 10.1	Thermal conductivity vs. temperature	S-glass, uniaxial S-glass/epoxy, filament-wound S-glass/epoxy (Al/A_{cr} = 2.0)
Fig. 10.2	Thermal conductivity vs. temperature	Manganin, stainless steel, Teflon
Fig. 10.3	Thermal conductivity vs. temperature	6063-T5 Aluminum
Table 10.1	Density, modulus of elasticity, ultimate tensile strength, yield strength	Uniaxial S-glass/epoxy, S-glass, filament-wound S-glass/epoxy, Invar, 6Al4V titanium, 6061-T6 aluminum, 347 stainless steel
Fig. 10.4	Thermal contraction vs. temperature	Invar, S-glass, 6Al4V titanium, 347 stainless steel, 6061 aluminum

THERMAL CONDUCTIVITY OF DOUBLE ALUMINIZED MYLAR, SILK NET INSULATION (Btu/hr ft ^{o}R)

$$k = \left[(6.72\times10^{-11})(\bar{N})^{1.56}\, k_s(T_H+T_c) + \frac{9.17\times10^{-13}\,\varepsilon(T_H^{4.67}-T_c^{4.67})}{(T_H-T_c)\bar{N}}\right] 1.4 \qquad \text{REF 10-1}$$

WHERE $\bar{N}$ IS THE LAYER DENSITY (L/IN), ε THE ROOM TEMPERATURE EMISSIVITY, T IN ^{o}R AND A 40% DEGRADATION FACTOR (1.4) FOR INSTALLATION

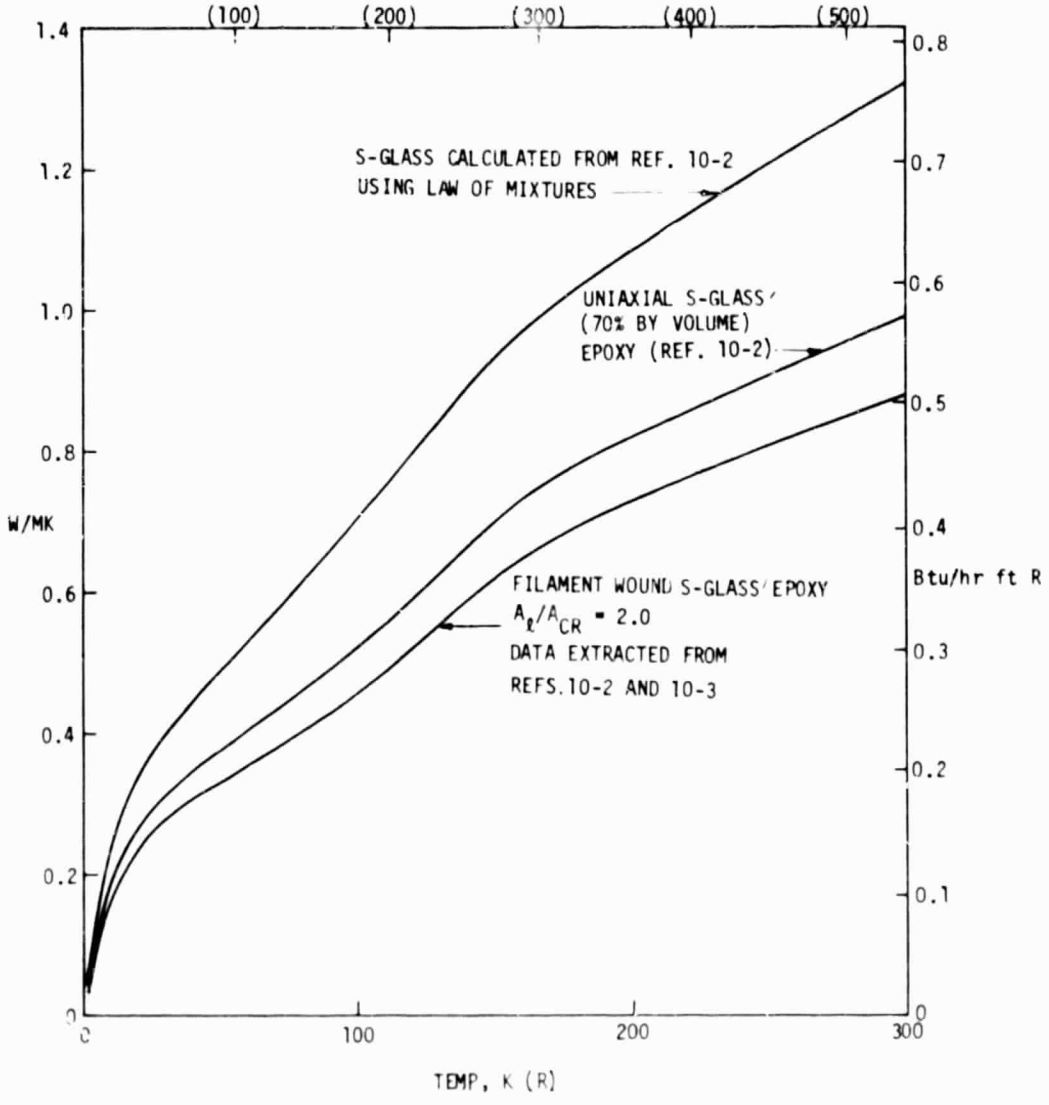

Fig. 10.1 Thermal Conductivity of S-Glass, S-Glass Composites and Multilayer Insulation

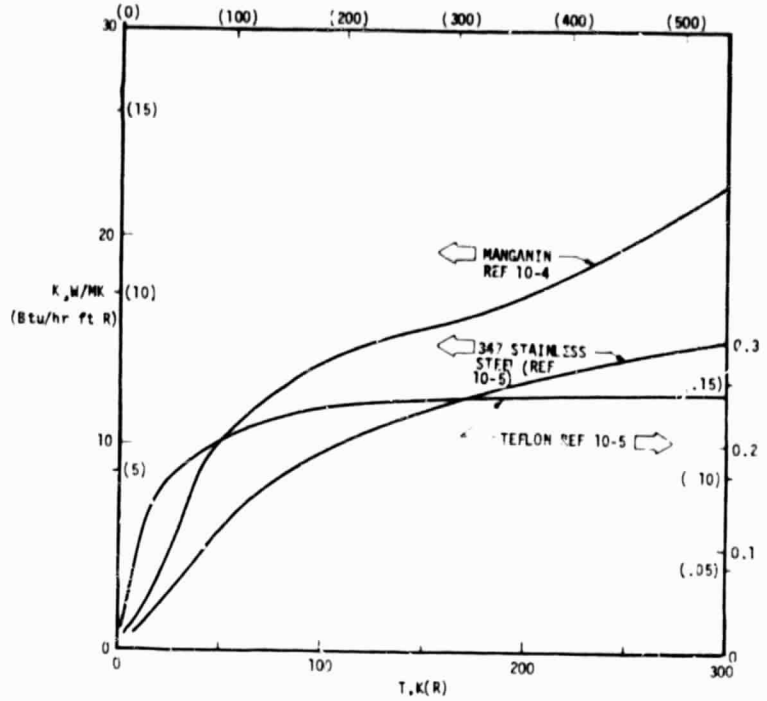

Fig. 10.2 Thermal Conductivity of Manganin, Stainless Steel and Teflon

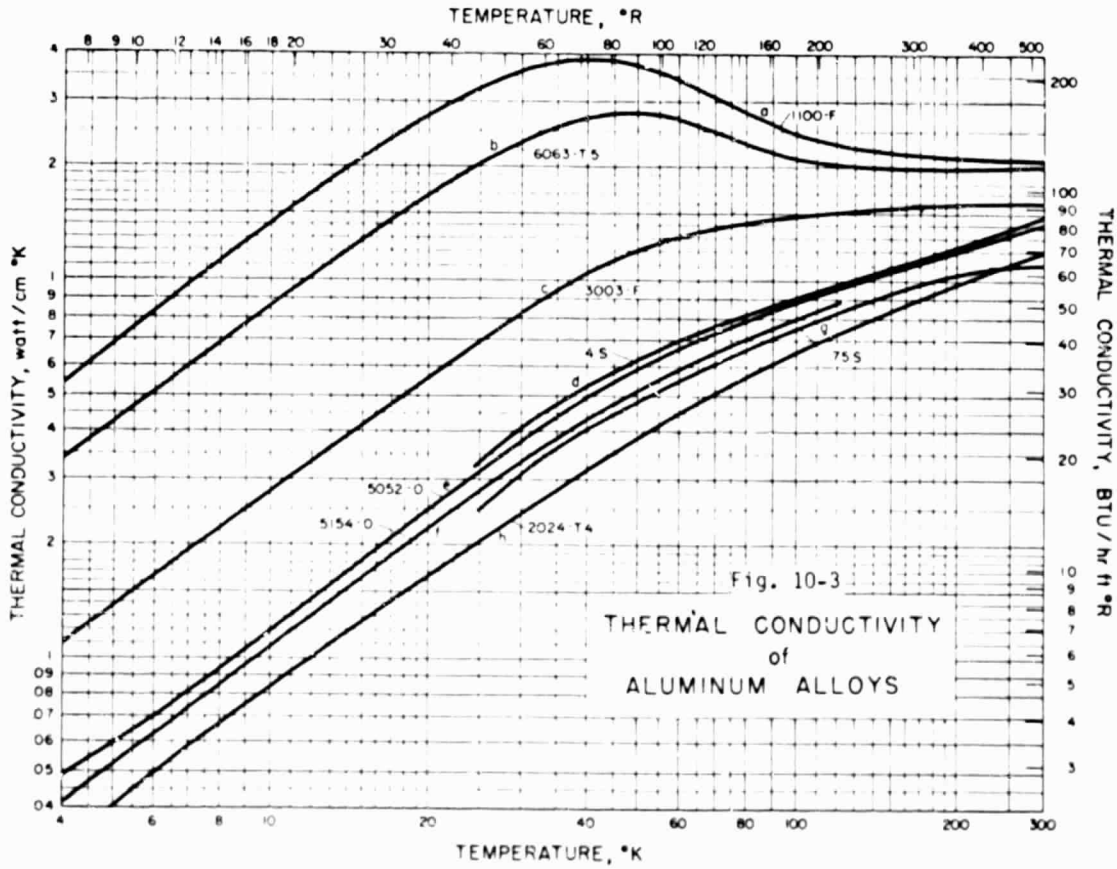

Table 10.1 MECHANICAL PROPERTIES OF METALS AND S-GLASS AT 300K (540R)

Ref.	Materials	Density kg/m^3 (lb/in^3)	Modulus of Elasticity 10^9 N/m^2 (PSI)	Ultimate Tensile Strength 10^9 N/m^2 (KSI)	Yield Strength 10^9 N/m^2 (KSI)
10.2	Uniaxial S-glass/ epoxy (70% by volume glass)	2120 (0.077)	51.7 ($7.5x10^6$)	1.17 (162)	---
10.9	S-glass	2490 (0.090)	86.9 ($12.6x10^6$)	4.59 (665)	---
10.2, 10.3	Filament-wound S-glass/epoxy (Al/A_{cr} = 2.0)	2120 (0.077)	41.4 ($6.0x10^6$)	0.74 (108)	---
10.7	Invar (annealed)	8050 (0.291)	141 ($20.5x10^6$)	0.45 (65)	0.28 (40)
10.8	6Al4V titanium	4430 (0.160)	114 ($16.5x10^6$)	0.95 (138)	0.82 (120)
10.8	6061-T6 aluminum	2710 (0.098)	69 ($10x10^6$)	0.31 (45)	0.25 (36)
10.8	347 stainless steel	8020 (0.29)	193 ($28x10^6$)	0.65 (95)	0.28 (40)

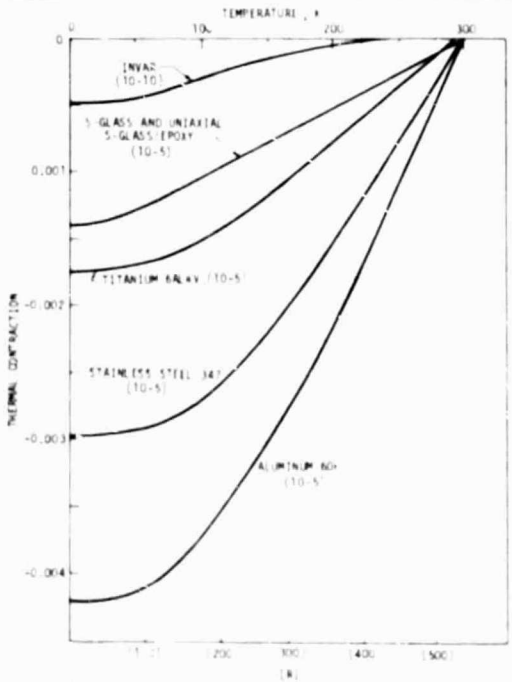

Fig. 10.4 Thermal Contraction Values of Metals and S-Glass